

การผลิตไฮโดรเจนผ่านปฏิกิริยารีฟอร์มมิงแก๊สชีวภาพด้วยไอน้ำที่ส่งเสริมด้วยการดูดซับโดยใช้никเกล
บนแคลเซียมออกไซด์ที่ถูกต้องแปร



บทคัดย่อและแฟ้มข้อมูลฉบับเต็มของวิทยานิพนธ์ตั้งแต่ปีการศึกษา 2554 ที่ให้บริการในคลังปัญญาจุฬาฯ (CUIR)
เป็นแฟ้มข้อมูลของนิสิตเจ้าของวิทยานิพนธ์ ที่ส่งผ่านทางบัณฑิตวิทยาลัย

The abstract and full text of theses from the academic year 2011 in Chulalongkorn University Intellectual Repository (CUIR)
are the thesis authors' files submitted through the University Graduate School.

วิทยานิพนธ์นี้เป็นส่วนหนึ่งของการศึกษาตามหลักสูตรปริญญาวิศวกรรมศาสตรดุษฎีบัณฑิต
สาขาวิชาวิศวกรรมเคมี ภาควิชาวิศวกรรมเคมี
คณะวิศวกรรมศาสตร์ จุฬาลงกรณ์มหาวิทยาลัย
ปีการศึกษา 2559
ลิขสิทธิ์ของจุฬาลงกรณ์มหาวิทยาลัย

HYDROGEN PRODUCTION FROM SORPTION ENHANCED STEAM REFORMING OF BIOGAS
VIA NICKEL OVER MODIFIED CaO SORBENT

Mr. Janewit Phromprasit



A Dissertation Submitted in Partial Fulfillment of the Requirements
for the Degree of Doctor of Engineering Program in Chemical Engineering

Department of Chemical Engineering

Faculty of Engineering

Chulalongkorn University

Academic Year 2016

Copyright of Chulalongkorn University

Thesis Title	HYDROGEN PRODUCTION FROM SORPTION ENHANCED STEAM REFORMING OF BIOGAS VIA NICKEL OVER MODIFIED CaO SORBENT
By	Mr. Janewit Phromprasit
Field of Study	Chemical Engineering
Thesis Advisor	Professor Suttichai Assabumrungrat, Ph.D.

Accepted by the Faculty of Engineering, Chulalongkorn University in Partial
Fulfillment of the Requirements for the Doctoral Degree

.....Dean of the Faculty of Engineering
(Associate Professor Supot Teachavorasinskun, Ph.D.)

THESIS COMMITTEE

.....Chairman
(Associate Professor Anongnat Somwangthanaroj, Ph.D.)

.....Thesis Advisor
(Professor Suttichai Assabumrungrat, Ph.D.)

.....Examiner
(Akawat Sirisuk, Ph.D.)

.....Examiner
(Palang Bumroongsakulsawat, Ph.D.)

.....External Examiner
(Assistant Professor Ratanawan (Wibulswas) Kiattikomol, Ph.D.)

เจนวิทย์ พรหมประสิทธิ์ : การผลิตไฮโดรเจนผ่านปฏิกิริยารีฟอร์มมิงแก๊สชีวภาพด้วยไอน้ำ ที่ส่งเสริมด้วยการดูดซับโดยใช้นิกเกิลบนแคลเซียมออกไซด์ที่ถูกต้องแปร (HYDROGEN PRODUCTION FROM SORPTION ENHANCED STEAM REFORMING OF BIOGAS VIA NICKEL OVER MODIFIED CaO SORBENT) อ.ที่ปรึกษาวิทยานิพนธ์หลัก: ศ. ดร.สุทธิชัย อัสสะบำรุงรัตน์, 164 หน้า.

ในงานวิจัยนี้ประกอบด้วย 2 ส่วน ได้แก่ การศึกษาการดูดซับแก๊สคาร์บอนไดออกไซด์ และการทดสอบสมรรถนะการผลิตแก๊สไฮโดรเจนของตัวเร่งปฏิกิริยาหลายหน้าที่ ในส่วนการดูดซับแก๊สคาร์บอนไดออกไซด์ ได้ศึกษาการใส่โลหะกลุ่มที่หนึ่ง ได้แก่ Mg^{2+} Sr^{2+} และ Al^{3+} บนแคลเซียมออกไซด์ แล้วนำไปทดสอบประสิทธิภาพการดูดซับและคายซับแก๊สคาร์บอนไดออกไซด์จำนวน 10 รอบ พบว่า Mg-CaO-HW แสดงผลการดูดซับและคายซับที่เสถียร แต่ทว่า Al-CaO-HW และ Sr-CaO-HW แสดงการลดลงของความจุการดูดซับแก๊สคาร์บอนไดออกไซด์ โดยลดลง 6 และ 12 % ตามลำดับ สำหรับการศึกษาโลหะกลุ่มที่สองที่ใส่บนแคลเซียมออกไซด์ ได้แก่ Zr^{4+} Ce^{4+} และ La^{3+} ผลชี้ว่า Zr-CaO-HW และ Ce-CaO-HW แสดงความเสถียรทางความจุแก๊สคาร์บอนไดออกไซด์ ในการทดลอง 10 รอบ ในทางกลับกัน La-CaO-HW แสดงการลดลงของความจุการดูดซับแก๊สคาร์บอนไดออกไซด์ 16% ทั้งนี้เนื่องมาจากคุณสมบัติการเก็บออกซิเจนที่อุณหภูมิต่ำของ Zr-CaO-HW และ Ce-CaO-HW ซึ่งช่วยเพิ่มความสามารถในการเคลื่อนที่ของออกซิเจน

ในส่วนของการผลิตแก๊สไฮโดรเจน มีการศึกษาลำดับการใส่ Ni^{2+} บนแคลเซียมออกไซด์ที่ถูกต้องแปร ผลการทดลองแสดงให้เห็นว่า Ni-Al-CaO-HW คือตัวเร่งปฏิกิริยาหลายหน้าที่ที่ดีที่สุด ความเสถียรของ Ni-Al-CaO-HW แสดงการแปลงผันของมีเทน มีค่ามากกว่า 90% ขณะช่วงเวลา pre-breakthrough สำหรับ 5 รอบการปฏิบัติการ นอกจากนี้เมื่อศึกษาผลของการเติม Ni^{2+} ลงบนตัวดูดซับที่ถูกต้องแปร Zr-CaO-HW Ce-CaO-HW และ La-CaO-HW ผลการทดลองพบว่า Ni-Zr-CaO-HW และ Ni-Ce-CaO-HW มีความเสถียรในการผลิตแก๊สไฮโดรเจนที่มีความบริสุทธิ์สูง แต่อย่างไรก็ตาม การแปลงผันของมีเทนจะลดลง ทั้งนี้เนื่องจากการหายไปของตำแหน่งวงโคจรของนิกเกิลที่พื้นผิวของตัวเร่งปฏิกิริยาหลายหน้าที่ ซึ่งเกิดจากการเกิดขึ้นของแคลเซียมคาร์บอเนต

ภาควิชา วิศวกรรมเคมี

ลายมือชื่อนิสิต

สาขาวิชา วิศวกรรมเคมี

ลายมือชื่อ อ.ที่ปรึกษาหลัก

ปีการศึกษา 2559

5671407421 : MAJOR CHEMICAL ENGINEERING

KEYWORDS: H₂ PRODUCTION / CO₂ CAPTURE / SORPTION ENHANCED STEAM REFORMING OF BIOGAS / MULTIFUNCTIONAL CATALYST

JANEWIT PHROMPRASIT: HYDROGEN PRODUCTION FROM SORPTION ENHANCED STEAM REFORMING OF BIOGAS VIA NICKEL OVER MODIFIED CaO SORBENT. ADVISOR: PROF. SUTTICHAJ ASSABUMRUNGRAT, Ph.D., 164 pp.

This research composed of two parts: (i) CO₂ sorption study and (ii) hydrogen production performance tests using multifunctional catalysts. In the CO₂ sorption section, the first group of metals (Mg²⁺, Sr²⁺ and Al³⁺) was loaded on CaO and tested the CO₂ sorption and desorption performance over 10 cycles. Mg-CaO-HW offered the best stability in terms of CO₂ sorption/desorption. Whereas Al-CaO-HW and Sr-CaO-HW exhibited a decrease in CO₂ sorption capacity corresponding to 6 and 12% reduction. The second group of metals loading on CaO were Zr⁴⁺, Ce⁴⁺ and La³⁺. The results indicated that Zr-CaO-HW and Ce-CaO-HW possessed stable CO₂ capacities over the 10 cycles. On the other hand, La-CaO-HW showed a decrease in the CO₂ sorption capacity of 16%. This was due to the low-temperature oxygen storage properties of Zr-CaO-HW and Ce-CaO-HW, which enhanced the mobility of oxygen.

In the section of H₂ production, three sequences of Ni²⁺ loading on modified CaO were investigated. The results showed that Ni-Al-CaO-HW is the best multifunctional catalyst. The stability of Ni-Al-CaO-HW shows that CH₄ conversion is still higher than 90% during the pre-breakthrough period for 5 cycle operations. Furthermore, Ni²⁺ was loaded on the modified sorbents Zr-CaO-HW, Ce-CaO-HW and La-CaO-HW. The results showed that Ni-Zr-CaO-HW and Ni-Ce-CaO-HW produced H₂ at stable purities but with decreasing CH₄ conversions. This was attributed to the loss of nickel active sites at the surface of the multifunctional catalysts due to the formation of CaCO₃.

Department: Chemical Engineering Student's Signature

Field of Study: Chemical Engineering Advisor's Signature

Academic Year: 2016

ACKNOWLEDGEMENTS

The author would like to thank his advisor, Professor Suttichai Assabumrungrat, and Dr. Jon Powell for their advices and suggestion to successful life, study and research. Their suggestions give him to be good person in society, positive thinking, strength and happiness when he did this thesis. Moreover, the author was grateful to Associate Professor Anongnat Somwangthanaroj, as the chairman, Dr. Akawat Sirisuk, Dr. Palang Bumroongsakulsawat, Assistant Professor Ratanawan (Wibulswas) Kiattikomol, as the examiners for their useful comments.

The author would like to thank the Royal Golden Jubilee Ph.D. Program from the Thailand Research Fund and Chulalongkorn University, and the Thailand Research Fund for financial support. Furthermore, the author would like to thank his friends in Center of Excellence of Catalysis and Catalytic Reaction Engineering, Department of Chemical Engineering, Faculty of Engineering, Chulalongkorn University for helps and suggestion leading to success in this project.

Finally, the author would like to thank his beloved family including dad, mom and older sister. They always support the author everything that they can do. The author cannot finish his thesis without their encouragements. The author would like to say he love his family.

CONTENTS

	Page
THAI ABSTRACT	iv
ENGLISH ABSTRACT	v
ACKNOWLEDGEMENTS	vi
CONTENTS	vii
CHAPTER I INTRODUCTION.....	1
1.1 Rationale	1
1.2 Objectives	9
1.3 Scope of research	9
1.4 Organization of thesis.....	10
CHAPTER II THEORY	13
2.1 Biogas	13
2.2 Hydrogen production reaction and mechanisms	18
2.2.1 Chemical reaction.....	18
2.2.2 Surface reaction mechanism.....	19
2.3 Fixed bed adsorption [86-88].....	21
CHAPTER III LITERATURE REVIEWS	25
3.1 Hydrogen production via reforming process	25
3.2 CO ₂ sorption	30
3.2.1 Calcium Oxide	30
3.2.2 Hydrotalcite.....	43
3.3 Sorption enhanced process	44
3.3.1 Sorption enhanced steam methane reforming	45

	Page
CHAPTER IV EXPERIMENTAL	52
4.1 Materials and method	52
4.1.1 Sorbent synthesis.....	52
4.1.2 Catalyst synthesis.....	53
4.2 Characterization.....	54
4.2.1 X-ray diffraction technique	54
4.2.2 N ₂ adsorption/desorption isotherm	54
4.2.3 Scanning electron microscope.....	54
4.2.4 X-ray photoelectron spectroscopy	55
4.2.5 Temperature-programmed reduction.....	55
4.3 CO ₂ sorption/desorption testing.....	55
4.4 H ₂ production.....	56
CHAPTER V Metals (Mg, Sr and Al) modified CaO based sorbent for CO ₂ sorption/desorption stability in fixed bed reactor for high temperature application ..	57
5.1 Effect of support	57
5.2 Effect of temperature.....	59
5.3 Effect of synthesis method	62
5.3.1 Dry powder mixing method.....	62
5.3.2 Wet mixing method.....	64
5.4 Effect of CO ₂ concentration	69
5.5 Stability of modified sorbents by CaO hydration followed with by wet mixing method	71

	Page
CHAPTER VI Activity and stability performance of multifunctional catalyst (Ni/CaO and Ni/Ca ₁₂ Al ₁₄ O ₃₃ -CaO) for bio-hydrogen production from sorption enhanced steam reforming of biogas	78
6.1 CO ₂ sorption/desorption testing of Ni- and Al-modified CaO sorbents	78
6.2 H ₂ production by using multifunctional catalysts	83
6.3 Stability of multifunctional catalyst	95
6.4 Effect of ultrasonic assistant in preparation method for CO ₂ sorption/desorption multiple cycles	100
6.5 Performance of multifunctional catalysts with/without ultrasonic assistant ...	101
CHAPTER VII H ₂ production from sorption enhanced steam reforming of biogas using multifunctional catalysts of Ni over Zr-, Ce- and La-modified CaO sorbents..	104
7.1 CO ₂ sorption stability of Zr-, Ce- and La-modified CaO sorbents	104
7.2 H ₂ production by using Ni over Zr-, Ce- and La-modified CaO multifunctional catalyst.....	111
7.3 Stability of Ni over Zr-, Ce- and La-modified CaO multifunctional catalysts for 5 cycles H ₂ production	115
CHAPTER VIII Conclusions and recommendations.....	124
8.1 Conclusions	124
8.1.1 CO ₂ sorption.....	124
8.1.2 H ₂ production	125
8.2 Recommendations	127
REFERENCES	128
APPENDIX A CALCULATIONS OF ADSORPTION CAPACITY	151
APPENDIX B CALCULATIONS FOR SORPTION ENHANCED BIOGAS STEAM REFORMING PROCESS.....	155

	Page
APPENDIX C CALIBRATION CURVES	157
APPENDIX D LIST OF PUBLICATIONS	162
International Publications	162
International Conferences.....	163
Awards.....	163
VITA.....	164



Figures

Figure 1.1 World primary energy demand.....	1
Figure 1.2 Flowsheet for a conventional methane steam reforming process	4
Figure 1.3 Proposed mechanism for the formation of the inert support materials.....	7
Figure 2.1 The CO ₂ close cycle in anaerobic digestion (AD).....	15
Figure 2.2 The anaerobic digestion stages.....	15
Figure 2.3 Fixed-dome type bio-gas plant.....	16
Figure 2.4 Floating gas-holder type bio-gas plant.....	16
Figure 2.5 Scheme of digester.....	17
Figure 2.6 Two-stage process.....	17
Figure 2.7 Scheme of UASB tank.....	18
Figure 2.8 Stoichiometric (equilibrium) concentration front for ideal fixed bed adsorption.....	22
Figure 2.9 Solute wave fronts in a fixed bed adsorber with mass transfer effects.....	24

Figure 3.1 Conversion of methane at 800 °C in the presence of nickel catalyst on various substrates including Mg doped alumina. Stability is seen as a loss of conversion rate over time.....	28
Figure 3.2 Catalytic activity of various nickel doped Ce-ZrO ₂ catalysts at temperature of 750 °C.....	29
Figure 3.3 Proposed mechanism for the formation of the inert support materials. ...	37
Figure 5.1 Breakthrough curves of various supports (MgO, SrO, CaO and Al ₂ O ₃) at temperature of 600 °C, pressure of 1 atm and 8% CO ₂ feed stream.....	58
Figure 5.2 Breakthrough curves of CaO at temperature of 500-700 °C, pressure of 1 atm and 8% CO ₂ feed stream: (1) refers to step 1 - surface reaction and (2) refers to step 2 - CO ₂ diffusion.....	59
Figure 5.3 Proposed mechanisms: (a) CO ₂ sorption step and (b) densification phenomena at sorption temperature of 600 and 700 °C.	61
Figure 5.4 Breakthrough curves of modified sorbents by dry powder mixing method (Mg-CaO-D, Sr-CaO-D, Al-CaO-D and CaO) at temperature of 600 °C, pressure of 1 atm and 8% CO ₂ feed stream.....	63
Figure 5.5 XRD patterns of modified sorbents by dry powder mixing method: ● CaO, ■ MgO, ✕ SrO, ▲ Al ₂ O ₃ and ★ Ca(OH) ₂	64

- Figure 5.6** CO₂ sorption/desorption cycles of modified sorbents by wet mixing method at temperature of 600 °C, pressure of 1 atm and 8% CO₂ in feed stream. ... 65
- Figure 5.7** SEM images of fresh and used modified sorbents by wet mixing method: (a) Al-CaO-W, (b) Mg-CaO-W, (c) Sr-CaO-W, (d) CaO commercial and (e) Al-CaO-HW..... 66
- Figure 5.8** Proposed mechanism of occurring the dopant phases (MgO, Ca_{0.2}Sr_{0.8}O and Ca₁₂Al₁₄O₃₃) on CaO by wet mixing method and their densification phenomena. 68
- Figure 5.9** CO₂ sorption/desorption cycles of Al-CaO-HW at temperature of 600 °C, pressure of 1 atm and CO₂ concentration of 8 and 15%. 69
- Figure 5.10** XRD patterns of modified sorbents by CaO hydration followed by wet mixing method (Mg-CaO-HW, Sr-CaO-HW and Al-CaO-HW): ● CaO, ■ MgO, ✕ Ca_{0.2}Sr_{0.8}O and ▲ Ca₁₂Al₁₄O₃₃..... 72
- Figure 5.11** CO₂ sorption/desorption cycles of modified sorbents by CaO hydration followed with wet mixing method (Mg-CaO-HW, Sr-CaO-HW and Al-CaO-HW) at temperature of 600 °C, pressure of 1 atm and 15% CO₂ feed stream..... 73
- Figure 5.12** SEM images of fresh and used of modified sorbents synthesized by CaO hydration followed by wet mixing method: (a) Al-CaO-HW, (b) Mg-CaO-HW, (c) Sr-CaO-HW and (d) CaO commercial. 74

- Figure 5.13** Proposed mechanism of metal precursors doped on CaO and their resisting sintering phenomena: (a) Al^{3+} doped on CaO and (b) Mg^{2+} doped on CaO... 76
- Figure 5.14** SEM-EDX images of modified sorbents by CaO hydration followed by wet mixing method (a) Mg-CaO-HW and (b) Al-CaO-HW..... 77
- Figure 6.1** Sorption capacity of Ni-CaO-HW and Al-CaO-HW at 600 °C, 1 atm and CO_2 concentration of 15% v/v for different sorption/desorption cycles..... 80
- Figure 6.2** SEM images of (a) Ni-CaO-HW and (b) Al-CaO-HW freshly prepared and after 10 CO_2 sorption/desorption cycles. 81
- Figure 6.3** XRD pattern of modified sorbents Al-CaO-HW and Ni-CaO-HW: ● CaO, ★ Ca(OH)_2 , ▲ NiO, ✕ $\text{Ca}_{12}\text{Al}_{14}\text{O}_{33}$ and ■ CaCO_3 82
- Figure 6.4** SEM-EDS images of (a) Ni-CaO-HW and (b) Al-CaO-HW after 10 CO_2 sorption/desorption cycles..... 83
- Figure 6.5** XRD pattern of different catalytic sorbents: ● CaO, ★ Ca(OH)_2 , ▲ NiO, ✕ $\text{Ca}_{12}\text{Al}_{14}\text{O}_{33}$ and ■ Al_2O_3 84
- Figure 6.6** Temperature programmed reduction (TPR) profiles of Ni over multifunctional catalytic sorbents. 86
- Figure 6.7** The performance of Ni- Al_2O_3 -HW for hydrogen production from sorption enhanced steam reforming of biogas. 87



Figure 6.8 The performance of Ni-CaO-HW for hydrogen production from sorption enhanced steam reforming of biogas.....	88
Figure 6.9 The performance of Ni-Al-CaO-HW for hydrogen production from sorption enhanced steam reforming of biogas.	88
Figure 6.10 The performance of Ni-Al-CaO-HWO for hydrogen production from sorption enhanced steam reforming of biogas.	89
Figure 6.11 The performance of Ni-Al-CaO-HWC for hydrogen production from sorption enhanced steam reforming of biogas.	89
Figure 6.12 CH ₄ conversions of Ni-Al ₂ O ₃ -HW, Ni-CaO-HW, Ni-Al-CaO-HW, Ni-Al-CaO-HWO and Ni-Al-CaO-HWC ( refers the pre-breakthrough period and  refers the post-breakthrough period).....	90
Figure 6.13 SEM images of multifunctional catalysts: (a) Ni-CaO-HW and (b) Ni-Al-CaO-HW.....	93
Figure 6.14 Gas product compositions and CH ₄ conversion of Ni-Al-CaO-HW sample: (a) hydrogen concentration, (b) methane concentration, (c) carbon dioxide concentration, (d) carbon monoxide concentration and (e) CH ₄ conversion.....	95
Figure 6.15 SEM-EDS images of Ni-Al-CaO-HW: (a) fresh and (b) used catalyst.	98

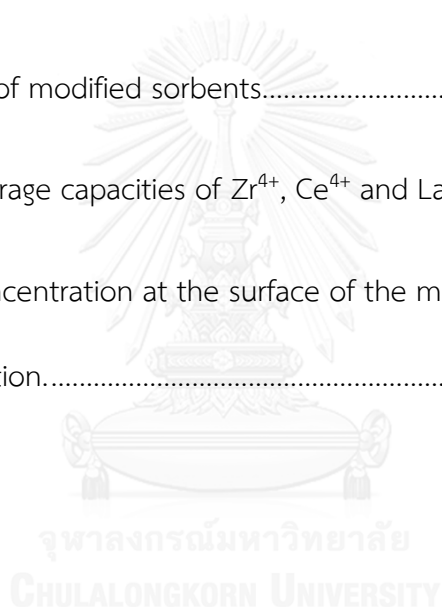
Figure 6.16 Schematic diagram of our proposed sorption enhanced H_2 production mechanism of (a) Ni-Al-CaO-HW and (b) Ni-CaO-HW at pre-breakthrough and post-breakthrough periods.....	99
Figure 6.17 CO_2 sorption capacity using Al-CaO-HW and Al-CaO-UHW for 10 cycle operations.	100
Figure 6.18 H_2 concentration and CH_4 conversion of Ni-Al-CaO-HW and Ni-Al-CaO-UHW.	102
Figure 7.1 XRD patterns of modified sorbents: ● CaO, ■ $CaCO_3$, ▲ $CaZrO_3$, ✕ CeO_2 and ★ La_2O_3	105
Figure 7.2 CO_2 sorption capacities of Zr^{4+} , Ce^{4+} and La^{3+} modified CaO after the indicated number of sorption/desorption cycles.	106
Figure 7.3 SEM images of modified sorbents: (a) Zr-CaO (Fresh), (b) Zr-CaO (Used), (c) Ce-CaO (Fresh), (d) Ce-CaO (Used), (e) La-CaO (Fresh) and (f) La-CaO (Used).....	108
Figure 7.4 O_2 consumption from the temperature-programmed reduction oxidation of Zr^{4+} , Ce^{4+} and La^{3+} modified CaO.	110
Figure 7.5 XRD patterns of multifunctional catalysts: ● CaO, ■ NiO, ▲ $CaZrO_3$, ✕ CeO_2 and ★ $(La_{1.7}Ca_{0.3})(NiO_4)$	111

Figure 7.6 H ₂ consumption from the temperature-programmed reduction of Ni over Zr ⁴⁺ , Ce ⁴⁺ and La ³⁺ modified CaO.....	112
Figure 7.7 H ₂ concentrations from sorption enhanced steam reforming of biogas with various multifunctional catalysts.....	113
Figure 7.8 The hydrogen production performance of Ni-Zr-CaO: (a) H ₂ concentration and (b) CH ₄ conversion.....	115
Figure 7.9 The hydrogen production performance of Ni-Ce-CaO: (a) H ₂ concentration and (b) CH ₄ conversion.....	116
Figure 7.10 The hydrogen production performance of Ni-La-CaO: (a) H ₂ concentration and (b) CH ₄ conversion.....	117
Figure 7.11 SEM images of multifunctional catalysts: (a) Ni-Zr-CaO (Fresh), (b) Ni-Zr-CaO (Used), (c) Ni-Ce-CaO (Fresh), (d) Ni-Ce-CaO (Used), (e) Ni-La-CaO (Fresh) and (f) Ni-La-CaO (Used).....	122
Figure 7.12 Proposed mechanism of the densification of CaCO ₃	123

Tables

Table 1.1 Melting and Tammann temperatures of CaO, CaCO ₃ , and the dopants.....	6
Table 2.1 Anaerobic digestion feedstock and biogas yield.	14
Table 3.1 Comparison between different reforming processes.....	27
Table 3.2 Melting and Tammann temperatures of CaO, CaCO ₃ , and the dopants.....	33
Table 3.3 Relative weight change after carbonation	34
Table 3.4 Summary of sorbents for CO ₂ sorption at high temperature.....	38
Table 3.5 BET surface area, CO ₂ capture capacity, and molecular formula of synthesized Mg ₃ Al ₁ -CO ₃ , Mg ₃ Al ₁ -NO ₃ , Mg ₃ Al ₁ -SO ₄ , Mg ₃ Al ₁ -Cl and Mg ₃ Al ₁ -HCO ₃	44
Table 3.6 Ni content on support, their properties and activity in sorption enhanced methane steam reforming reaction.....	49
Table 3.7 Summaries catalysts and sorbents for hydrogen production via sorption enhanced methane steam reforming (SEMSR).....	50
Table 5.1 Sources of CO ₂	71
Table 6.1 BET surface areas and crystallite sizes of different catalytic sorbents.	85

Table 6.2 XPS analysis results of the multifunctional catalysts.....	92
Table 6.3 XPS analysis results of Ni-Al-CaO-HW catalyst.....	97
Table 6.4 Atomic concentrations at the surface of modified sorbents.....	101
Table 6.5 XPS analysis of Ni-Al-CaO-HW and Ni-Al-CaO-UHW before and after reaction.....	103
Table 7.1 Properties of modified sorbents.....	109
Table 7.2 Oxygen storage capacities of Zr ⁴⁺ , Ce ⁴⁺ and La ³⁺ modified CaO.....	110
Table 7.3 Atomic concentration at the surface of the multifunctional catalysts before and after reaction.....	121



CHAPTER I

INTRODUCTION

1.1 Rationale

Historically the world energy demand has been increasing due to an increasing human population and industrialization, in particular for countries such as Brazil, China and India [1]. The most abundant energy sources are fossil fuels such as petroleum, natural gas and coal which shown in Figure 1.1, the combustion of which results in the emission of carbon dioxide amongst other emissions, contributing to a decrease in local air quality and the global warming effect. These problems can be alleviated or mitigated by the use of fossil fuels along with renewable energy sources [2] or by capturing and sequestering the CO₂.

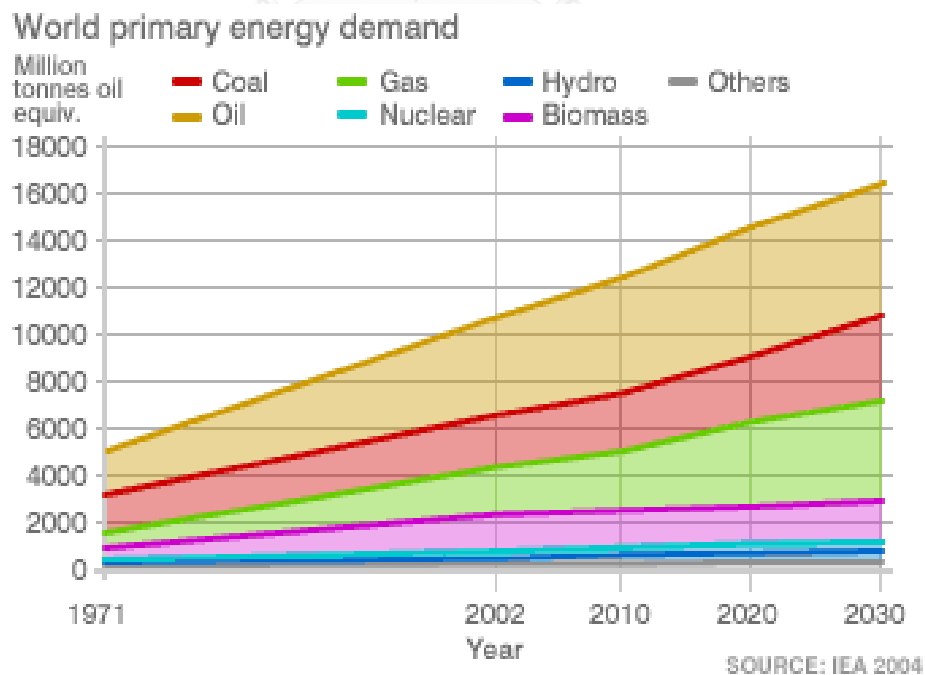
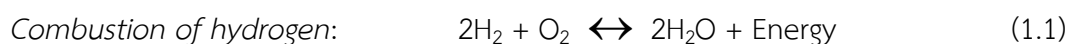


Figure 1.1 World primary energy demand [3]

Renewable energy sources include but are not limited to solar, hydro, tidal, wind, biomass and bio-fuels. None of these energy sources solve all of the mentioned issues. Solar, hydro and wind energy although having no CO₂ emissions are limited in their applications due to their reliability, their ability to provide power at demand, coupled with the ongoing challenge to develop technology that can efficiently store electrical energy on large scales. Furthermore solar, hydro and wind energy are associated with large construction, large maintenance costs and limited suitable locations. Unlike electricity generated from these three energy sources, biomass can be easily stored and although having no net CO₂ emissions, does have a negative impact upon local air quality.

Although not an energy source, hydrogen can be used as an energy carrier, having been produced via electrolysis from renewable energy sources or from fossil fuels or biomass. Production of hydrogen from fossil fuels and biomass also releases CO₂, but if produced centrally there is the opportunity to capture and store the CO₂. The produced hydrogen can be used as a fuel in which case the only combustion product is water (Eq. 1.1). The specific energy density of H₂ is approximately 142 MJ/kg, a value which is four times higher than that of coal and three times higher than that of methane. This makes it particularly interesting for transportation applications, where the mass needs to be minimized for improved efficiency.



Hydrogen gas can be produced by various processes, i.e. electrolysis [4-8] which is a process to separate water into hydrogen and oxygen (Eq. 1.2). Electrolysis reactors operate under high pressure conditions (100-700 atm), meaning a significant amount of unrecoverable energy is used during the electrolysis process, thus making this a relatively inefficient option to store electrical energy produced from renewable sources [9].

Solar biological processes use the cyanobacteria and the sunlight to produce O_2 , with H_2 gas as a side product, but is currently limited by poor H_2 yields [10]. Photocatalysis [11-16] is a process that uses ultraviolet or visible light and a photocatalyst to produce hydrogen. Photocatalysts such as TiO_2 [17] and B modified for ultraviolet light, and Cr, Fe, V and Pt over TiO_2 for visible light [11, 17-19] require a large production plants due to the small H_2 production rates, for example Fe-doped TiO_2 and Cr-doped TiO_2 have H_2 production rates of 15.5 $\mu\text{mole/h}$ and 5.3 $\mu\text{mole/h}$, respectively [11]. However, the most widely known process is the steam reforming process which can produce hydrogen from various hydrocarbons such as oxygenated hydrocarbons i.e. methanol steam reforming (Eq. 1.3) [20-23] and ethanol steam reforming (Eq. 1.4) [24-26], or hydrocarbons i.e. methane steam reforming (Eq. 1.5) [27-29] and dry methane reforming (Eq. 1.6) [30, 31]. The most conventional process for hydrogen production is methane steam reforming combined with the water gas shift reaction (Eq. 1.7) and a CO_2 capture unit, as shown in Figure 1.2.

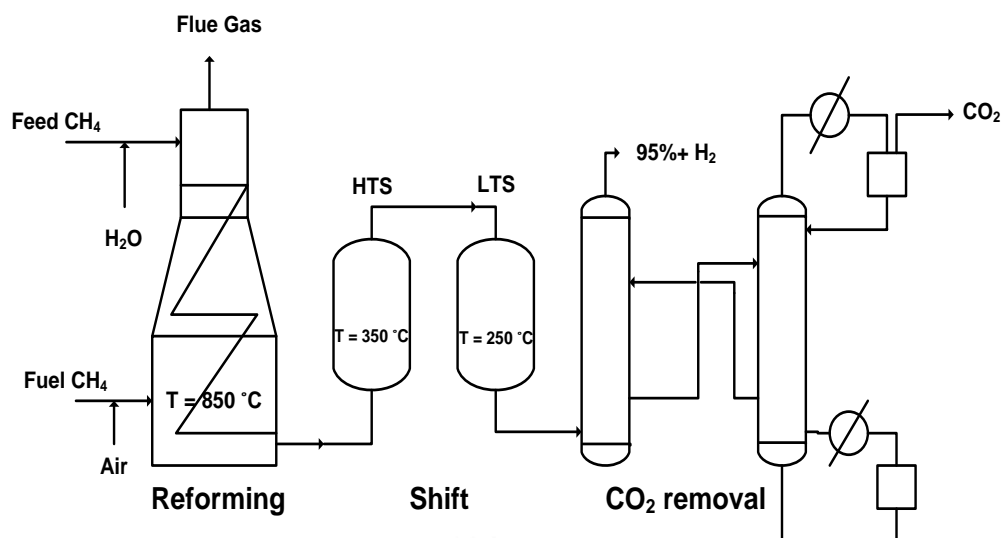
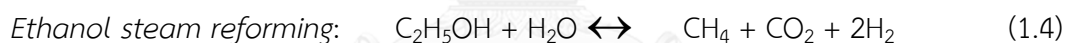
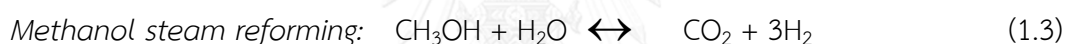
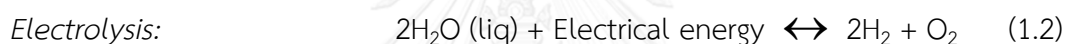


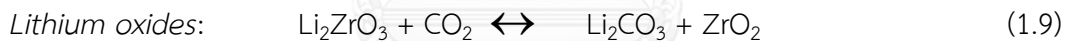
Figure 1.2 Flowsheet for a conventional methane steam reforming process [32]



Recently, several researchers have been investigating ways of increasing hydrogen production rates and purity by the addition of a sorbent into the reactor for the sorption of CO_2 , referred to as “sorption enhanced methane steam reforming”. Sorption enhanced methane steam reforming (SEMSR) is a process that combines the reactor and separator into one unit operation. This concept utilises Le Chatelier’s principle to increase the production yield and purity of hydrogen gas, driven by the

selective removal of CO₂ from the gas phase reaction zone (shift forward reaction). The advantages of the sorption enhanced methane steam reforming process are; (i) it is a process that combines the reaction unit and separation unit into one unit operation reducing the overall size of the process; (ii) it enhances the forward reaction rate for increased methane conversion and purity of hydrogen [33]; (iii) it reduces the operating cost by decreasing the operating temperature and capital cost due to decreased cost of reactor wall materials [34].

Various sorbents for high temperature CO₂ sorption were investigated including calcium oxide (Eq. 1.8) [35-37], hydrotalcite [38-42] and alkali metal sorbents such as lithium oxide and lithium orthosilicate (Eqs. 1.9-1.10) [36, 43-50].



Calcium oxide has the highest CO₂ adsorption capacity (0.495 g_{CO₂} / g_{sorbent}) when compared with Li₂ZrO₃ (0.271 g_{CO₂} / g_{sorbent}), Li₄SiO₄ (0.229 g_{CO₂} / g_{sorbent}), K-Li₂ZrO₃ (0.207 g_{CO₂} / g_{sorbent}) and Na₂ZrO₃ (0.163 g_{CO₂} / g_{sorbent}) at a temperature of 575 °C [36]. However, its stability is poor therefore researchers have been focused on improving the stability of CaO. Several researches have been investigated various metals doped to CaO for inhibiting the reduction of CO₂ sorption capacity when it was

used for multiple cycle operations. For example, Lu *et al.*, (2009) [51] studied refractory dopants (Si, Ti, Cr, Co, Zr and Ce) that aim to develop sorbents for more sorption stability. Table 1.1 shows the Tammann temperature of metal oxides, the temperature at which sintering begins to take place. However, the results indicated that when zirconia was added to calcia, the ZrO_2 has reacted with CaO to form $CaZrO_3$ as observed by XRD analysis. They proposed that the formation of calcium zirconate restrained the growth of CaO grains, inhibiting the sintering-agglomeration phenomenon.

Table 1.1 Melting and Tammann temperatures of CaO, $CaCO_3$, and the dopants [51]

Compound	Melting temperature (°C)	Tammann temperature (°C)
CaO	2898	1313
$CaCO_3$	1339	533
SiO_2	1722	725
CoO	1830	779
TiO_2	1843	785
Cr_2O_3	2329	1028
CeO_2	2400	1064
ZrO_2	2709	1218

Apart from CaO, ZrO_2 possesses the highest Tammann temperature, which correlates to the performance of FSP-made Zr/Ca sorbents.

Zhou *et al.*, (2012) [52] studied the synthesis of CaO incorporated with alumina/aluminate and its CO₂ capture performance. The sorbents were synthesized using the wet mixing method. The mechanism of calcium aluminate formation was proposed as shown in Figure 1.3. Steps 1-2, the calcium and alumina precursors are dehydrated and decarbonised forming CaO and Al₂O₃. Steps 3-4, the solid-solid state reaction does not go to completion as it is controlled by diffusion of Ca²⁺ through the reaction interface and relies upon the properties of the powder such as the composition, particle size, distribution and interface contact. Results of the CO₂ sorption tests using CaO-Ca₉Al₆O₁₈ sorbent (CaO content of 80 wt.% prepared from calcium citrate and aluminum nitrate) showed this to perform best in terms of CO₂ capacity and its stability, with the CO₂ capacity decreasing from 0.59 to 0.51 g_{CO2}/g_{sorbent} after 28 cycles.

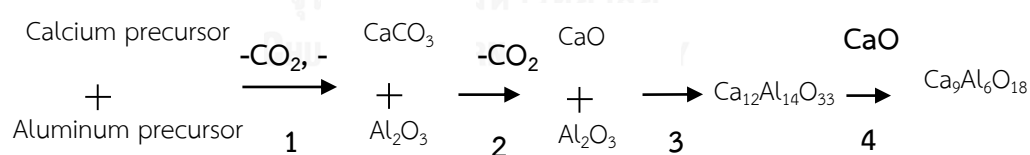


Figure 1.3 Proposed mechanism for the formation of the inert support materials [52]

Having improved the stability of the CaO with the addition of CaO-Ca₁₂Al₁₄O₃₃ (85:15), it was mixed with a commercial catalyst and its performance was tested in a sorption enhanced steam methane reforming reaction [35]. The results showed that more than 93% CH₄ conversion was obtained whilst operating at a temperature of 650

°C, pressure of 1 bar and steam to methane ratio of 3.4. Moreover, a hydrogen purity greater than 92% was achieved in this SESMR reaction compared to the 77% hydrogen purity achieved using the CaO alone. Multi-cycle testing showed a moderate decrease in the CaO-Ca₁₂Al₁₄O₃₃ sorption capacity over a period of 15 cycles. However, steam reforming studies have been carried out using other feedstocks such as propane [53], methanol [54-59], ethanol [60-68], glycerol [69], n-butanol [70] biomass [71-75] and biogas [76-78].

Biogas is produced by the anaerobic digestion of residual biomass such as animal waste, industrial waste water, landfills and agriculture waste [79]. Typically, the gas compositions of biogas are 55-70% CH₄, 27-44% CO₂, <1% H₂ and <3% H₂S as well as traces of NH₃ [80]. However, biogas is not widely used as a fuel, partly because it has a high CO₂ content which decreases the heating value and flame stability of the gas mixture [81]. Therefore to extract the latent energy from biogas, the decomposition of biogas to hydrogen by sorption enhanced steam reforming is a good alternative for investigation.

However, the work on the steam reforming of biogas containing a high content of CO₂ in the feed has not been well investigated. Therefore, this study will focus on the hydrogen production via sorption enhanced steam reforming of biogas. The optimum operating conditions such as type of sorbents, effect of sorption temperature, effect of synthesis method and so on is to be studied and the selection of sorbent that

can handle the sorption of CO₂ at the pervading operating temperatures are also investigated.

1.2 Objectives

To improve the stability of CaO for CO₂ sorption/desorption multiple cycles at high temperature and prepare multifunctional material (catalyst and sorbent) for hydrogen production via sorption enhanced steam reforming of biogas process.

1.3 Scope of research

- 1) The improvement in the stability of calcium oxide for using in CO₂ capture and hydrogen production via sorption enhanced steam reforming of biogas process.
- 2) The catalyst and sorbent are synthesized by three methods; dry powder mixing; wet mixing; hydration of CaO followed by wet mixing.
- 3) The catalyst and sorbent are characterized to determine their physical properties. The techniques include X-ray diffraction (XRD), N₂ adsorption desorption (BET surface area), scanning electron microscope (SEM), temperature programmed reduction (TPR) and X-ray photoelectron spectroscopy (XPS).
- 4) The CO₂ sorption testing are carried out at various temperatures within the range 500-700 °C and pressure of 1 atm. Specifically they were tested in terms

of sorption capacity and stability of the sorbent (sorption/desorption testing for 10 cycles).

- 5) The multifunctional catalysts are tested for hydrogen production via sorption enhanced steam reforming of biogas at a temperature of 600 C, pressure of 1 atm, steam to methane ratio of 3, methane to carbon dioxide ratio of 3:2 balanced nitrogen with total flow rate of 50 mL/min.

1.4 Organization of thesis

This dissertation is organized as the list below:

Chapter II shows the theories of methods for producing the biogas, hydrogen production reaction and mechanisms which included chemical reaction and surface reaction mechanism, and fixed bed adsorption.

Chapter III exhibits the literature reviews in topic of hydrogen production via reforming process, CO₂ sorption by CaO sorbent and sorption enhanced steam reforming of methane process.

Chapter IV indicates the materials and methods for using in sorbent and catalyst preparation section. The characterizations of modified sorbents and multifunctional catalysts have been performed including (i) X-ray diffraction technique, N₂ adsorption/desorption isotherm, scanning electron microscope, temperature

programmed reduction and X-ray photoelectron spectroscopy. Finally, CO₂ sorption and H₂ production testing have been presented.

Chapter V shows the investigations of the effect of various factors pertinent to these applications, namely the effect of supports, the effect of sorption temperatures and the effect of CO₂ concentration. Furthermore, the synthesis methods - physical mixing (dry powder mixing); wet mixing; CaO hydration followed by wet mixing - have been investigated, comparing samples produced using compounds of Mg²⁺, Sr²⁺ and Al³⁺ with CaO.

Chapter VI is composed of two parts: (i) studies on CO₂ sorption stability and (ii) hydrogen production performance using a multifunctional catalyst (nickel catalyst over calcium aluminate sorbent). Performances of modified sorbents produced by adding compounds of Ni²⁺ or Al³⁺ into CaO have been investigated in terms of CO₂ sorption capacity. The hydrogen production and stability of the multifunctional catalyst over 5 reaction cycles are tested using the sorption enhanced steam reforming of biogas reaction.

Chapter VII shows various metal ions (Zr⁴⁺, Ce⁴⁺ and La³⁺) doped on CaO, of which the corresponding metal oxides have Tammann temperatures greater than the calcination temperature (900 °C), by hydration followed by wet mixing and tested over multiple operation cycles. Hydrogen production was conducted with three modified sorbents (Ni-Zr-CaO-HW, Ni-Ce-CaO-HW and Ni-La-CaO-HW).

Chapter VIII is composed of two sections which are conclusions and recommendations. The conclusion has been separated into two parts included (i) CO₂ sorption/desorption part and (ii) H₂ production part.



CHAPTER II

THEORY

2.1 Biogas

Biogas or landfill gas can be produced by the anaerobic digestion (AD) of residual biomass such as animal waste, industrial waste water, and agricultural landfill waste [79] as shown in Table 2.1, which presents data for different types of feedstock, their yield and the biogas methane content. Typically, the gas compositions of biogas consist of 55-70% CH₄, 27-44% CO₂, <1% H₂ and <3% H₂S as well as traces of NH₃ [80]. This process not only produces CH₄ but also produces CO₂ as a by-product; however, this CO₂ is consumed in a closed cycle via photosynthesis [82] as shown in Figure 2.1. The AD process is composed of four steps namely; hydrolysis, acidogenesis, acetogenesis and methanogenesis as summarized in Figure 2.2 [82].

Biogas is commonly produced by one of several processes which include the fixed dome floating drum and channel balloon processes. They are easy to build, comfortable, durable and low maintenance. Figures 2.3 and 2.4 show fixed dome type biogas plant and floating gas-holder type biogas plant, respectively. For example, biogas reactors used in Ukraine and other ex USSR countries, use a single stage process as shown in Figure 2.5. However, in Poland a two-stage process is used which is composed of (i) an acidogenesis tank and (ii) a methanogenesis tank as shown in Figure 2.6 and 2.7 [83].

Table 2.1 Anaerobic digestion feedstock and biogas yield. [82]

Substrates	Biogas yield (m ³ /tFFa)	Methane percent
Liquid pig manure	28	65
Liquid cattle manure	25	60
Distillers grains with soluble	40	61
Pig manure	60	60
Cattle manure	45	60
Chicken manure	80	60
Organic waste	100	61
Beet	88	53
Sweet sorghum	108	54
Grass silage	172	54
Corn silage	202	52
Forage beet	111	51

a tFF is tons fresh feed

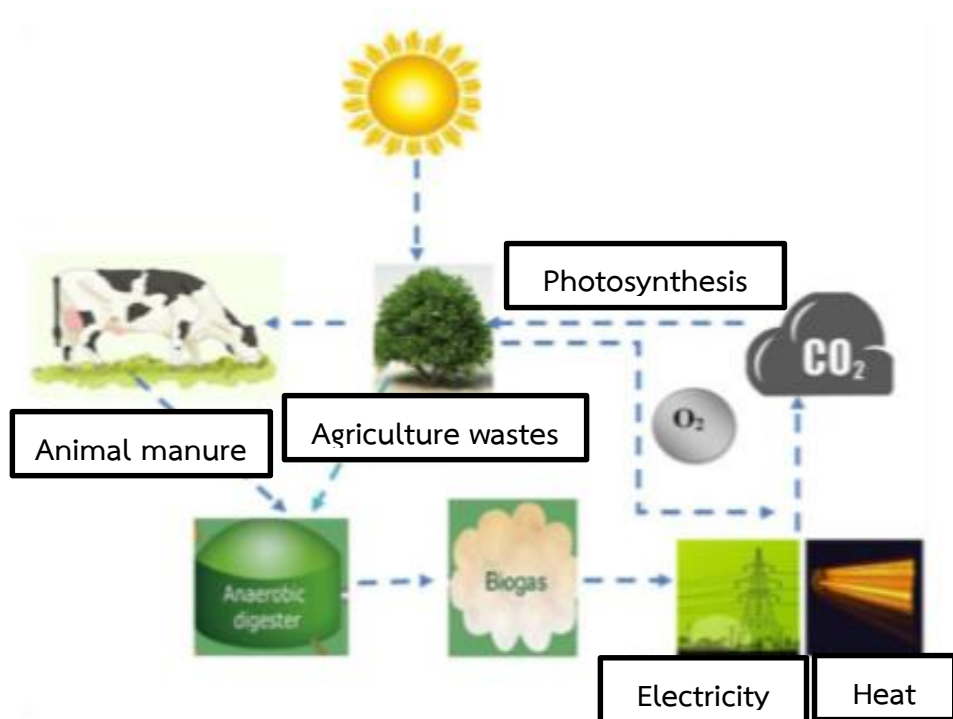


Figure 2.1 The CO₂ close cycle in anaerobic digestion (AD) [82]

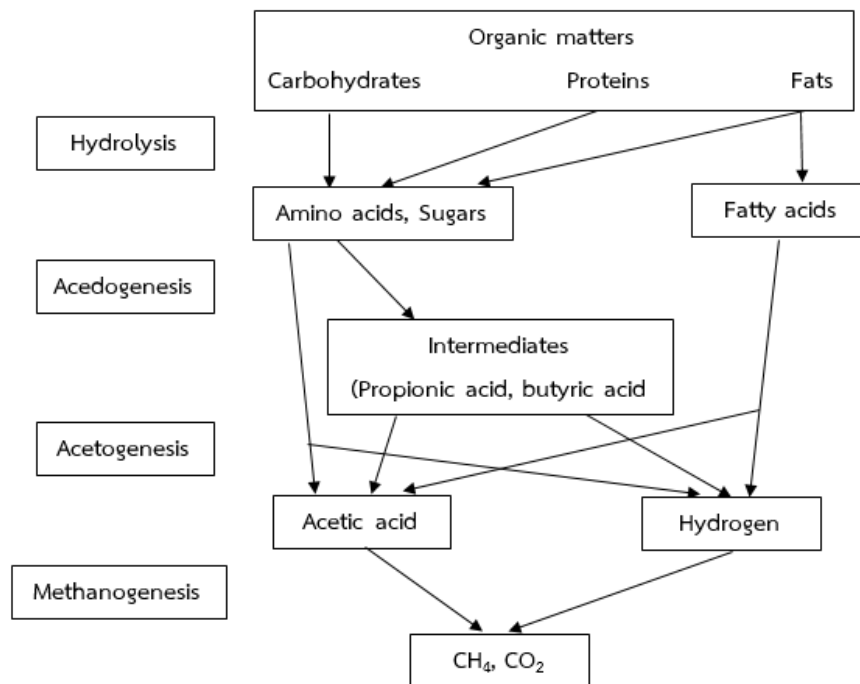


Figure 2.2 The anaerobic digestion stages [82]

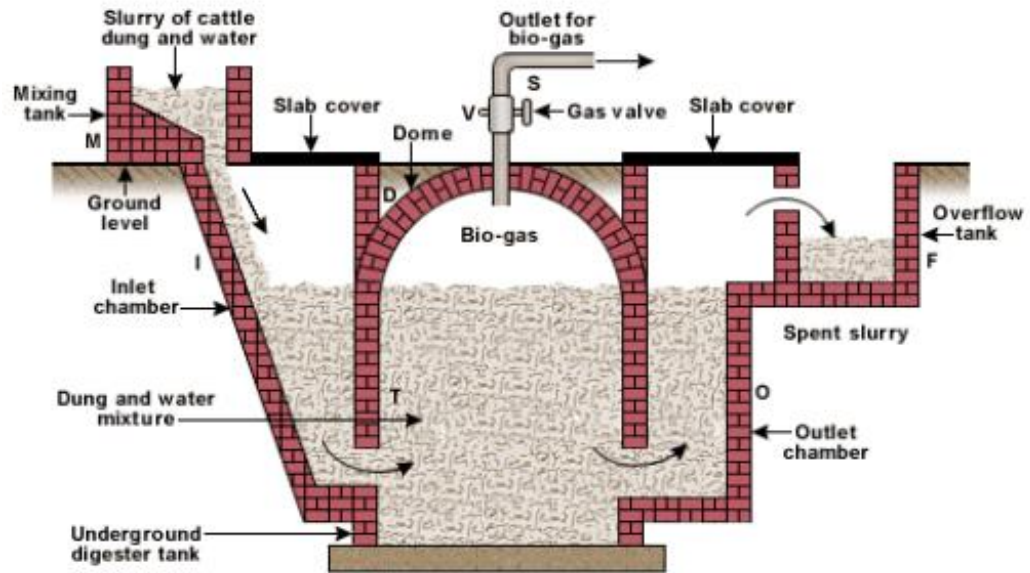


Figure 2.3 Fixed-dome type bio-gas plant [84]

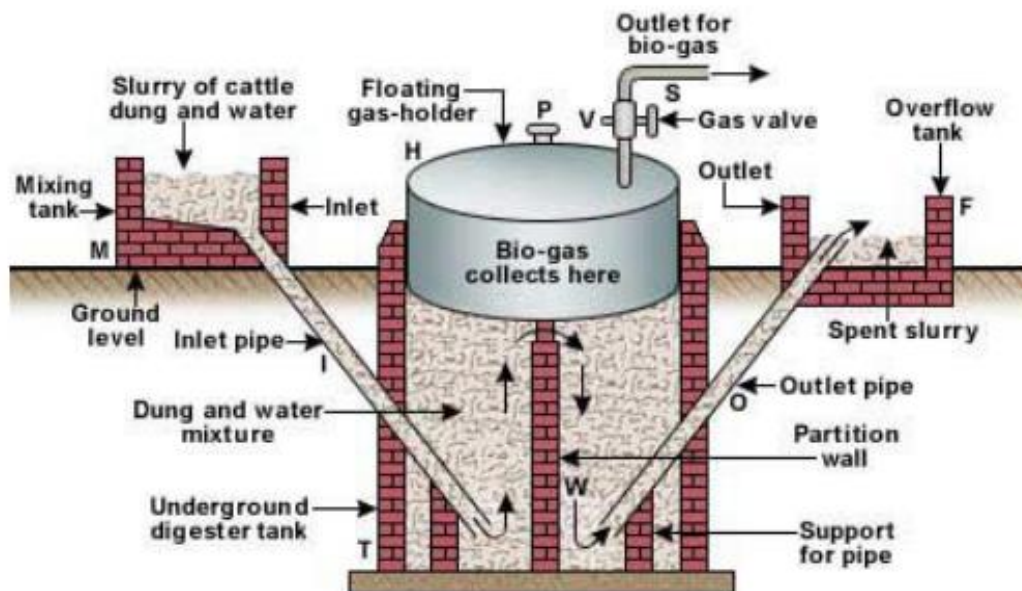


Figure 2.4 Floating gas-holder type bio-gas plant [84]

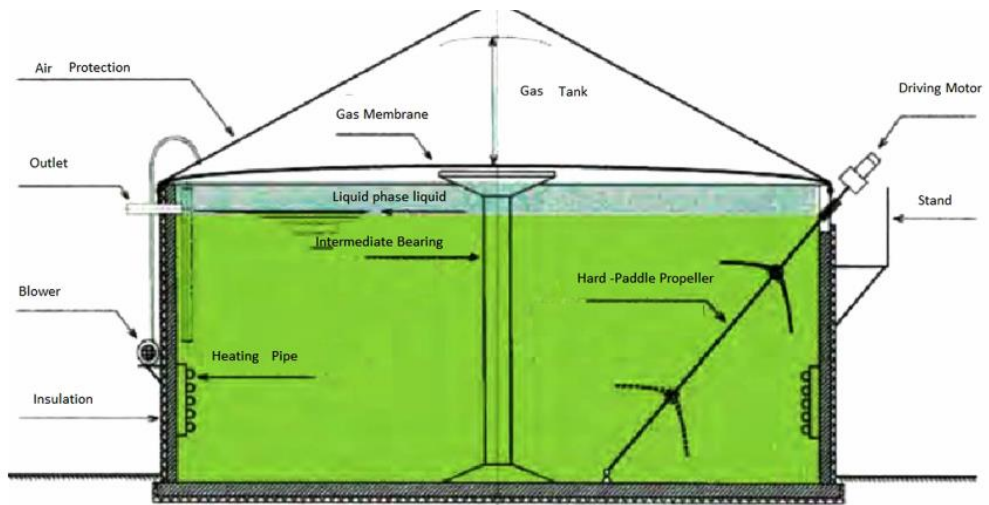


Figure 2.5 Scheme of digester [83]



Figure 2.6 Two-stage process [83]

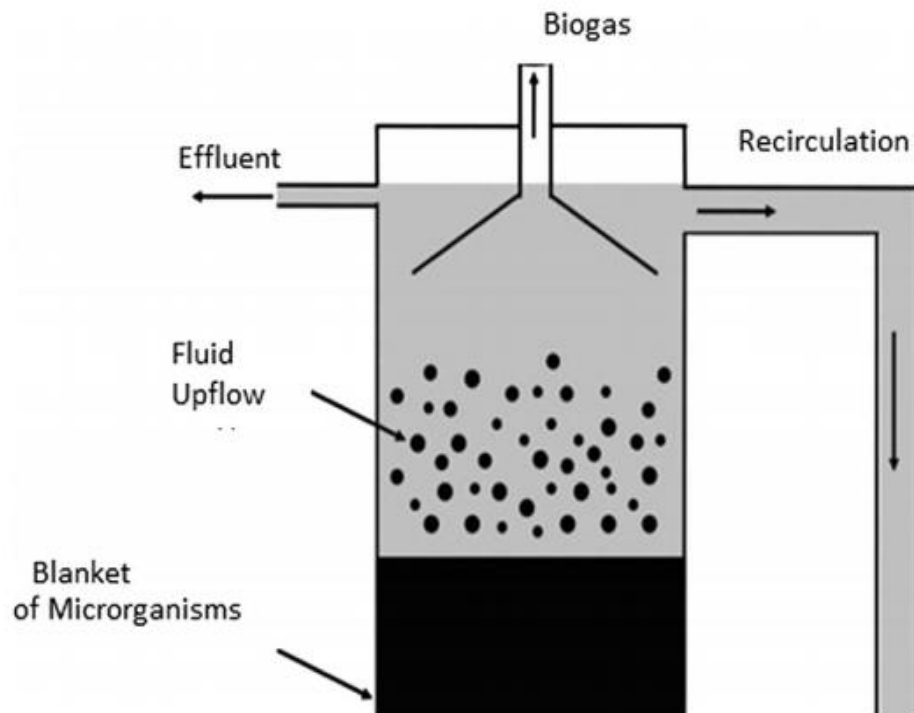


Figure 2.7 Scheme of UASB tank [83]

The biogas cannot be used directly from the reactor(s) due to its high CO_2 content which decreases the heating value and flame stability of the gas mixture [81]. To extract the latent energy from the biogas, the decomposition of biogas to hydrogen by sorption enhanced steam reforming is a good alternative for investigation.

2.2 Hydrogen production reaction and mechanisms

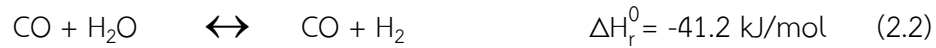
2.2.1 Chemical reaction [85]

The chemical reactions for the steam reformation of methane, carbon formation, methane cracking and gasification of carbon by steam or oxygen are shown in Eqs. 2.1-2.7:

Endothermic methane steam reforming



Exothermic water gas shift



Overall reaction



Carbon formation by Boudouard reaction



Methane cracking



Gasification of carbon by steam or oxygen

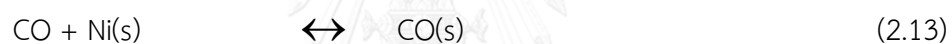
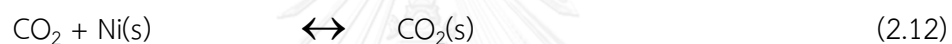
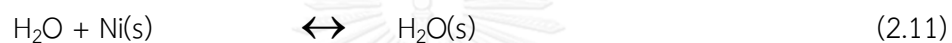
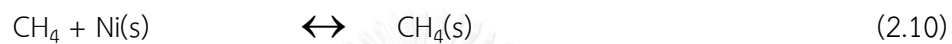
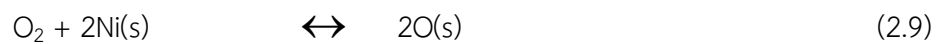
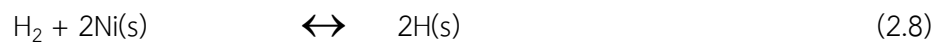


2.2.2 Surface reaction mechanism [85]

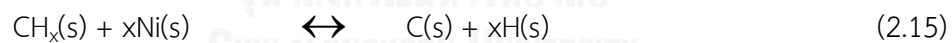
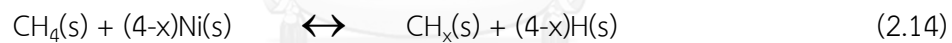
Proposed details of the surface reaction mechanism were developed by *Maier et al.* to model the reformation of methane on nickel, including all of the global reactions given above in Eqs. 2.8-2.23. The reaction mechanism consists of 16 reactions and 6 gas phase species. It suggests that the adsorbed carbon species $\text{CH}_x(\text{s})$ ($x = 0, 1, 2, 3$ - formed from activated methane - reacts with adsorbed atomic oxygen $\text{O}(\text{s})$ -

formed from the adsorption of oxygen or from the decomposition of water and CO_2 - to produce carbon oxide. The total reforming process on Ni catalyst is described as follows:

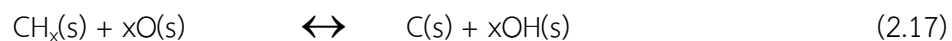
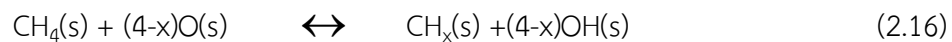
Adsorption-desorption of reactants and products



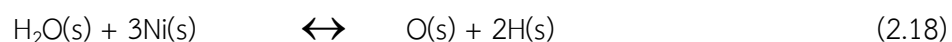
Activation of methane without oxygen



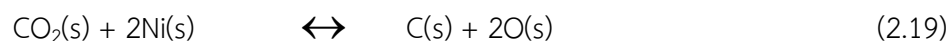
Activation of methane with oxygen



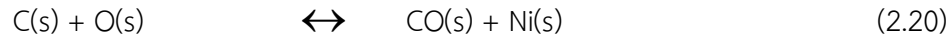
Decomposition of water



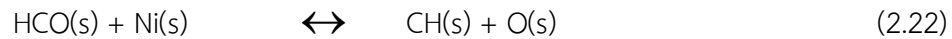
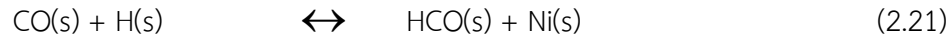
Decomposition of carbon dioxide



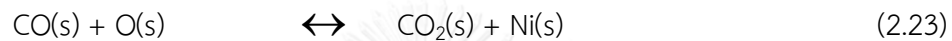
Reaction of adsorbed species and production of CO



Reaction of adsorbed species and production of H₂



Reaction of adsorbed species and production of CO₂



2.3 Fixed bed adsorption [86-88]

In a fixed bed reactor the surface concentration of adsorbed fluid phases changes with time and position in the bed. The adsorption front is initially at the inlet for the adsorbate fluid and propagates along the bed until equilibrium between the adsorption and desorption takes occurs. This movement of the stoichiometric front is depicted in Figure 2.8, where the concentration of solute moves as a sharp concentration front through the bed. This is *ideal fixed bed adsorption*. Upstream of the front, the adsorbents are saturated with adsorbate and the concentration of solute in the fluid phase feed is called c_F . The loading of adsorbate on the adsorbent is denoted as q_F and is an equilibrium quantity at bulk fluid concentration c_F . The length and weight of the bed are LES and WES, respectively, where ES is an initialization of equilibrium section. Downstream of the stoichiometric front at the outlet, the

concentration of the solute in the stream is zero. The length and weight of this bed section are LUB and WUB, respectively, where UB is unused bed.

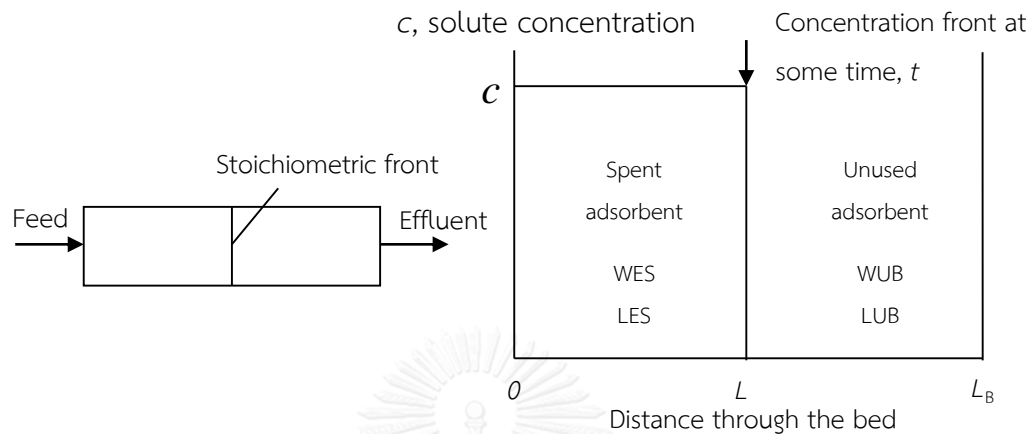


Figure 2.8 Stoichiometric (equilibrium) concentration front for ideal fixed bed adsorption [86]

After a period of time, the concentration of the solute at the outlet rises to the inlet values, c_F , and no further adsorption is possible - the adsorption step is terminated. This point is referred to as the *breakthrough point* (normally, c/c_F equal to 0.05 or 0.10) and the stoichiometric wave front becomes the ideal *breakthrough curve*. For ideal fixed bed adsorption, the material balance on the adsorbate before breakthrough occurs is: amount in the inlet = amount adsorbed:

$$Q_F c_F t_{ideal} = q_F S L_{ideal} / L_B \quad (2.24)$$

Where Q_F is the inlet volumetric flow rate, c_F is the inlet concentration of the solute, t_{ideal} is the time for an ideal front to reach the outlet, q_F is the loading per unit mass of in equilibrium with the feed concentration, S is the total mass of adsorbent in the bed, and L_B is the total bed length.

In a real fixed bed adsorber, the assumptions of leading to equation are not valid. Typically, solute concentration profiles for the adsorbate fluid are shown as a function of distance along the bed with increasing time (t_1 , t_2 , and t_b) from the start of flow through the bed as shown in Figure 2.9 (a). At t_1 no part of the bed is saturated. At t_2 , the bed is almost saturated for a distance L_s . Beyond L_f little mass transfer occurs at t_2 and the adsorbent is still unused. The region between L_s and L_f is called the mass transfer zone, MTZ, and at t_2 L_f is defined as the zone where $c/c_F = 0.05$, whilst L_s is defined as the zone where $c/c_F = 0.95$. During the period from t_2 to time t_b , the S shape concentration profile moves through the bed. At t_b , the leading point of MTZ reaches the end of the bed. This is the breakthrough point. Rather than using $c/c_F = 0.05$, the breakthrough concentration can be taken as the minimum detectable or maximum allowable solute concentration in the effluent fluid.

A typical plot of the ratio of the outlet to inlet solute concentration in the fluid as a function of time is shown in Figure 2.9 (b). The S-shaped curve is called breakthrough curve. Prior to t_b , the solute concentration is less than $c_{out}/c_F = 0.05$. At t_b flow is normally discontinued and regeneration of the adsorbent is begun. At $t > t_b$, the outlet solute concentration increases rapidly. The time to reach $c_{out}/c_F = 0.95$ is designated t_e

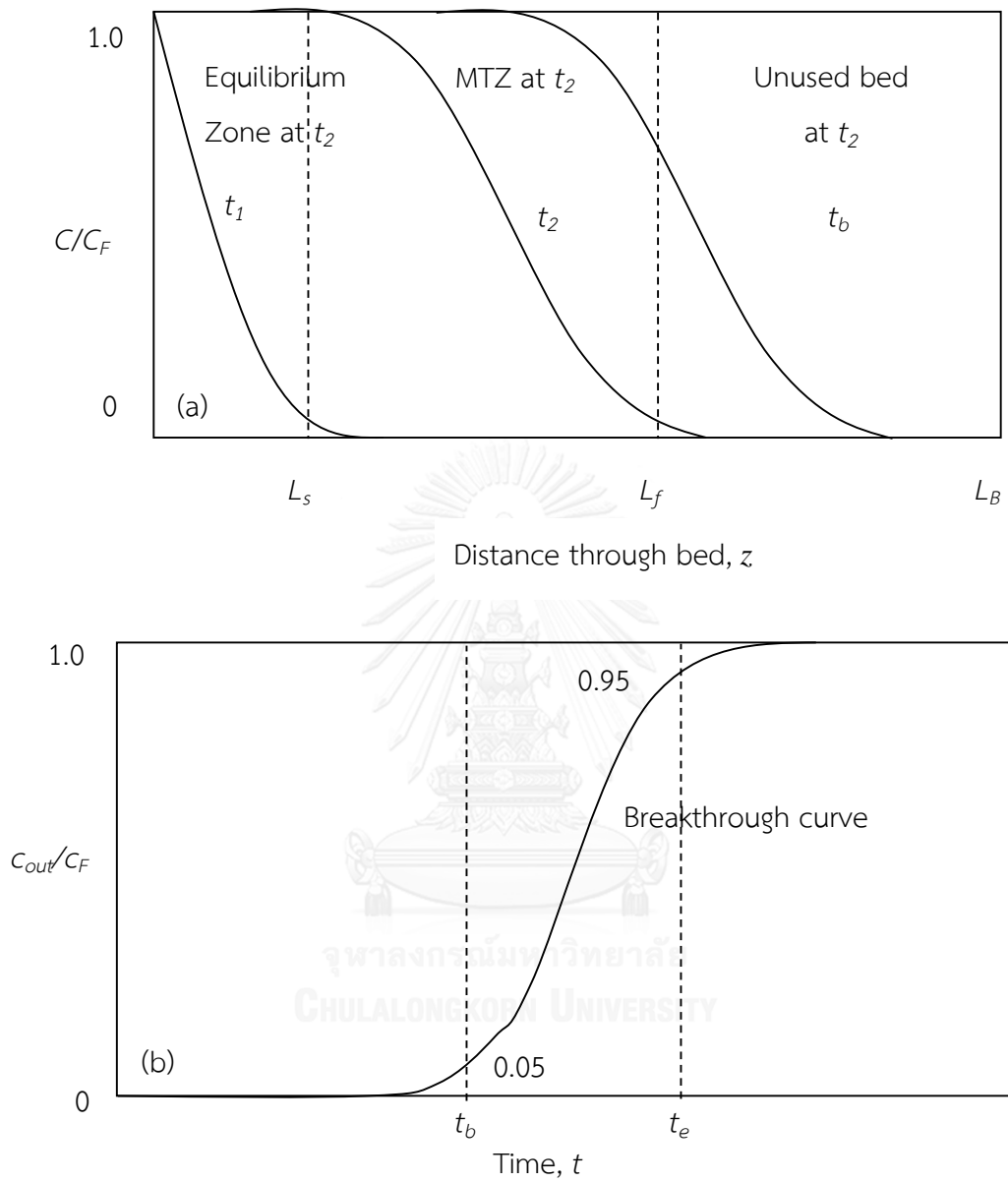


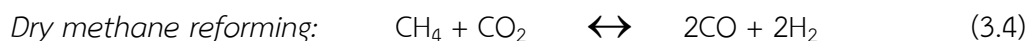
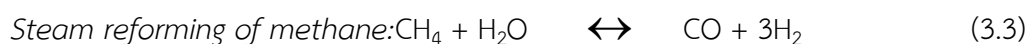
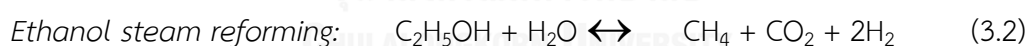
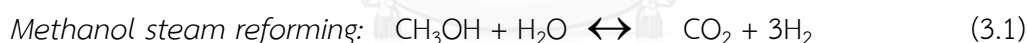
Figure 2.9 Solute wave fronts in a fixed bed adsorber with mass transfer effects:
 (a) Concentration-distance profiles. (b) Breakthrough curve [88]

CHAPTER III

LITERATURE REVIEWS

3.1 Hydrogen production via reforming process

Hydrogen gas is produced by several reaction processes such as steam reforming, partial oxidation and autothermal reforming. A comparison of the various hydrogen production processes is provided in Table 3.1. The most common process is the steam reforming process which can use various reactants such as oxygenated hydrocarbons such as methanol (Eq. 3.1) [20-23] and ethanol (Eq. 3.2) [24-26], or hydrocarbons such as the steam reformation of methane (Eq. 3.3) [27-29] or dry methane reforming (Eq. 3.4) [30, 31].



Steam methane reforming (SMR) is a process that uses steam to reform methane producing carbon monoxide and hydrogen. Combined with the water gas shift reaction (Eq. 3.5) higher hydrogen production yields and concentrations can be

achieved. However, SMR production process is a highly endothermic highly energy intensive process. Several researchers have investigated various supports such as MgO, Al₂O₃, ZrO₂ and CeO₂ for improved stability and activity.

Roh *et al.*, (2007) [89] investigated Mg/Ni/Al catalysts for hydrogen production, observing CH₄ conversion greater than 90% at the feed (H₂O + CO₂)/CH₄ ratio of 1.2 and space velocity of 265,000 cm³ gas fed/g_{cat}-h. The addition of Mg led to an improvement in stability, where without Mg addition large amounts of coke formation were observed and a drop in CH₄ conversion from 75% to 30% over 5 h. Figure 3.1 shows the change in CH₄ conversion due to the steam reforming reaction in the presence of Ni/Al catalysts with and without Mg, as well as Ni with Mg, Ce, and Zr for comparison.

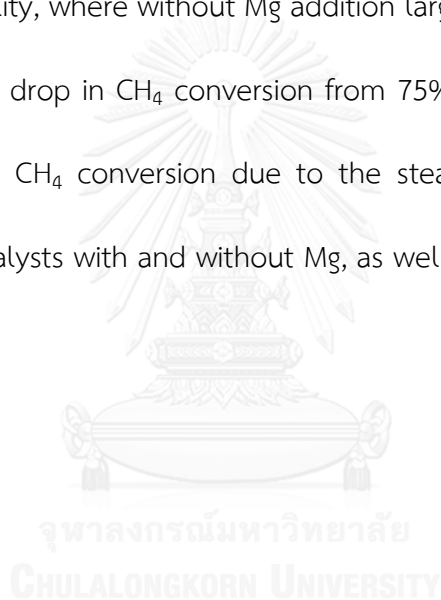


Table 3.1 Comparison between different reforming processes [90]

Technology	Advantages	Disadvantages
SMR	<ul style="list-style-type: none"> ● O₂ not required ● Lowest temp. ● Best H₂/CO ratio ● High efficiency ● Cost for large unit ● Mostly used process 	<ul style="list-style-type: none"> ● Highest CO₂ emission ● System is complex ● System is sensitive to natural gas qualities
POx	<ul style="list-style-type: none"> ● No catalyst required ● Low methane slip ● Simple process ● Cost for small unit ● Requires less desulphurization 	<ul style="list-style-type: none"> ● Low H₂/CO ratio ● Very high temperature ● Soot formation/handling adds complexity ● Pure O₂ requires
ATR	<ul style="list-style-type: none"> ● Lower operating temperature than PO_x ● Low methane slip ● Requires less O₂ than Pox 	<ul style="list-style-type: none"> ● Limited commercial experience ● Requires air or O₂

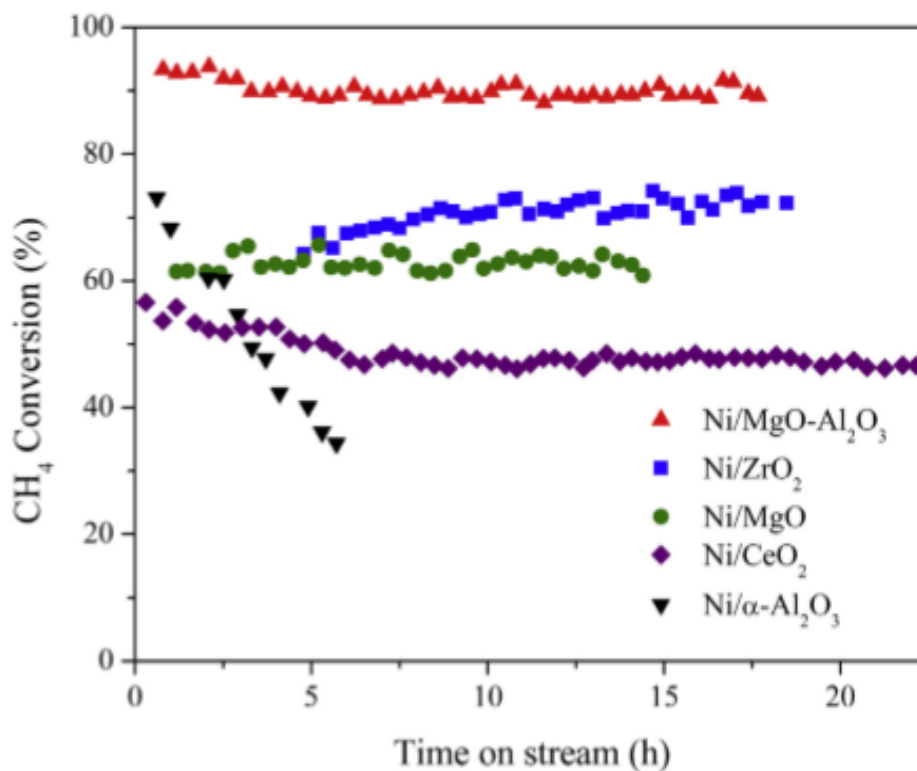


Figure 3.1 Conversion of methane at 800 °C in the presence of nickel catalyst on various substrates including Mg doped alumina. Stability is seen as a loss of conversion rate over time [89, 91].

Dong *et al.*, (2002) [92] examined Ni/Ce/Zr with various percentages of Ni and found that with 15% Ni, methane conversions of 97%, a CO selectivity of 67% and a H₂/CO ratio of 4.7 can be achieved [92]. At higher Ni concentrations, the availability of oxygen from the CeZrO support is not as high. The increase in nickel concentration vs. CH₄ conversion is shown in Figure 3.2. The stability of Ni/Ce/Zr is shown to be constant for 12 h leading to a highly stable and potentially highly active catalyst.

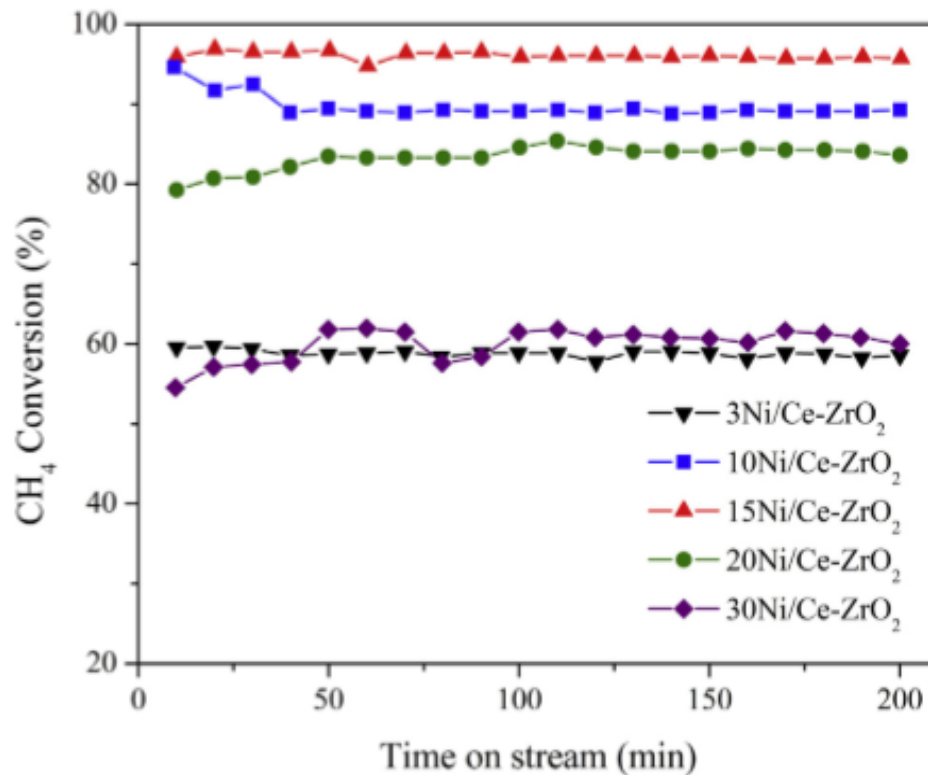


Figure 3.2 Catalytic activity of various nickel doped Ce-ZrO₂ catalysts at temperature of 750 °C [91, 92].

This process emitted CO₂ gas, with this being one of the reaction products, hence this would need to be removed in a separate unit operation in order to prevent the emission of greenhouse gases. It is preferable to separate the CO₂ from the hydrogen in the same unit operation as the hydrogen production. To remove CO₂ gas from the outlet stream in one unit operation, solid sorbent is loaded into the reactor. This process is called the sorption enhanced steam reforming process and not only has the benefit of removing the CO₂ - meaning the outlet stream is high purity H₂ - but

also CH₄ conversion equilibrium position is shifted forward. In this sense, the use of a solid sorbent in the steam reforming reaction offers significant advantages.

3.2 CO₂ sorption

CO₂ capture is an important technology for several processes and may be used to purify gases or to reduce CO₂ emissions to the atmosphere. CO₂ sorbents can be classified in terms of CO₂ sorption temperature i.e. low and high temperature. Low temperature sorbents (<200 °C) include organic sorbents, zeolite based sorbents, alkali metal carbonate based sorbents and amine based solid sorbents. High temperature sorbents (>400 °C) include calcium oxide, hydrotalcite and alkali metal oxide. This study has focused on higher temperature CO₂ sorbents as they can be used in a sorption enhanced biogas steam reforming process (next section).

3.2.1 Calcium Oxide

Calcium oxide is an effective sorbent for CO₂ sorption due to its high CO₂ sorption capacity ($0.495 \text{ g}_{\text{CO}_2} / \text{g}_{\text{sorbent}}$) when compared to other sorbents such as Li₂ZrO₃ ($0.271 \text{ g}_{\text{CO}_2} / \text{g}_{\text{sorbent}}$), Li₄SiO₄ ($0.229 \text{ g}_{\text{CO}_2} / \text{g}_{\text{sorbent}}$), K-Li₂ZrO₃ ($0.207 \text{ g}_{\text{CO}_2} / \text{g}_{\text{sorbent}}$) and Na₂ZrO₃ ($0.163 \text{ g}_{\text{CO}_2} / \text{g}_{\text{sorbent}}$) at typical operating temperatures for steam reformation, with the quoted values relating to a study carried out at 575°C [36]. However, the physical stability of CaO at these temperatures is not good and the improvement of CaO for long time sorption/desorption cycles is an important for area

of development. Lu *et al.*, (2006) [93] investigated calcium oxide based sorbents for high temperature carbon dioxide capture. Various precursors including $\text{Ca}(\text{NO}_3)_2 \cdot 4\text{H}_2\text{O}$, $\text{Ca}(\text{OH})_2$, CaCO_3 , $\text{Ca}(\text{CH}_3\text{COO})_2 \cdot \text{H}_2\text{O}$ and CaO were investigated. The sorbent prepared from calcium acetate ($\text{CaAc}_2\text{-CaO}$) resulted in the best characteristics for CO_2 sorption such as a higher BET surface area of $20.2 \text{ m}^2/\text{g}$ and a larger pore volume of $0.23 \text{ cm}^3/\text{g}$. When silicon was doped on $\text{CaAc}_2\text{-CaO}$ (0-50% wt.) the results indicated a poorer performance after four cycles, at a temperature of $700 \text{ }^\circ\text{C}$ and under 30 % CO_2 in helium. Reddy *et al.*, (2004) [94] investigated the improvement of CO_2 sorption capacity by doping alkali metals on the CaO support. A wet impregnation method was used for preparing the catalyst. Initially they compared three sorbents including MgO , BaO and CaO . CaO exhibited the greatest sorption capacity after a period of 70 min. They also tested the performance at various temperatures with the results indicating $700 \text{ }^\circ\text{C}$ to the optimum temperature with the highest wt.% increase of 12.5% after 70 min. Finally they investigated the various alkali metal chlorides including Li , Na , K , Rb and Cs at 20 wt.% loading and a temperature of $50 \text{ }^\circ\text{C}$. The results showed Cs/CaO to exhibit the highest wt.% increase of 1.25% when compared with the other sorbents ($\text{Li} < \text{Na} < \text{K} < \text{Rb} < \text{Cs}$). The trend follows the trend in electro-positivity of alkali metals, increasing from the top to the bottom of the periodic group. Cs/CaO sorbents were produced using various precursors including CsOH , Cs_2CO_3 and CsCl with the CsOH sample exhibiting the greatest percentage mass increase of 30% under 40% CO_2 in helium, at a temperature of $450 \text{ }^\circ\text{C}$ and a total flow rate of 50 mL/min . As well as the alkalis earth

metals dopants, various transition metals (i.e. Cr, Mn, Co, Cu and Ce) have been tested. For example, Lu *et al.*, (2009) [51] studied refractory dopants (Si, Ti, Cr, Co, Zr and Ce) that aim to develop sorbents with improved mechanical strength. They explained that the solid material begins to sinter at or higher than their Tammann temperature which is roughly about 50-75% of their bulk melting temperature. The Tammann temperatures of metal oxides are shown in Table 3.2. The results indicated that when zirconia was added to calcia, the ZrO_2 reacts with CaO to form $CaZrO_3$, as observed by XRD results. They proposed that calcium zirconate restrains the growth of CaO grains, inhibiting the sintering-agglomeration phenomenon. Furthermore, they investigated various Zr/Ca ratios of 1:1, 3:10, 1:5, 1:10, 1:20 and 1:50, and results indicated that a Zr/Ca ratio of 3:10 led to the best stability (X_{CaO} 1st cycles of 64% and X_{CaO} 100th cycles of 64%) when using a feed gas of 30% CO_2 in helium and operating at a temperature of 700 °C. The CaO carbonation was calculated by the following equation:

$$X_{CaO} \% = \frac{DF_d + CF_{CaO}}{CF_{CaO} X_t} W_{CaO} \% \quad (3.6)$$

Table 3.2 Melting and Tammann temperatures of CaO, CaCO₃, and the dopants [51]

Compound	Melting temperature (°C)	Tammann temperature (°C)
CaO	2898	1313
CaCO ₃	1339	533
SiO ₂	1722	725
CoO	1830	779
TiO ₂	1843	785
Cr ₂ O ₃	2329	1028
CeO ₂	2400	1064
ZrO ₂	2709	1218

ZrO₂ possesses the highest Tammann temperature, which correlates with the observed performance of the FSP-made Zr/Ca sorbents

Lu *et al.*, (2009) [95] investigated the calcium oxide doped sorbents for CO₂ capture with and without SO₂ at high temperature. The catalysts were prepared by the co precipitation method. All of the metal precursors (Cr, Mn, Co, Cu and Ce) were nitrates. The results in Table 3.3 indicate that the best performing sorbent was the Ce/Ca sorbnet with Ce:Ca ratio of 1:10, tested at a temperature of 750 °C, over 60 min with a feed gas of 30 % CO₂ in helium.

The weight increase (%) is calculated with the following equation:

$$\text{Weight increased \%} = \frac{(W_t - W_0)}{W_0} \times 100\% \quad (3.7)$$

Table 3.3 Relative weight change after carbonation [95]

Sorbent	wt.% increase ^a (g g ⁻¹)	wt.% increase ^b (g g ⁻¹)	Capacity for CO ₂ uptake (g g ⁻¹)
Mn/Ca	47	0.3	47
Ce/Ca	44	0.1	44
Cr/Ca	40	0.8	40
Co/Ca	26	0.2	26
Cu/Ca	24	0.05	24

^a is after carbonation

^b is after carbonation and regeneration

Vielle *et al.*, (2012) [96] investigated the improvement of calcium oxide based sorbent over multiple CO₂ capture cycles. Various percentages of titanium ethoxide (0-50%) were impregnated on CaO. The 50% of titanium ethoxide resulted in the best multiple CO₂ capture (conversion rate 1st cycles of approx. 98% and conversion rate 25th cycles of approx. 50%) at a temperature of 650°C and with a feed gas of 67% CO₂ in nitrogen. Moreover, the BET surface area and pore volume increased with increasing percentages of titanium ethoxide. Other investigations have looked into the use of complex materials such as Ca₁₂Al₁₄O₃₃ and Ca₉Al₆O₁₈.

Complex materials have been investigated for improving the stability of CaO adsorbents. Zhou *et al.*, (2012) [52] studied the synthesis of CaO materials that incorporate alumina/aluminate and their performance in terms of CO₂ capture. The adsorbents were synthesized by the wet mixing method. The CO₂ sorption capacity (C_t) and maximum carbonation conversion (α_{\max}) were calculated using the following equations:

$$C_t = \frac{W_t - W_0}{W_0} \quad (3.8)$$

$$\alpha_{\max} = \frac{(W_{30} - W_0)}{W_0 x} \frac{M_{\text{CaO}}}{M_{\text{CO}_2}} \quad (3.9)$$

Where W_0 is the sorbent weight after complete calcination, W_t is the sorbent weight at time t of carbonation, W_{30} is the sorbent weight after 30 min of carbonation for each cycle, x is the weight fraction of CaO in the sorbent, and M_{CaO} and M_{CO_2} are the molar weights of CaO and CO₂, respectively. The CO₂ capture performance of a sorbent depends on C_t and α_{\max} . High values of C_t and α_{\max} mean high CO₂ capture performance. Moreover, the stability of the sorbent was measured in terms of the change in performance over multiple carbonation/calcinations cycles.

Samples referred to as CG-AN-80, CC-AN-80, CA-AN-80 and CF-AN-80 - where CG, CC, CA, CF and AN refer to the precursors calcium gluconate monohydrate ($\text{Ca}(\text{C}_6\text{H}_{11}\text{O}_7)_2 \cdot \text{H}_2\text{O}$), calcium citrate tetrahydrate ($\text{Ca}_3(\text{C}_6\text{H}_5\text{O}_7)_2 \cdot 4\text{H}_2\text{O}$), calcium acetate monohydrate ($\text{Ca}(\text{C}_2\text{H}_3\text{O}_2)_2 \cdot \text{H}_2\text{O}$), calcium formate ($\text{Ca}(\text{CHO}_2)_2$) and aluminum nitrate

nonahydrate ($\text{Al}(\text{NO}_3)_3 \cdot 9\text{H}_2\text{O}$), respectively – were shown by XRD analysis to have $\text{Ca}_9\text{Al}_6\text{O}_{18}$ and CaO present.

Samples denoted as CP-AN-80, CL-AN-80 and CL-AA-80 - where CP, CL and AA refer to calcium propionate ($\text{Ca}(\text{C}_3\text{H}_5\text{O}_2)_2$), calcium lactate pentahydrate ($\text{Ca}(\text{C}_3\text{H}_5\text{O}_3)_2 \cdot 5\text{H}_2\text{O}$) and basic aluminum acetate dehydrate ($\text{Al}(\text{OH})(\text{C}_2\text{H}_3\text{O}_2)_2 \cdot 2\text{H}_2\text{O}$), respectively – were shown by XRD analysis to have only CaO present.

It was confirmed by EDX analysis that Al was present in the sorbents. CL-AC-80 - where CL and AC refer to calcium lactate pentahydrate ($\text{Ca}(\text{C}_3\text{H}_5\text{O}_3)_2 \cdot 5\text{H}_2\text{O}$) and aluminum chloride hexahydrate ($\text{AlCl}_3 \cdot 6\text{H}_2\text{O}$), respectively – were shown by XRD analysis that CaO and the complex material $\text{Ca}_{12}\text{Al}_{14}\text{O}_{33}$ were present. A proposed mechanism for calcium aluminate formation is proposed in Figure 3.3. In stages 1-2, the calcium and alumina precursors undergo dehydration and decarbonation forming CaO and Al_2O_3 . In stages 3-4, a solid-solid state reaction takes place. This is controlled by the rate of Ca^{2+} diffusion through the reaction interface and relies on the features of powder reactant such as composition, particle size and distribution and the interface surface area. The $\text{CaO-Ca}_9\text{Al}_6\text{O}_{18}$ was shown to have the highest CO_2 sorption capacity and stability, which decreased from 0.59 to 0.51 by the 28th cycle. Mastin *et al.*, (2011) [97] investigated a new synthesis method for the production of $\text{CaO/Ca}_{12}\text{Al}_{14}\text{O}_{33}$ for high temperature CO_2 capture. The sorbents exhibited a high CO_2 sorption capacity – up to 20g CO_2 / 100g sorbent – and a total conversion of 90% after more than 140 carbonation/calcinations cycles, at a temperature of 870 °C with a feed gas of 50% H_2O

in CO₂. Table 3.4 shows the high temperature CO₂ sorption capacities and stabilities for various sorbents.

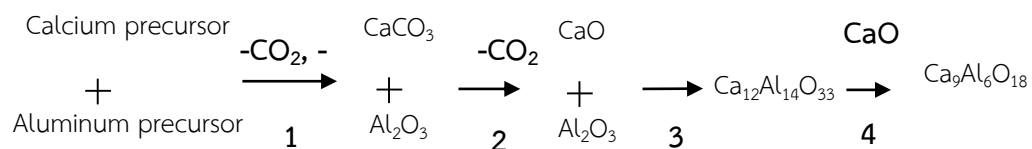


Figure 3.3 Proposed mechanism for the formation of the inert support materials. [52]



Table 3.4 Summary of sorbents for CO₂ sorption at high temperature.

Sorbent	Capacity (%)	Carbonation (%)	Temp. (°C)	Feed	Ref.
Effect of supports					
MgO	0	-	600	40%	Reddy <i>et al.</i> ,
BaO	0	-	600	CO ₂ /He	(2004)
CaO	11.5	-	600		[94]
Effect of metals					
20%Na/CaO	1	-	600		
20%Li/CaO	5	-	600		
20%K/CaO	8	-	600		
20%Rb/CaO	16	-	600		
20%Cs/CaO	49	-	600		
Effect of precursors					
CsOH	30	-	450		
Cs ₂ CO ₃	29	-	450		
CsCl	21	-	450		

Sorbent	Capacity (%)	Carbonation (%)	Temp. (°C)	Feed	Ref.
Effect of ratios					
CaO	5	-	450		
10%Cs/CaO	18	-	450		
20%Cs/CaO	31	-	450		
35%Cs/CaO	26	-	450		
Effect of precursor					
Ca(NO ₃) ₂ -CaO		2.5	600	30%	Lu <i>et al.</i> ,
CaO		25	600	CO ₂ /He	(2006)
Ca(OH) ₂ -CaO		63	600		[37]
CaCO ₃ -CaO		66	600		
CaAc ₂ -CaO		97	600		
Effect of temp.					
CaAc ₂ -CaO		9	200		
CaAc ₂ -CaO		20	300		
CaAc ₂ -CaO		50	400		
CaAc ₂ -CaO		87	500		

Sorbent	Capacity (%)	Carbonation (%)	Temp. (°C)	Feed	Ref.
CaAc ₂ -CaO		94	550		
CaAc ₂ -CaO		98	700		
CaAc ₂ -CaO		98	800		
Varies ratios					
0%SiO ₂ /CaO	78 ^a , 76 ^a		700		
10%SiO ₂ /CaO	69 ^a , 67 ^a		700		
20%SiO ₂ /CaO	59 ^a , 55 ^a		700		
30%SiO ₂ /CaO	54 ^a , 52 ^a		700		
40%SiO ₂ /CaO	46 ^a , 42 ^a		700		
50%SiO ₂ /CaO	37 ^a , 33 ^a		700		
Effect of Metal					
Mn/Ca	47	-	750	30%	Lu <i>et al.</i> ,
Ce/Ca	44	-	750	CO ₂ /He	(2009)
Cr/Ca	40	-	750		[95]
Co/Ca	26	-	750		
Cu/Ca	24	-	750		

Sorbent	Capacity (%)	Carbonation (%)	Temp. (°C)	Feed	Ref.
Effect of metal					
Co/Ca (1:10)		72.5, 15	700	30%	Lu <i>et al.</i> ,
Cr/Ca (1:10)		77.5, 20	700	CO ₂ /He	(2009)
Si/Ca (1:10)		67.5, 27.5	700		[51]
Ti/Ca (1:10)		83, 35	700		
Ce/Ca (1:10)		72.5, 35	700		
Zr/Ca (1:10)		83, 45	700		
Effect of ratios					
Zr/Ca (1:1)		14, 16	700		
Zr/Ca (3:10)		64, 64	700		
Zr/Ca (1:5)		72, 68	700		
Zr/Ca (1:10)		83, 44	700		
Zr/Ca (1:20)		88, 34	700		
Zr/Ca (1:50)		92, 32	700		

Sorbent	Capacity (%)	Carbonation (%)	Temp. (°C)	Feed	Ref.
Effect of precursors					
CA-AN-80	63, 48	-	650	15%	Zhou <i>et al.</i> ,
CC-AN-80	59, 51	-	650	CO ₂ /N ₂	(2012)
CG-AN-80	52, 42	-	650		[52]
CaO	49, 16	-	650		
CC-AN-70	55, 48	-	650		
CC-AN-90	50, 33	-	650		
Effect of ratios					
CaO	-	74, 17	650		
CaTi-0.1	-	82, 11	650		Vieille <i>et al.</i> ,
CaTi-1	-	88, 9	650	67%	(2012)
CaTi-10	-	83, 20	650	CO ₂ /N ₂	[96]
CaTi-20	-	85, 71	650		
CaTi-30	-	83, 68	650		
CaTi-40	-	95, 80	650		
CaTi-50	-	98, 79	650		

^a is weight increased (%) and ^b is cycles #5

3.2.2 Hydrotalcite

Hydrotalcite is a complex material that is a combination of magnesium and aluminium oxides. Advantages of hydrotalcite include its high stability (adsorption/desorption multiple cycles), however, the activity (CO_2 capacity) is too low and so this represents area of interest for investigation. For example, Oliveira *et al.*, (2008) [39] investigated commercial hydrotalcite at different Mg/Al ratios. Three ratios of magnesium and aluminium oxide were tested (i.e. MG30, MG50 and MG70) and compared at temperatures of 403 °C, a total pressure of 2 bar and a CO_2 partial pressure of 0.4 bar in the presence of water vapor. The results showed all of the hydrotalcites to have similar CO_2 capacities (approx. 0.8-1.2 mol/kg). They also studied the effect of two alkali metals (K and Cs) loaded on hydrotalcite (MG30, MG50 and MG70). The alkali-modified samples exhibited a maximum loading at a temperature of 403 °C with the MG30-K sample having the highest capacity (0.76 mol/kg wet basis at 0.40 bar of CO_2 partial pressure). A study on the cyclic stability of this material was performed, showing only a small loss in capacity after 75 sorption/desorption cycles. Wang *et al.*, (2010) [98] studied the effect of charge compensating anions and the pH on the hydrotalcite synthesis. A series of $\text{Mg}_3\text{Al}_1\text{-A}$ ($\text{A} = \text{CO}_3^{2-}$, HCO_3^- , NO_3^- , SO_4^{2-} and Cl^-) HTs were synthesized and tested as high temperature CO_2 adsorbents. Among various HTs, $\text{Mg}_3\text{Al}_1\text{-CO}_3$ exhibited the highest CO_2 sorption capacity of 0.53 mmol/g. Next, the influence of pH on the Mg/Al ratio, BET surface area, pore size, and CO_2 sorption capacity of $\text{Mg}_3\text{Al}_1\text{-CO}_3$ was investigated. Table 3.5 shows results obtained for

the synthesized sorbents. $Mg_3Al_1-CO_3$ synthesized at a pH of 10–12 was shown to have the highest CO_2 sorption capacity.

Table 3.5 BET surface area, CO_2 capture capacity, and molecular formula of synthesized $Mg_3Al_1-CO_3$, $Mg_3Al_1-NO_3$, $Mg_3Al_1-SO_4$, Mg_3Al_1-Cl and $Mg_3Al_1-HCO_3$ [98]

	BET, before calcinatino, (m^2/g)	BET, after calcinatino, (m^2/g)	CO_2 capture capacity ($mmol/g$)	Molecular formula
$Mg_3Al_1-CO_3$	114.3	239.0	0.53	$Mg_3Al_1(OH)_8(CO_3)_{0.5} \cdot 2H_2O$
$Mg_3Al_1-NO_3$	8.1	114.9	0.21	$Mg_3Al_1(OH)_8NO_3 \cdot 2H_2O$
$Mg_3Al_1-SO_4$	5.2	41.9	0.10	$Mg_3Al_1(OH)_8(SO_4)_{0.5} \cdot 2H_2O$
Mg_3Al_1-Cl	4.9	136.5	0.18	$Mg_3Al_1(OH)_8Cl \cdot 2H_2O$
$Mg_3Al_1-HCO_3$	5.9	135.6	0.18	$Mg_3Al_1(OH)_8HCO_3 \cdot 2H_2O$

3.3 Sorption enhanced process

Recently, several researches have been investigating methods to increase the hydrogen production yield and hydrogen purity from steam reformation by adding the CO_2 sorbent into the reactor, referred to as sorption enhanced methane steam reforming (SEMSR). This concept takes advantage of Le Chatelier's principle selectively removing CO_2 from the reaction zone and thus promoting the forward reaction. Advantages of the sorption enhanced methane steam reforming process are (i) it is a

process that combines the reaction unit and the separation unit into one unit operation (reduces size of overall process), (ii) increases the rate of the forward reaction, the steam reformation of methane [33], (iii) it reduces the operating cost (reduces the operating temperature) and the capital cost (reduces cost of wall materials of reactor) [34].

3.3.1 Sorption enhanced steam methane reforming

Several researchers have investigated the sorption enhanced steam methane reforming (SESMR) process, including Chanchanasiri *et al.*, (2011) [99] who investigated the use of a Ni/CaO multifunctional catalyst for hydrogen production via sorption enhanced steam methane reforming. They found that 12.5 wt% Ni/Al₂O₃+CaO provided the highest CH₄ conversion (89%) when compared with 12.5 wt% Ni/CaO (86%) and 12.5 wt% Ni/Al₂O₃ (84%, without CO₂ sorption). Moreover, the 12.5 wt% Ni/Al₂O₃+CaO provided the highest purity of H₂ (83%) when compared with 12.5 wt% Ni/CaO (82%), 12.5 wt% Ni/MG30-K (75%) and 12.5 wt% Ni/Al₂O₃ (72%). Chen *et al.*, (2011) [100] studied a two dimensional transient model for steam methane reforming (SMR) and tested different sorbents including hydrotalcite (HTC), CaO, Li₄SiO₄ and Li₂ZrO₃. The results showed that H₂ purities greater than 94% were obtained when using HTC, CaO and Li₄SiO₄ at a temperature of 550 °C and a pressure of 0.1 MPa. The sorbents used led to SMR performances ranked according to the following order from highest to lowest HTC>CaO>Li₄SiO₄>Li₂ZrO₃, tested at temperatures ranging from 500 °C – 600 °C. However, the sorption times at a temperature of 600 °C were approx. 15

min, 25 min, 50 min and 100 min (wide range of mass transfer zone) for HTC, CaO, Li_4SiO_4 and Li_2ZrO_3 , respectively.

CaO can provide the highest CO_2 sorption capacities but its stability requires improvement. Incorporation of Al into the CaO to produce $\text{CaO-Ca}_{12}\text{Al}_{14}\text{O}_{33}$ and using this with a commercial catalyst in sorption enhanced methane steam reforming [35], led CH_4 conversion greater than 93% at a temperature of 650 °C, a pressure of 1 bar and a steam to methane ratio of 3.4. Moreover, a hydrogen purity greater than 92% was reached using SESMR whilst only 77% hydrogen purity was reached when conventional reaction was performed. Multi-cycle testing showed a moderate decrease in the $\text{CaO-Ca}_{12}\text{Al}_{14}\text{O}_{33}$ sorption capacity for the sorption enhanced reaction over 15 cycles.

The operating window of sorption enhanced steam methane reforming using a $\text{CaO-Ca}_{12}\text{Al}_{14}\text{O}_{33}$ sorbent was investigated [101]. The results indicate a shifts of the equilibrium position to a higher hydrogen concentration of hydrogen (>93%) when compared with the conventional steam methane reforming reaction at a temperature of 650 °C. Moreover, a CH_4 conversion of over 95% was attained with outlet gases containing only 2-3% CO_2 and 3-4% CO.

Another complex material produced by modifying $\text{NiO-CaO/Al}_2\text{O}_3$ with La_2O_3 was investigated by Feng *et al.*, (2012) [102]. This complex catalyst was prepared by impregnating the $\text{NiO-CaO/Al}_2\text{O}_3$ with lanthanum nitrate. The sorption enhanced reaction, which was carried out in a fixed bed reactor, showed that $\text{NiO-CaO/Al}_2\text{O}_3$

modified with La_2O_3 , was stable for 30 cycles, whilst without the La_2O_3 it was only stable for 7 cycles. The La_2O_3 modified sample was also stable for 10 more cycles than the ZrO_2 modified $\text{NiO-CaO/Al}_2\text{O}_3$ [103]. Addition of the La_2O_3 helped improve the stability of the catalyst by inhibiting the formation of NiAl_2O_4 . As a result of this, the Ni particle size and surface area were stable for many multiple cycles at reaction temperatures of 600 °C and regeneration temperatures of 800 °C.

As well as CaO being used as a sorbent in the sorption enhanced methane steam reforming reaction, other sorbents such as hydrotalcite [104] and alkali metal oxides have been investigated [105, 106]. For example, Li_2ZrO_3 and Na_2ZrO_3 were tested and compared as CO_2 acceptors for hydrogen production via sorption enhanced methane steam reforming [106]. The reforming reaction was performed at 575 °C, 5 atm and a steam to carbon ratio, S/C of 5. The results showed high H_2 yields (95%) when used Na_2ZrO_3 as a sorbent. Furthermore, lithium oxides including Li_4SiO_4 and Li_2ZrO_3 were compared for hydrogen production using the SESMR process [105]. This reaction was carried out at pressure of 20 bar, a temperature of 575 °C and a steam to carbon ratio of 5. The results show that hydrogen purities as high as 87% could be achieved. In addition, Li_4SiO_4 enabled higher CH_4 conversions and hydrogen production yields at lower steam to carbon ratios.

Catalyst and sorbent activity is also of concern. The size of the surface nickel deposits and the catalyst preparation technique were investigated by Ochoa-Fernández *et al.*, (2007) [104]. Various amounts (12.5%, 40% and 77.5%) of Ni were

loaded on hydrotalcite support. Table 3.6 shows information on the Ni content, the dimensions of the deposits, their dispersions and catalytic activity. The results indicated that use of the co-precipitation method led to a stronger support-catalyst interaction than for the incipient wetness method. Use of the co-precipitation method also leads to smaller Ni crystallites which provide higher catalytic activity and more stable in sorption enhanced steam methane reforming reaction. The dispersion and crystal size are independent of the Ni loading for loadings between 12.5 wt% and 40 wt%. Table 3.7 shows a summary of data for catalysts and sorbents used for sorption enhanced methane steam reforming hydrogen production.

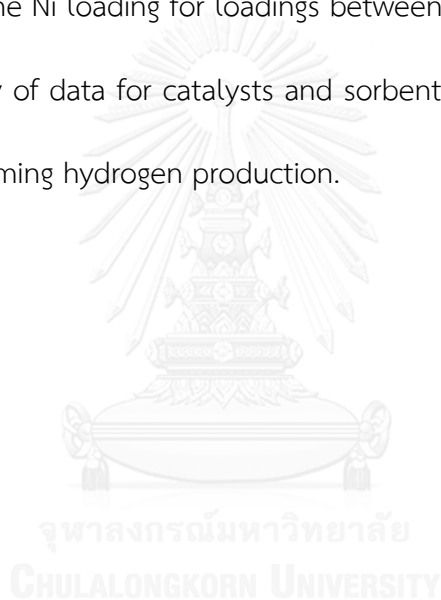


Table 3.6 Ni content on support, their properties and activity in sorption enhanced methane steam reforming reaction [104]

Catalyst	Ni loading (wt%)	Ni dispersion (%)	d_{Ni}^a (nm)	d_{NiO}^b (nm)	CH ₄ conversion (%)
12.5 Ni/HT	12.5	11.9	8	4	40
40 Ni/HT	40	10.8	9	4	57
77.5 Ni/HT	77.5	5.5	18	7	41
12.5 Ni/HT70	12.5	4.2	24	29	24
CC ^c	12.5	1.5	65	65	10

^a calculated from H₂ chemisorption

^b calculated from X-ray diffraction

^c commercial catalyst

However, the work on the steam reforming of biogas containing high levels of CO₂ has not been well investigated. Therefore, this study will focus on sorption-enhanced biogas steam reforming and feed biogas containing high levels of CO₂. Of particular interest and focus is the catalyst-sorbent used to handle the high content of CO₂ in the reaction system.

Table 3.7 Summaries catalysts and sorbents for hydrogen production via sorption enhanced methane steam reforming (SEMSR)

Catalyst	Sorbent	Conditions		CH ₄ conversion (%)	H ₂ purity (%)	Ref.
		Temp (°C)	S/C			
16wt%Ni/						Martavalt
Hybrid material	CaO-Ca ₁₂ Al ₁₄ O ₃₃	650	3.4	80	90	zi <i>et al.</i> , [107]
Commercial catalyst	CaO-Ca ₁₂ Al ₁₄ O ₃₃	650	3.4	93	>92	Martavalt zi <i>et al.</i> , [35]
Commercial nickel based catalyst	CaO-Ca ₁₂ Al ₁₄ O ₃₃	550 600 650	3.4	72 88 95	- - 93	Martavalt zi <i>et al.</i> , [101]
Simulation	HTC	500 550 600	-	-	92 99 99	YuMing <i>et al.</i> , [100]

Catalyst	Sorbent	Conditions		CH ₄ conversion (%)	H ₂ purity (%)	Ref.
		Temp (°C)	S/C			
	CaO	500			90	
		550			97	
		600			99	
	Li ₄ SiO ₄	500			88	
		550			95	
		600			96	
Nickel	La ₂ O ₃ -NiO-	600		90	92	Feng <i>et al.</i> ,
	CaO/Al ₂ O ₃					(2012)
	NiO-	600		77	92	[102]
	CaO/Al ₂ O ₃					
Rh/Ce α Zr ₁₋	K ₂ CO ₃ /HTC	450		82	94.7	Halabi <i>et al.</i> ,
α O ₂		450		92.7	98.0	(2012)
		450		98	99.5	[108]
		450		99.6	99.8	

CHAPTER IV

EXPERIMENTAL

4.1 Materials and method

4.1.1 Sorbent synthesis

Three synthesis methods have been investigated including methods referred to as the physical mixing method (dry powder mixing), the wet mixing method and the CaO hydration with mixing method. Firstly, the dry powder mixing method involved mixing dry metal oxide powders - namely magnesium oxide (MgO, Sigma-Aldrich), strontium oxide (SrO, Aldrich) and aluminum oxide (Al_2O_3 , Sigma-Aldrich) - with calcium oxide powder (CaO, Sigma-Aldrich). Compositions of 80% w/w CaO and 20% w/w of each metal oxide (MgO, SrO and Al_2O_3) were dry mixed by shaking by hand for 10 min until uniform mixture was obtained, which was then calcined at 900 °C for 3 h in air. In this report, samples produced using the dry powder mixing method are denoted with a D i.e. Mg-CaO-D, Sr-CaO-D and Al-CaO-D for samples containing MgO, SrO and Al_2O_3 as precursors, respectively.

The metal precursors used for synthesis of the modified sorbents by wet mixing and CaO hydration followed by wet mixing, were calcium oxide (CaO, Sigma-Aldrich), magnesium nitrate hexahydrate ($\text{Mg}(\text{NO}_3)_2 \cdot 6\text{H}_2\text{O}$, Merck), strontium nitrate anhydrous ($\text{Sr}(\text{NO}_3)_2$, Fluka) and aluminum nitrate nanohydrate ($\text{Al}(\text{NO}_3)_3 \cdot 9\text{H}_2\text{O}$, Sigma-Aldrich). The wet mixing process involved dispersing CaO in deionized water and then adding the metal precursors (magnesium nitrate, strontium nitrate and aluminum nitrate) into the

CaO suspension at a temperature of 75 °C for 3 h. After that they were dried in an oven at a temperature of 110 °C overnight and calcined at 900 °C for 3 h in air. In this report, samples produced using the wet mixing method are denoted with a W i.e. Mg-CaO-W, Sr-CaO-W and Al-CaO-W for samples produced using magnesium nitrate, strontium nitrate and aluminum nitrate precursors, respectively.

The modified sorbents were synthesized by CaO hydration followed by wet mixing. Firstly, CaO was added to DI water at a temperature of 75 °C for 2 h and then 20 wt% each of Al₂O₃, ZrO₂, CeO₂, La₂O₃ or NiO are added to the solution, which was then kept at 75 °C for 2 h. Aluminum nitrate nanohydrate (Sigma-Aldrich), zirconium(IV) oxynitrate hydrate (Aldrich), cerium(III) nitrate hexahydrate (Aldrich), lanthanum(III) nitrate hexahydrate (Fluka) or nickel nitrate hexahydrate (Sigma-Aldrich) were used as precursors for the Al₂O₃, ZrO₂, CeO₂, La₂O₃ or NiO, respectively. The solution was dried at 100 °C overnight to produce a powder, after that the resulting powder was further dried at 500 °C for 3 h and then calcined at 900 °C for 3 h in an air atmosphere.

4.1.2 Catalyst synthesis

Multifunctional catalysts containing Ni and a modified sorbent (CaO/Ca₁₂Al₁₄O₃₃) were also synthesized by hydration followed wet mixing. Ni deposited on a commercial support (Al₂O₃, Fluka) or a commercial sorbent (CaO, Sigma-Aldrich) were synthesized by hydration followed by wet mixing, which was used for comparison to the multifunctional catalysts in terms of H₂ production performance. First, CaO or Al₂O₃ were added to DI water and stirred at 75 °C for 2 h. 20 mL of solution of Ni(NO₃)₂·6H₂O

dissolved in DI water (equal to 12.5 wt.% Ni) was then added to the CaO or Al₂O₃ suspension then stirred at a temperature of 75 °C for 2 h. The mixture was then dried at 100 °C overnight and heated up to 500 °C for 3 h. The resulting powder then was calcined at 900 °C for 3 h.

4.2 Characterization

4.2.1 X-ray diffraction technique

Phases and crystallite sizes of the modified sorbents and multifunctional catalysts were determined by X-ray diffraction technique (XRD) using a D8 Advance, Bruker equipped with a long fine focus Cu K α X ray source. The XRD patterns were recorded at $10^\circ < 2\theta < 80^\circ$ with a step of 0.04° , wavelength of 1.54056 nm and scan speed of 0.5 s/step.

4.2.2 N₂ adsorption/desorption isotherm

The surface area of each samples was determined by the Brunauer-Emmett-Teller (BET) method with nitrogen gas (Micromeritics Chemisorp 2750). Pore sizes and pore volumes of the samples were determined by desorption isotherm using Barret-Joyner-Halender (BJH) method.

4.2.3 Scanning electron microscope

The morphologies of the modified sorbents and multifunctional catalysts (both fresh and used) were analyzed using a scanning electron microscope, SEM, (Hitachi S-

3400N) coupled with X-ray energy dispersive spectroscopy, X-ray EDS, (AMETEK EDAX, APOLLO X) for analyzing the local dispersion of elements.

4.2.4 X-ray photoelectron spectroscopy

Atomic concentrations at the surface were characterized by X-ray photoelectron spectroscopy (XPS) using a Kratos Amicus X-ray photoelectron spectrometer. The analyses were carried out with a Mg K α X-ray source under a working pressure of 1×10^{-6} Pa at a current of 20 mA and 12 kV.

4.2.5 Temperature-programmed reduction

Temperature-programmed reduction (TPR) was used to determine reducibility of multifunctional catalyst. The samples were tested in a fixed bed quartz reactor connected to a mass spectrometer to analyze gaseous products (H₂ and N₂) at the outlet stream. For each experiment, a 0.5 g sample was packed in the reactor supported by quartz wool. The sample was pretreated at 850 °C for 30 min under N₂ flow to remove water and other contaminants before performing the experiment. TPR profile was recorded by heating the samples from 30 to 900 °C at a heating rate of 10 °C/min under 10% v/v H₂/N₂ flowing at 50 mL/min.

4.3 CO₂ sorption/desorption testing

Sorption/desorption tests have been performed in a fixed bed quartz reactor (15 mm inner diameter and 18 mm outer diameter). One gram of modified sorbent

was sandwiched within quartz wool in the fixed bed quartz reactor. The sorbents were pretreated at 850 °C for 30 min under flowing N₂ before running an experiment. To test the ability for CO₂ sorption, 15% v/v CO₂ concentration (balanced N₂) was fed through the reactor with a total flow rate of 60 mL/min at 600 °C and 1 atm. Outlet gas products were collected and analyzed by the mass spectrometer.

4.4 H₂ production

For each experiment, two grams of catalyst was placed in the fixed bed reactor supported by quartz wool. The catalyst was pretreated at 850 °C for 30 min under 100% N₂ flow and then reduced by 10% H₂ (balanced N₂) at 850 °C for 1 h. The temperature was thereafter decreased to the reaction temperature of 600 °C. The operating conditions were: a steam to methane molar ratio (S/C) of 3:1, a CH₄ to CO₂ ratio of 60%:40% [109] balanced with N₂ at a total flow rate of 50 mL/min, temperature of 600 °C and pressure of 1 atm. The product gas compositions were measured by gas chromatography (GC-8A, SHIMADZU) equipped with two columns - Molecular Sieve 5A and PoraPLOT Q.

CHAPTER V

Metals (Mg, Sr and Al) modified CaO based sorbent for CO₂ sorption/desorption stability in fixed bed reactor for high temperature application

This study investigates the effect of various factors pertinent to these applications, namely the effect of supports, the effect of sorption temperatures and the effect of CO₂ concentration. Furthermore, the synthesis methods - physical mixing (dry powder mixing); wet mixing; CaO hydration followed by wet mixing - have been investigated, comparing samples produced using compounds of Mg²⁺, Sr²⁺ and Al³⁺ with CaO. Samples were tested in terms of their CO₂ sorption/desorption performance over multiple cycles in a fixed bed reactor, measured in terms of sorption capacity and sorption stability.

5.1 Effect of support

Alkali earth metal oxides including MgO, CaO and SrO, and Al₂O₃ are commonly used as catalyst supports and were selected due to their ability to absorb CO₂ gas. All samples were tested in terms of CO₂ sorption by added 1 g of the solid powder into a fixed bed quartz reactor. The results (Figure 5.1) show the CaO exhibited the best sorption capacity ($0.571 \text{ g}_{\text{CO}_2} / \text{g}_{\text{sorbent}}$) when compared with MgO ($0.038 \text{ g}_{\text{CO}_2} / \text{g}_{\text{sorbent}}$),

SrO ($0.065 \text{ g}_{\text{CO}_2} / \text{g}_{\text{sorbent}}$) and Al_2O_3 ($0.037 \text{ g}_{\text{CO}_2} / \text{g}_{\text{sorbent}}$) at a temperature of $600 \text{ }^\circ\text{C}$, pressure of 1 atm and with an 8% CO_2 feed stream.

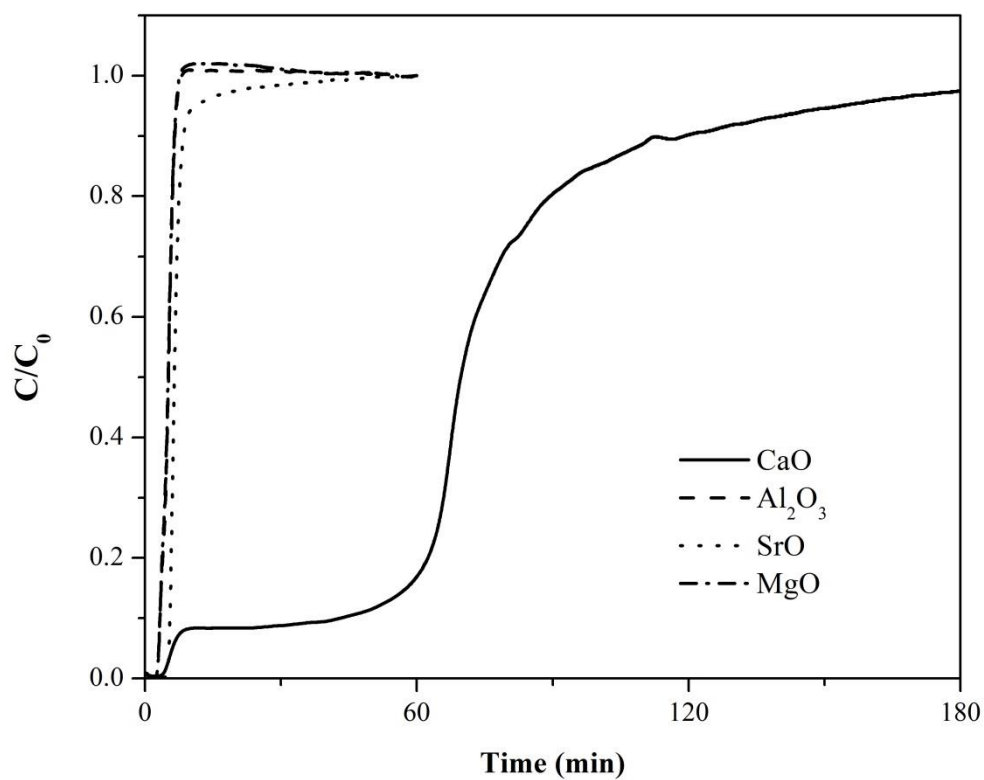


Figure 5.1 Breakthrough curves of various supports (MgO, SrO, CaO and Al_2O_3) at temperature of $600 \text{ }^\circ\text{C}$, pressure of 1 atm and 8% CO_2 feed stream.

5.2 Effect of temperature

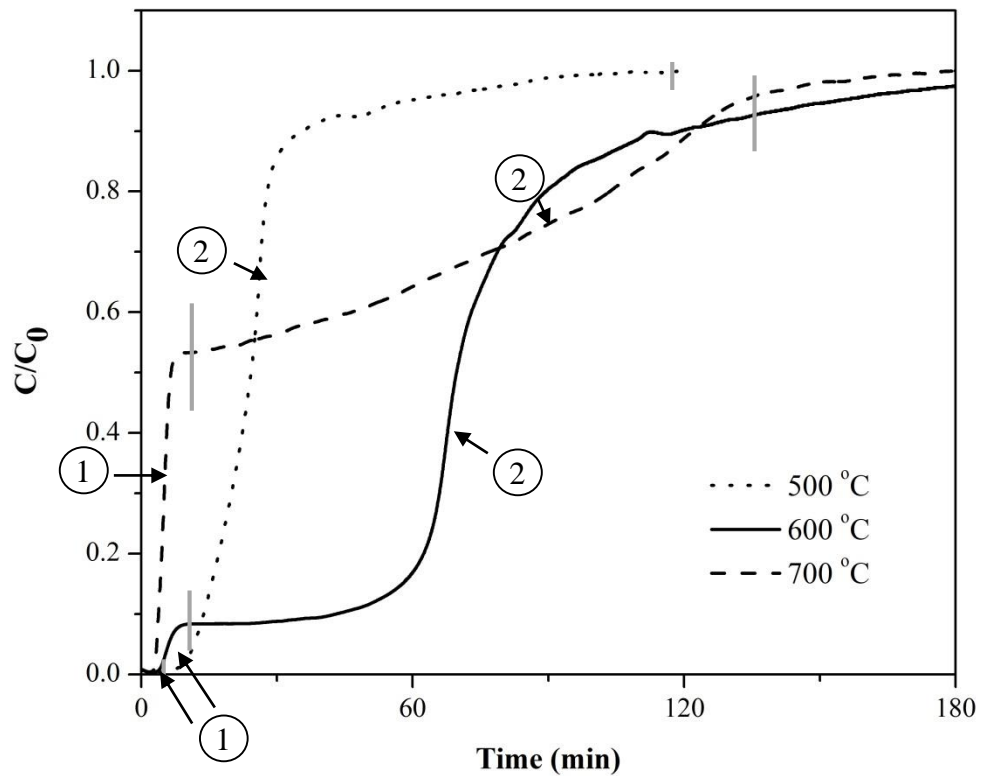


Figure 5.2 Breakthrough curves of CaO at temperature of 500-700 °C, pressure of 1 atm and 8% CO₂ feed stream: (1) refers to step 1 - surface reaction and (2) refers to step 2 - CO₂ diffusion.

For the test on the CaO sorbent, temperatures were varied from 500 to 700 °C, at a pressure of 1 atm and with an 8% CO₂ feed stream. The sorption capacity increased with increasing temperature from 500 to 600 °C (sorption capacity at 500 °C of 0.211 g_{CO₂} / g_{sorbent} and at 600 °C of 0.571 g_{CO₂} / g_{sorbent}). For temperatures of 700 °C and above CO₂ sorption capacity decreased with increasing temperature. The optimum temperature for CO₂ sorption capacity in the fixed bed reactor was found to be

approximately 600 °C. However, with increasing sorption temperature, the breakthrough time consistently decreased (11.67, 9.66, 3.41 min for 500, 600 and 700 °C, respectively), meaning that the time required for CO₂ gas to reach the outlet of the reactor decreased with increasing temperature. The breakthrough curves for CaO (Figure 5.2) indicated a two-step sorption process was taking place. It is proposed that for the first step the sorption occurred at the surface only (Step 1: $\text{CaO} + \text{CO}_2 \leftrightarrow \text{CaCO}_3$). It is proposed that the second step is related to the diffusion of CO₂ into the CaO particles, as indicated in Figure 5.3(a). At a temperature of 500 °C, the sorption capacity is limited by step 2 the diffusion of CO₂ into the CaO particles, meaning the slow diffusion of CO₂ below the surface but relatively fast adsorption of CO₂ onto the CaO surface because CaCO₃ generated at the surface layers were not sintered by thermal activity because sorption temperature (500 °C) was lower than the Tammann temperature (533 °C) therefore CO₂ sorption at surface continued. In contrast, at temperatures of 600 and 700 °C an increase in CO₂ concentration at the outlet indicates less adsorption of CO₂ taking place at the CaO surface (step 1) due to sintering of the CaCO₃ at surface (proposed mechanism in Figure 5.3(b)) which reduces the surface area and reduces the open porosity. However, the sorption capacity at a temperature of 700 °C ($0.363 \text{ g}_{\text{CO}_2} / \text{g}_{\text{sorbent}}$) was observed to be lower than at 600 °C. This is due to two reasons: (i) carbonation is an exothermic reaction and so desorption of CO₂ is

avored by higher temperature; (ii) the CO_2 diffusion rate into sub surface CaO layers (step 2) is low due to reduced surface area as a result of surface sintering.

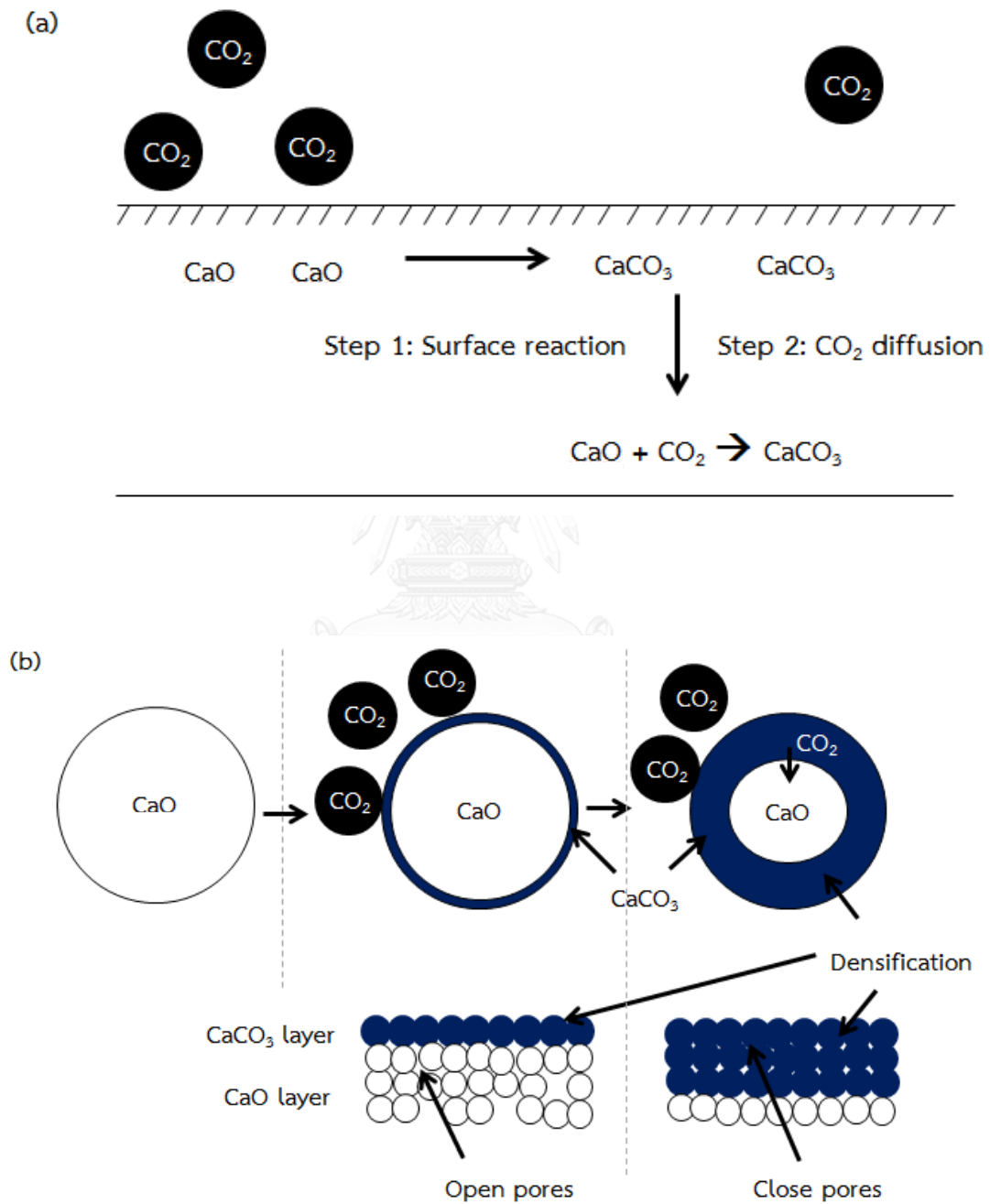


Figure 5.3 Proposed mechanisms: (a) CO_2 sorption step and (b) densification

phenomena at sorption temperature of 600 and 700 °C.

5.3 Effect of synthesis method

5.3.1 Dry powder mixing method

Experimental results obtained for the sorbents produced by the dry powder mixing method (Mg-CaO-D, Sr-CaO-D and Al-CaO-D), as shown in Figure 5.4, indicate that the CO₂ sorption capacities are similar to each other (0.256, 0.219, 0.248 g_{CO₂} / g_{sorbent} for Mg-CaO-D, Sr-CaO-D and Al-CaO-D, respectively). This is partly because the same mass of each metal oxide (MgO, SrO and Al₂O₃) was loaded on to the CaO (20% by weight) reducing the mass of CaO in the sorbent mixture by the same mass each time; moreover, the metal oxides and CaO remained as separate phases as confirmed by XRD patterns as shown in Figure 5.5, for example XRD pattern of the Al-CaO-D sample showed Al₂O₃ phase, CaO showed CaO and Ca(OH)₂ phases. The fact that none of the samples contained complex materials or materials resulting from chemical interactions between each other, is due to the Tammann temperature (>900 °C) of the metal oxides being higher than the temperature of the calcination process (900 °C), and so migration of the respective ions and hence solid state reactions and sintering would not be expected.

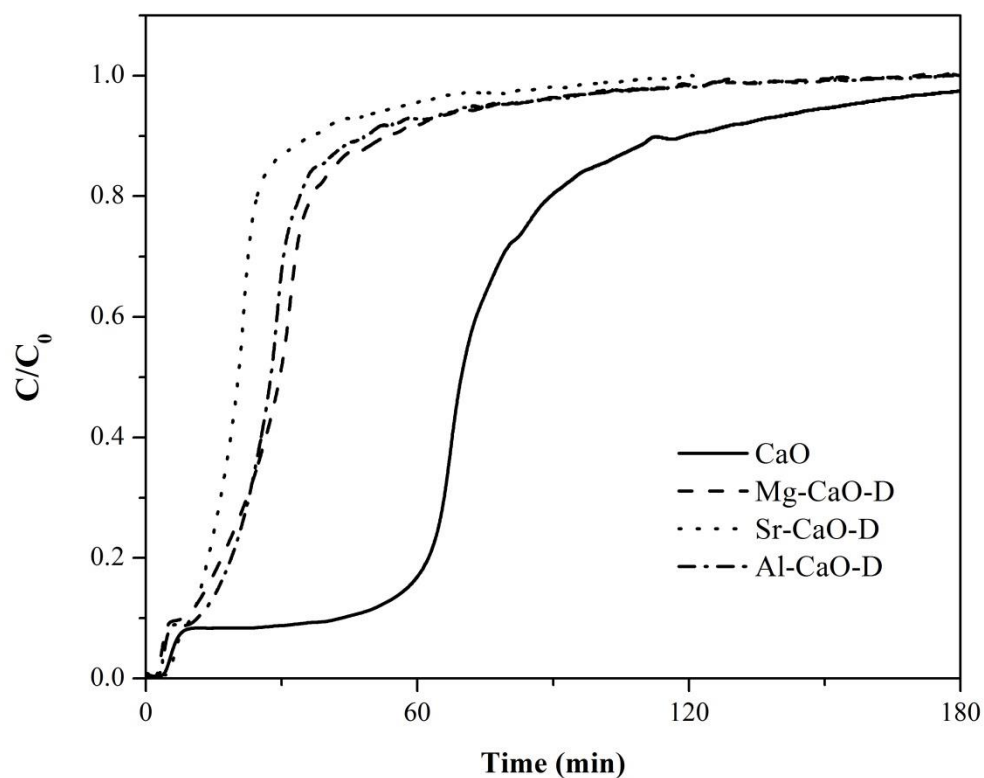


Figure 5.4 Breakthrough curves of modified sorbents by dry powder mixing method (Mg-CaO-D, Sr-CaO-D, Al-CaO-D and CaO) at temperature of 600 °C, pressure of 1 atm and 8% CO₂ feed stream.

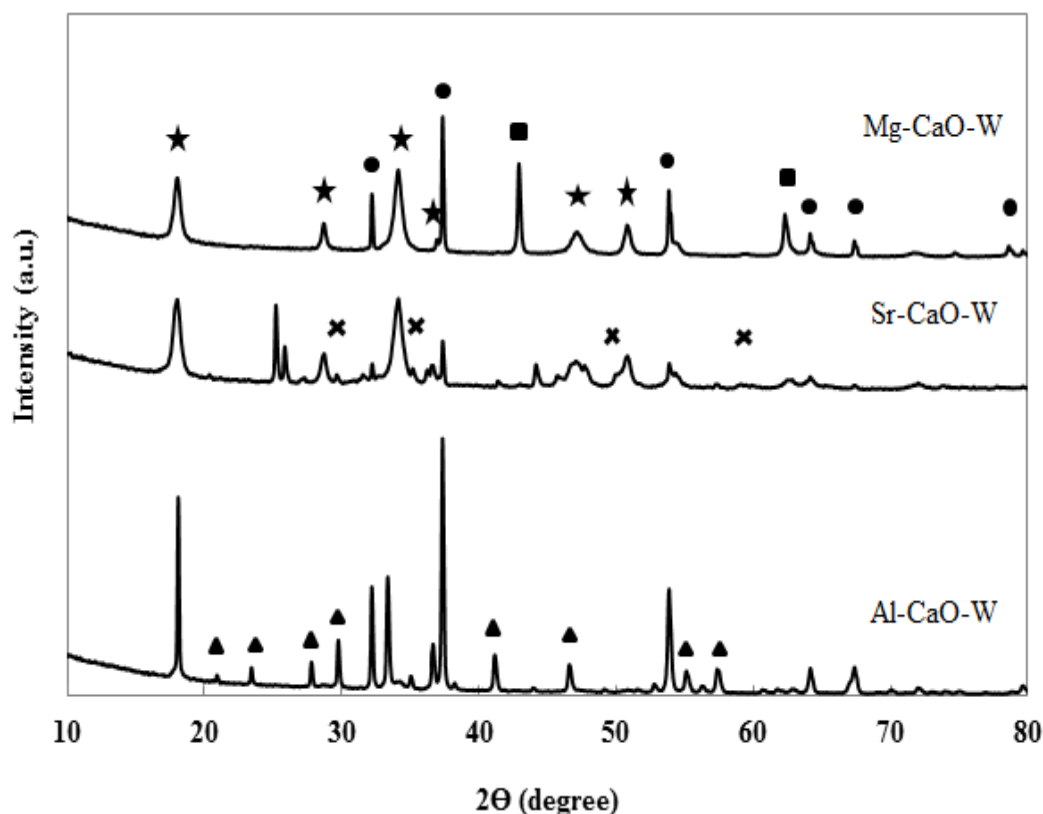


Figure 5.5 XRD patterns of modified sorbents by dry powder mixing method:

● CaO, ■ MgO, × SrO, ▲ Al₂O₃ and ★ Ca(OH)₂.

5.3.2 Wet mixing method

Modified sorbents produced by wet mixing (Mg-CaO-W, Sr-CaO-W and Al-CaO-W) were tested by CO₂ sorption/desorption over multiple cycles as shown in Figure 5.6. The CaO showed decreasing CO₂ sorption capacity with an increasing number of cycles (0.390 g_{CO₂}/g_{sorbent} at 1st cycle to 0.168 g_{CO₂}/g_{sorbent} at 25th cycle which decreasing of 56.92%). This is due to the sintering of particles resulting in pores decreasing in size or even closing as shown in Figure 5.7(d). To reduce this effect some

metal oxides with Tammann temperatures greater than 900 °C were selected and added to CaO structure. The modified sorbents (Mg-CaO-W, Sr-CaO-W and Al-CaO-W) showed the same trend with decreasing sorption capacity with increasing number of cycles, however the degree to which it took place was much lower. This decrease in sorption capacity is attributed to the agglomeration of particles due to sintering as shown in Figure 5.7(a), (b) and (c).

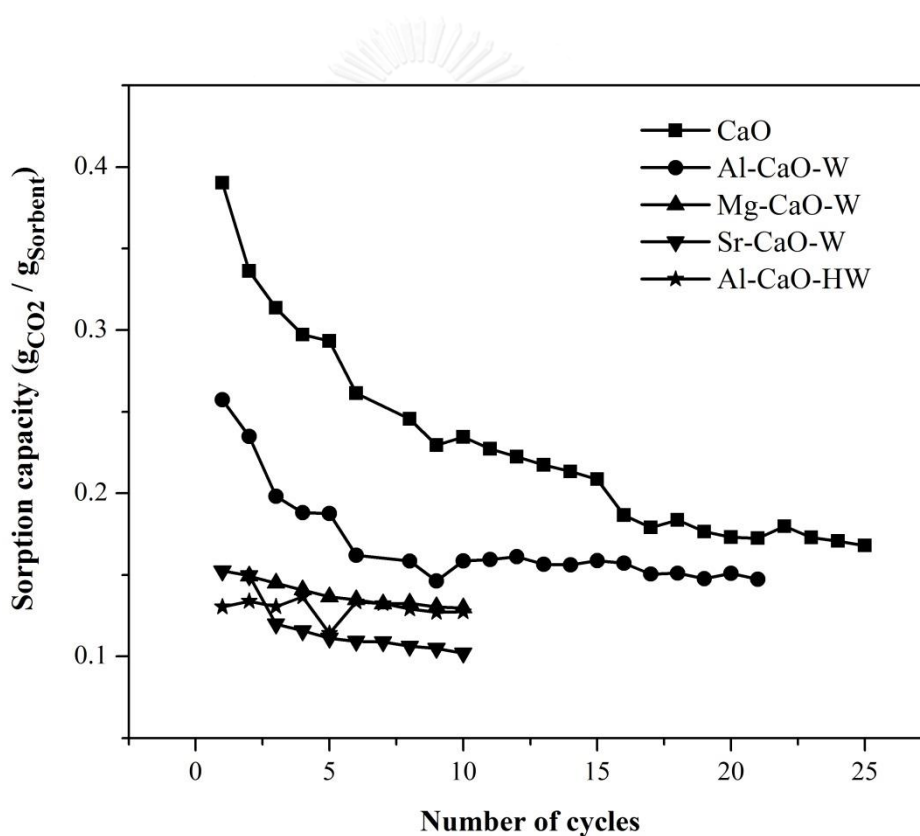


Figure 5.6 CO₂ sorption/desorption cycles of modified sorbents by wet mixing method at temperature of 600 °C, pressure of 1 atm and 8% CO₂ in feed stream.

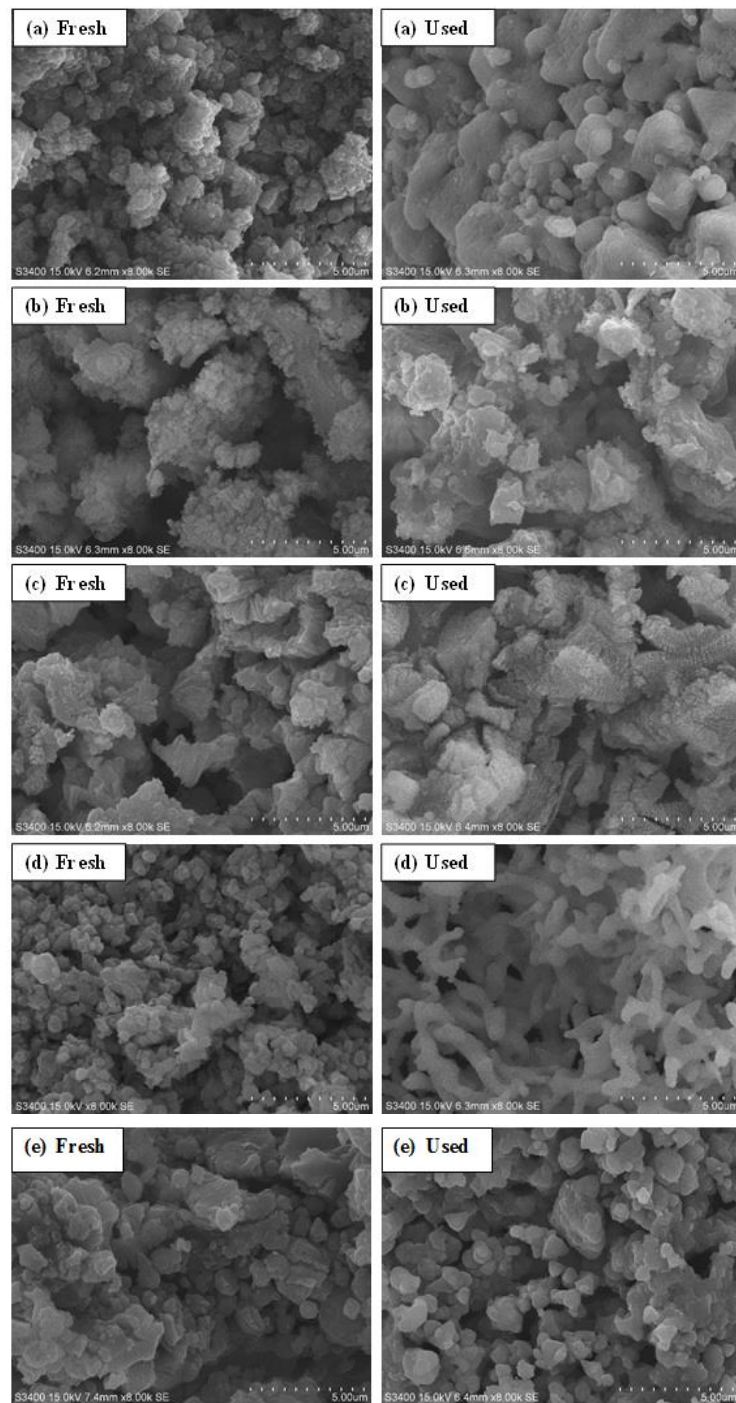


Figure 5.7 SEM images of fresh and used modified sorbents by wet mixing method:

(a) Al-CaO-W, (b) Mg-CaO-W, (c) Sr-CaO-W, (d) CaO commercial and (e) Al-CaO-HW.

All modified sorbents produced by the wet mixing method (Mg-CaO-W, Sr-CaO-W and Al-CaO-W) exhibited low stability performance. This is possibly due to incomplete formation of CaO and poor dispersion of metal dopants (Mg^{2+} , Sr^{2+} and Al^{3+}) within the CaO. Furthermore, due to a low surface area of the CaO, metal dopants (Mg^{2+} , Sr^{2+} and Al^{3+}) were deposited on CaO surface meaning that dopant phases (MgO , $Ca_{0.2}Sr_{0.8}O$ and $Ca_{12}Al_{14}O_{33}$) were occurred only at the surface resulting in occurred the densification of particles when CO_2 sorption/desorption were tested as shown propose mechanism in Figure 5.8. In order to increase the CaO surface area, the CaO hydration step was implemented before adding the dopant (Mg^{2+} , Sr^{2+} and Al^{3+}). The results indicated the Al-CaO-HW to be stable for more than 10 cycles ($0.130 \text{ g}_{CO_2} / \text{g}_{sorbent}$ at 1st cycle and $0.127 \text{ g}_{CO_2} / \text{g}_{sorbent}$ at 10th cycle). This is attributed to the hydration of CaO to form $Ca(OH)_2$, increasing the pore volume [47] therefore allowing the Al^{3+} precursor to diffuse in to the $Ca(OH)_2$ structure, resulting in it being more highly dispersed on the CaO and subsequently more highly dispersed $Ca_{12}Al_{14}O_{33}$ after calcination. In addition, the inert phase ($Ca_{12}Al_{14}O_{33}$) - which has defect of oxygen vacancies [53] - can promote absorption of adsorbed CO_2 to below the CaO surface and also during CO_2 regeneration subsurface CaO can be released to the surface [54]. Furthermore, $Ca_{12}Al_{14}O_{33}$ also resisted the agglomeration between CaO particles therefore the sintering was not observed as shown in Figure 5.7(e).

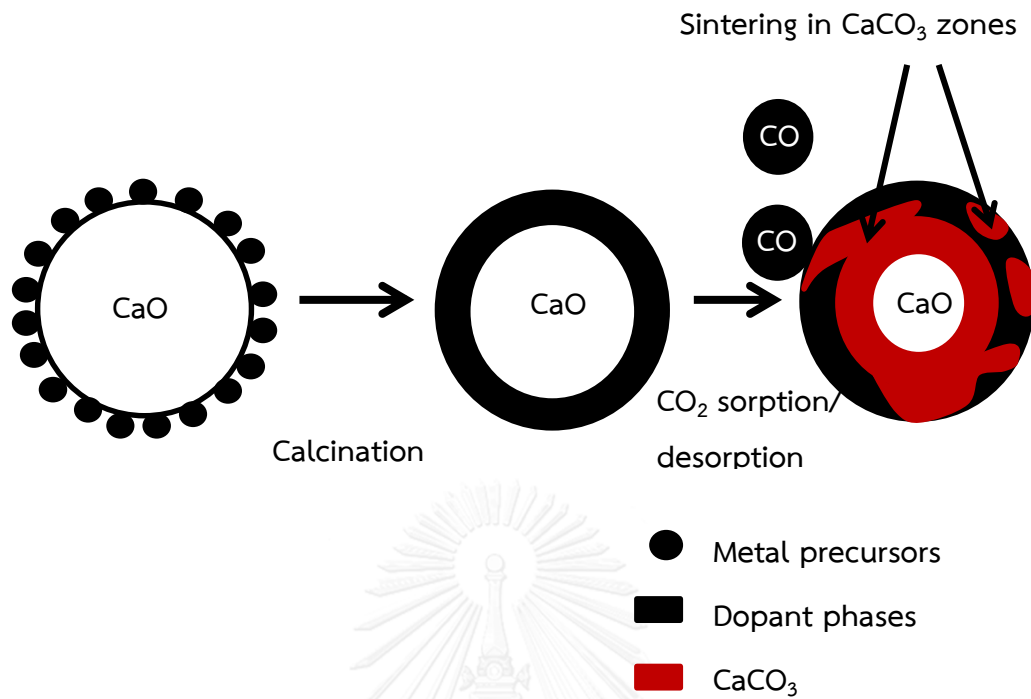


Figure 5.8 Proposed mechanism of occurring the dopant phases (MgO, Ca_{0.2}Sr_{0.8}O and Ca₁₂Al₁₄O₃₃) on CaO by wet mixing method and their densification phenomena.

5.4 Effect of CO₂ concentration

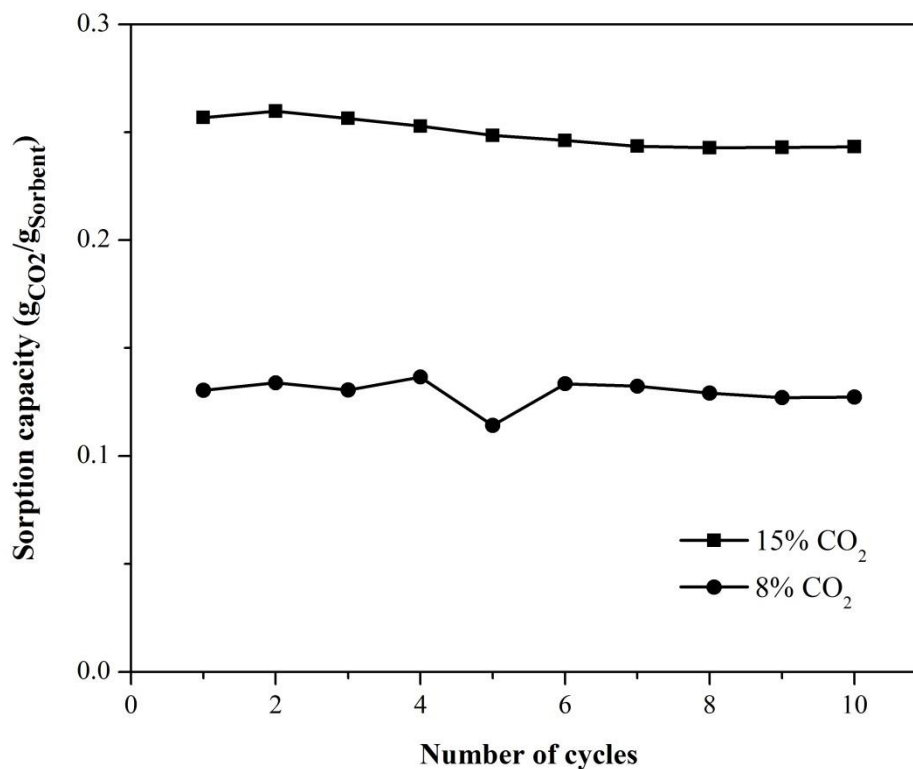


Figure 5.9 CO₂ sorption/desorption cycles of Al-CaO-HW at temperature of 600 °C, pressure of 1 atm and CO₂ concentration of 8 and 15%.

The Al-CaO-HW samples synthesized by hydration of the CaO followed by wet mixing, were tested with an 8% CO₂ feed gas and a 15% CO₂ feed gas, both with a N₂ balance. These concentrations were tested as they represent a typical range in CO₂ concentrations in emissions from various industrial sources such as flue gas from power plants, fired heaters from oil refineries and petrochemical plants as shown in Table 5.1. Furthermore, several researchers have investigated the modified sorbent for CO₂ sorption in a 15% CO₂ atmosphere and at high temperatures [52, 55-57]. This was done to enable the comparison of our modified sorbents with the sorption capacity results

from other studies. As would be expected the results indicate that when the feed CO₂ concentration is increased, the CO₂ sorption capacity also increases (1st cycle: 0.130 g_{CO₂} / g_{sorbent} at 8% CO₂ in feed to 0.257 g_{CO₂} / g_{sorbent} at 15% CO₂ in feed which increasing of 97.7 %) as shown in Figure 5.9. This increase in partial pressure of the CO₂ leads to a greater driving force for sorption and hence an increase in capacity [13]. Furthermore, this phenomena was supported by equilibrium partial pressure of CO₂ resulting from the decomposition of CaCO₃ [44, 58] which indicated that the increasing of partial pressure of CO₂ at constant temperature promoted further capture of CO₂ by CaO. This in itself is not of particular interest, but we will see further on in this section that the increase in concentration of the CO₂ has a greater positive impact upon the sorption capacity of the modified sorbents.

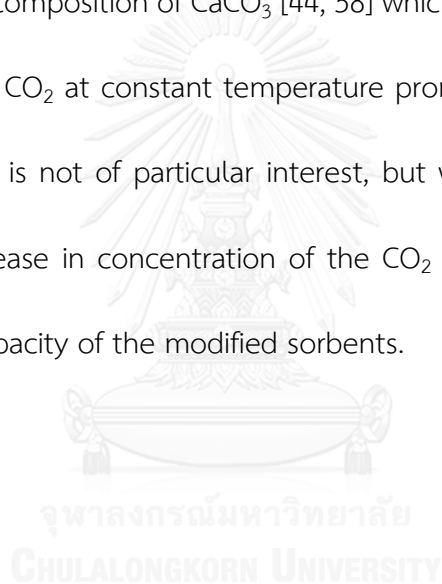


Table 5.1 Sources of CO₂ [110]

Source	CO ₂ concentration
	% vol (dry)
Power station flue gas:	
- Natural gas fired boilers	7-10
- Gas turbines	3-4
- Oil fired boilers	11-13
- Coal fired boilers	12-14
Oil refinery and petrochemical plant fired heaters	8
Chemical reaction (s)	
- Ethylene oxide	8
- Hydrogen production	15
- Methanol production	10

5.5 Stability of modified sorbents by CaO hydration followed with by wet mixing method

Comparing Figure 5.11 to Figure 5.6 we see that the increase in CO₂ concentration had relatively little effect on the CO₂ capacity of the CaO sorbent but

had a relatively significant positive impact upon the sorption capacity of the modified sorbents. The results in Figure 5.11 imply that after 17 cycles the modified sorbents would start to out-perform the CaO at a CO₂ concentration of 15%. This, however, is conjecture based upon a possibly unreliable extrapolation of experimental data, but it does indicate a need for further investigation. Furthermore, 10 cycle CO₂ sorption capacity tests of CaO were repeated (Figure 5.11) with results having 4% variation between these two sets of data.

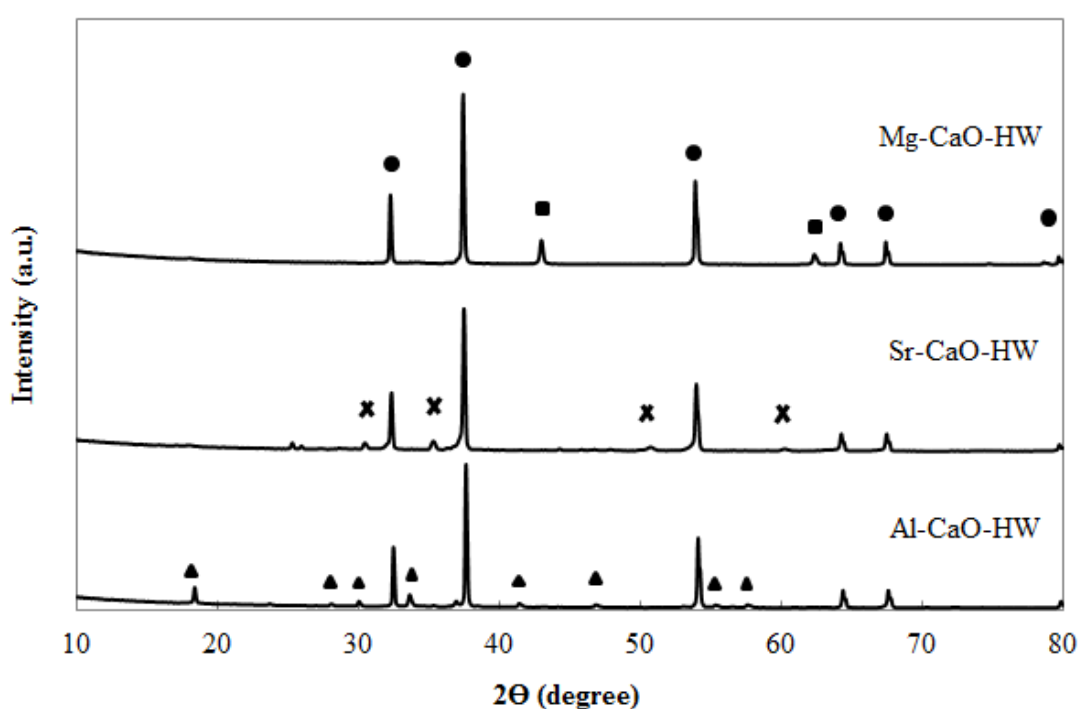


Figure 5.10 XRD patterns of modified sorbents by CaO hydration followed by wet

mixing method (Mg-CaO-HW, Sr-CaO-HW and Al-CaO-HW): ● CaO, ■ MgO,

× $\text{Ca}_{0.2}\text{Sr}_{0.8}\text{O}$ and ▲ $\text{Ca}_{12}\text{Al}_{14}\text{O}_{33}$.

The modified sorbents synthesized by CaO hydration followed by wet mixing (Mg-CaO-HW, Sr-CaO-HW and Al-CaO-HW) were characterized by XRD and results (Figure 5.10) indicate the following: the MgO and CaO exist as separate phases in the Mg-CaO-HW samples; Sr-CaO-HW is composed of $\text{Ca}_{0.2}\text{Sr}_{0.8}\text{O}$ and CaO phases; Al-CaO-HW is composed of $\text{Ca}_{12}\text{Al}_{14}\text{O}_{33}$ and CaO. The modified sorbents were tested over multiple CO_2 sorption/desorption cycles with the results shown in Figure 5.11. The results indicate that Mg-CaO-HW is the most stable with sorption capacities of $0.259 \text{ g}_{\text{CO}_2} / \text{g}_{\text{sorbent}}$ for 1st cycle and $0.252 \text{ g}_{\text{CO}_2} / \text{g}_{\text{sorbent}}$ for the 10th cycle.

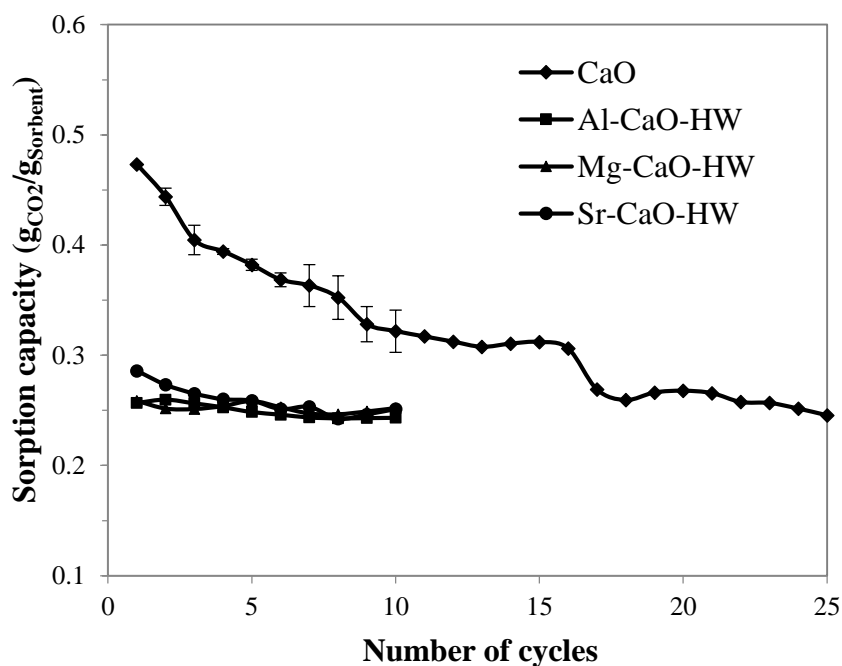


Figure 5.11 CO_2 sorption/desorption cycles of modified sorbents by CaO hydration followed with wet mixing method (Mg-CaO-HW, Sr-CaO-HW and Al-CaO-HW) at temperature of $600 \text{ }^\circ\text{C}$, pressure of 1 atm and 15% CO_2 feed stream.

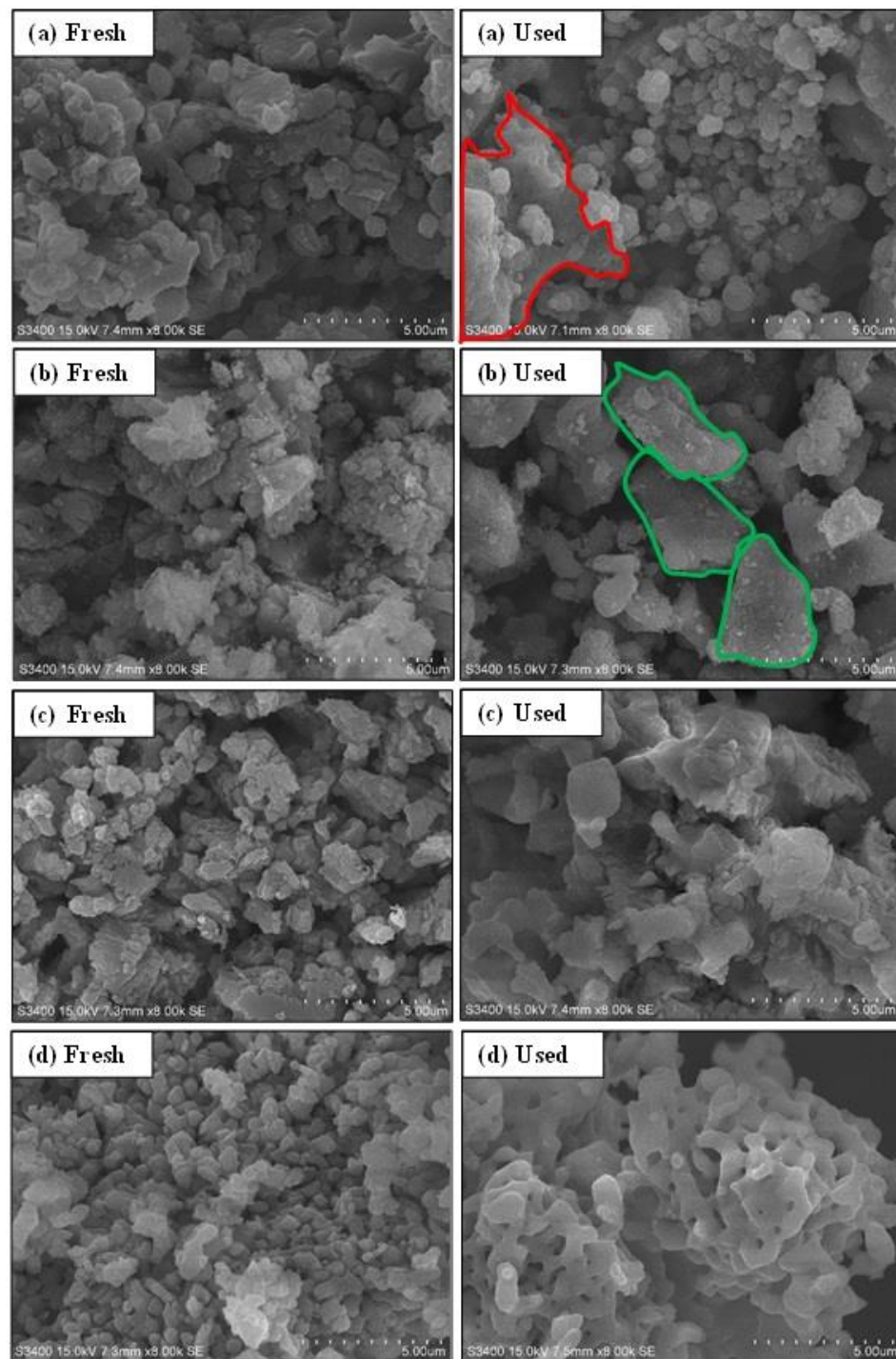


Figure 5.12 SEM images of fresh and used of modified sorbents synthesized by CaO hydration followed by wet mixing method: (a) Al-CaO-HW, (b) Mg-CaO-HW, (c) Sr-CaO-HW and (d) CaO commercial.

SEM images (Figure 5.12(b) used) also support the suggestion that Mg-CaO-HW has relatively small grains and less evidence of sintering than Al-CaO-HW, Sr-CaO-HW and CaO. However, the used Mg-CaO-HW sorbent (Blue circle line in Figure 5.12(b) used) is shown to have larger particles than the Mg-CaO-HW fresh sorbent (Figure 5.12(b) fresh) due to sintering of the exposed CaO particles and surfaces but on CaO particle surfaces covered by MgO as proposed in Figure 5.13(b) and supported by the SEM-EDX images showed the MgO prevented sintering, but in areas where CaO surfaces are exposed, sintering took place, as shown in Figure 5.14(a).

Al-CaO-HW was shown to have a sorption capacity of $0.257 \text{ g}_{\text{CO}_2} / \text{g}_{\text{sorbent}}$ for the 1st cycle dropping to only $0.243 \text{ g}_{\text{CO}_2} / \text{g}_{\text{sorbent}}$ for the 10th cycle representing a 6% decrease. This is attributed to the sorbent particulates being largely covered by the inert phase thus limiting the degree to which sintering could take place as shown in Figure 5.12. Figure 5.13(a) schematically represents the mechanism by which the inert phase prevented sintering. However, even with this partial coverage of the inert phase, sintering can still take place, but is nevertheless limited. The SEM-EDX images (Figure 5.14(b)) confirm the presence of this coating, shown by the elemental mapping (Al and Ca), which indicates a dispersion of Al on CaO, where there is only CaO but no Al (complex phase), there is sintering. On the other hand, Al (complex phase) prevents sintering where it is present at the surface. At the Sr-CaO-HW interface, $\text{Ca}_{0.2}\text{Sr}_{0.8}\text{O}$ complex was formed; however, the sorption capacity was still slightly decreased from

0.286 $\text{g}_{\text{CO}_2} / \text{g}_{\text{sorbent}}$ at 1st cycle to 0.251 $\text{g}_{\text{CO}_2} / \text{g}_{\text{sorbent}}$ at 10th cycle which decreasing of 12%. This is supported by evidence of sintering from the SEM images shown in Figure 5.12(c) used. In addition, Sr-CaO-HW complex prevents sintering as observed for Al-CaO-HW.

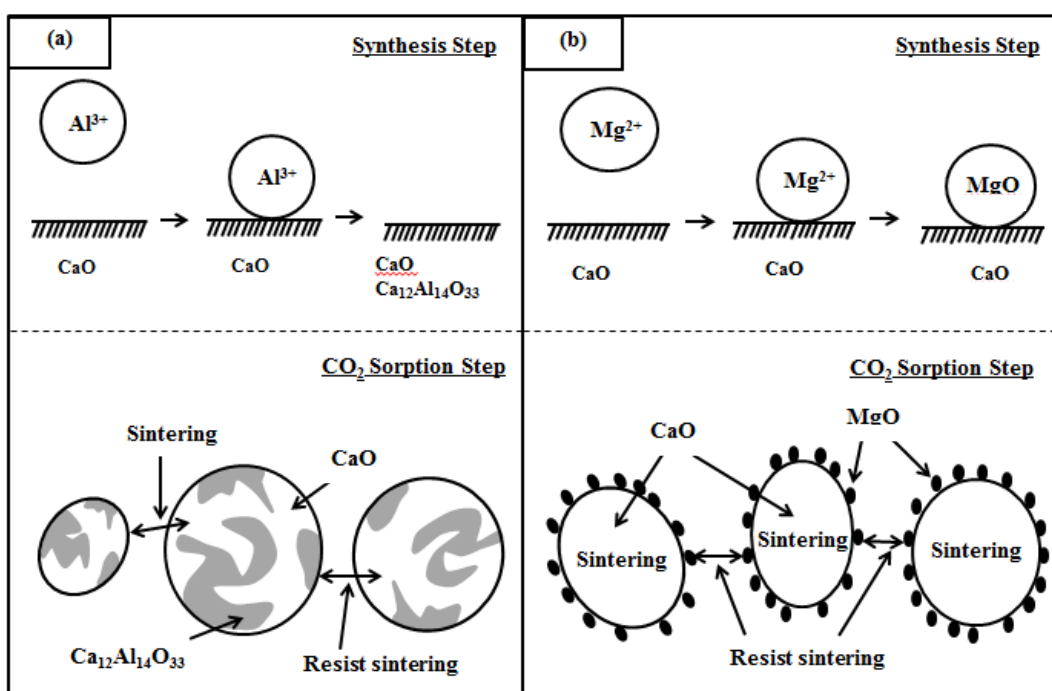


Figure 5.13 Proposed mechanism of metal precursors doped on CaO and their resisting sintering phenomena: (a) Al³⁺ doped on CaO and (b) Mg²⁺ doped on CaO.

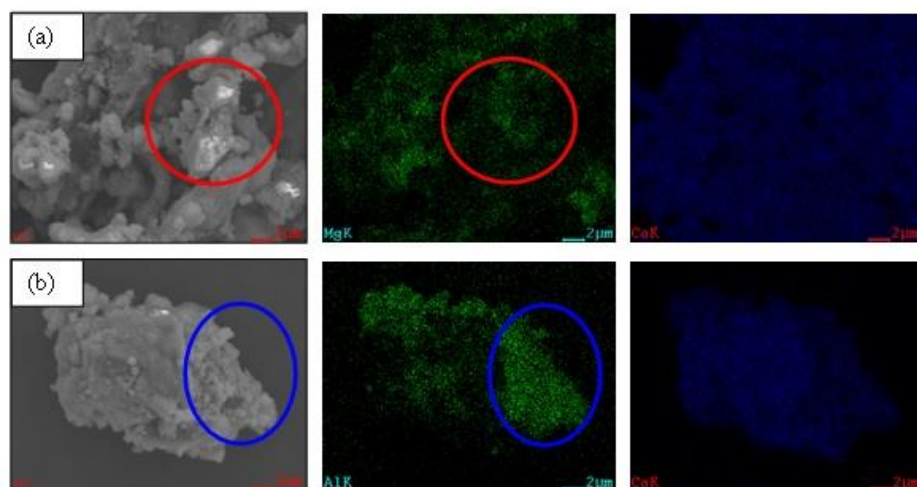
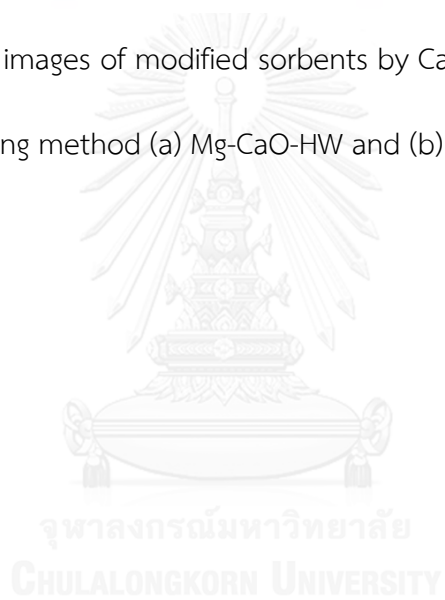


Figure 5.14 SEM-EDX images of modified sorbents by CaO hydration followed by wet mixing method (a) Mg-CaO-HW and (b) Al-CaO-HW.



CHAPTER VI

Activity and stability performance of multifunctional catalyst (Ni/CaO and Ni/Ca₁₂Al₁₄O₃₃-CaO) for bio-hydrogen production from sorption enhanced steam reforming of biogas

The work reported in this paper is composed of two parts: (i) studies on CO₂ sorption stability and (ii) hydrogen production performance using a multifunctional catalyst (nickel catalyst over calcium aluminate sorbent). Performances of modified sorbents produced by adding compounds of Ni²⁺ or Al³⁺ into CaO have been investigated in terms of CO₂ sorption capacity, sorption/desorption stability over 10 cycles in the fixed bed reactor. The hydrogen production and stability of the multifunctional catalyst over 5 reaction cycles are tested using the sorption enhanced steam reforming of biogas reaction.

6.1 CO₂ sorption/desorption testing of Ni- and Al-modified CaO sorbents

The performance of CaO as a sorbent in H₂ production was improved by incorporation of metal ions to enhance stability of the sorbent. In this section, the modified sorbents, Ni-CaO-HW and Al-CaO-HW, were tested for CO₂ sorption/desorption for 10 cycles. The results shown in Figure 6.1 indicate that the CO₂ sorption capacity increases from 0.275 g_{CO₂} / g_{sorbent} and 0.238 g_{CO₂} / g_{sorbent} in the 1st

cycle to $0.287 \text{ g}_{\text{CO}_2} / \text{g}_{\text{sorbent}}$ and $0.242 \text{ g}_{\text{CO}_2} / \text{g}_{\text{sorbent}}$ in the 2nd cycle for Ni-CaO-HW and Al-CaO-HW, respectively. After the 2nd cycle, the CO₂ sorption capacities slightly decreases to $0.276 \text{ g}_{\text{CO}_2} / \text{g}_{\text{sorbent}}$ and $0.227 \text{ g}_{\text{CO}_2} / \text{g}_{\text{sorbent}}$ in the 10th cycle for Ni-CaO-HW and Al-CaO-HW, respectively. The reason for the increase in CO₂ sorption capacity observed for the 2nd cycle is not yet clear; however, this behavior is in agreement with other literature data reported [34, 69, 70]. After 10 cycle tests, the CO₂ sorption capacity decreases slightly by about 4% for Ni-CaO-HW and 6% for Al-CaO-HW, which is significantly less than that of CaO of which the sorption capacity decreases by 37% as reported by Phromprasit *et al.* [71]. However, the slight decrease of CO₂ sorption capacity observed with Ni-CaO-HW and Al-CaO-HW is likely caused by partial densification of CaCO₃ as evidenced in Figure 6.2, resulting in pore closure [32], surface area reduction [31] and an increase of intraparticle diffusion resistance [34].

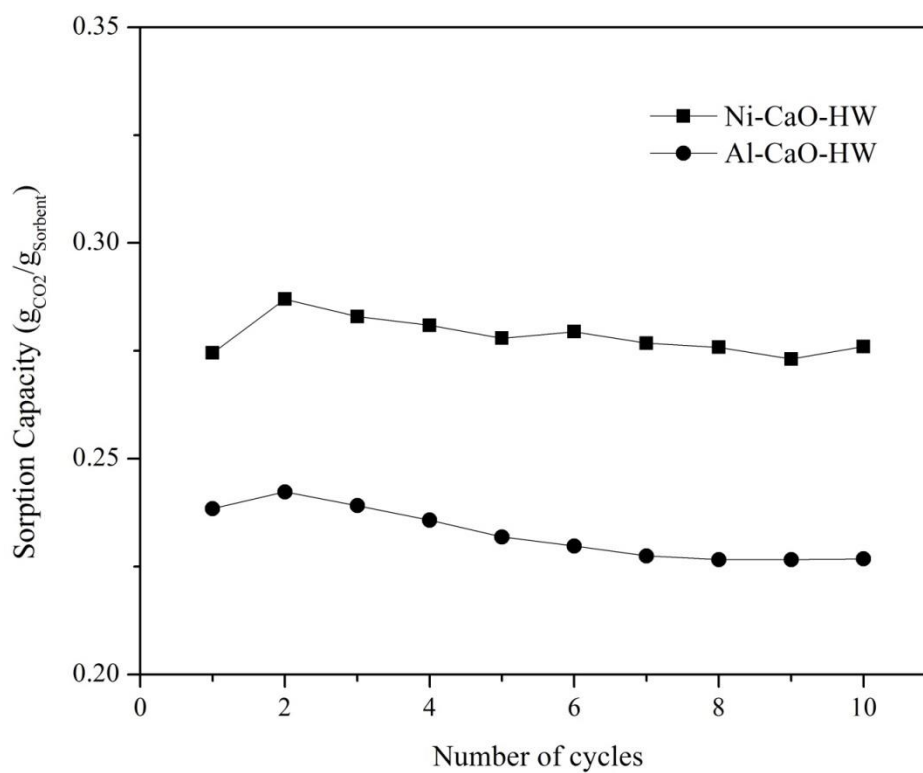


Figure 6.1 Sorption capacity of Ni-CaO-HW and Al-CaO-HW at 600 °C, 1 atm and CO₂ concentration of 15% v/v for different sorption/desorption cycles.

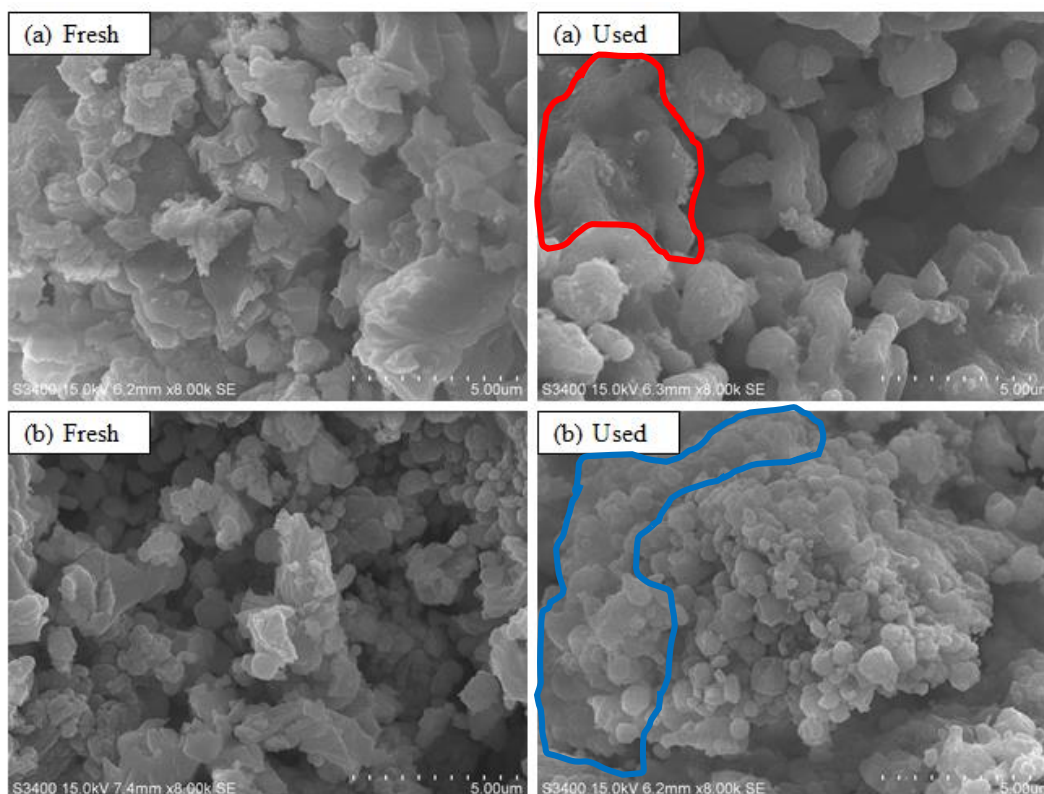


Figure 6.2 SEM images of (a) Ni-CaO-HW and (b) Al-CaO-HW freshly prepared and after 10 CO₂ sorption/desorption cycles.

As supported by the SEM images, the BET surface area analysis results show a decrease in surface area between the 1st and the 10th cycles (30.7 and 15.1 m²/g (fresh sorbent) to 17.1 and 12.4 m²/g (used sorbent) for Ni-CaO-HW and Al-CaO-HW, respectively). CO₂ sorption capacity of Ni-CaO-HW is higher than that of Al-CaO-HW and this is due to a higher content of CaO as Ni-CaO-HW consists of separate phases of NiO and CaO while Al-CaO-HW shows complex phases of Ca₁₂Al₁₄O₃₃ and CaO as evidenced by XRD results depicted in Figure 6.3. There was no significant difference in crystallite sizes for the fresh and used CaO (46.6 nm and 50.9 nm for fresh Ni-CaO-HW and used

Ni-CaO-HW, respectively, and 54.0 nm and 50.5 nm for fresh and used Al-CaO-HW. It is believed that the decrease in the sorption capacities was caused by partial densification of particles as confirmed by SEM-EDS images (Figure 6.4).

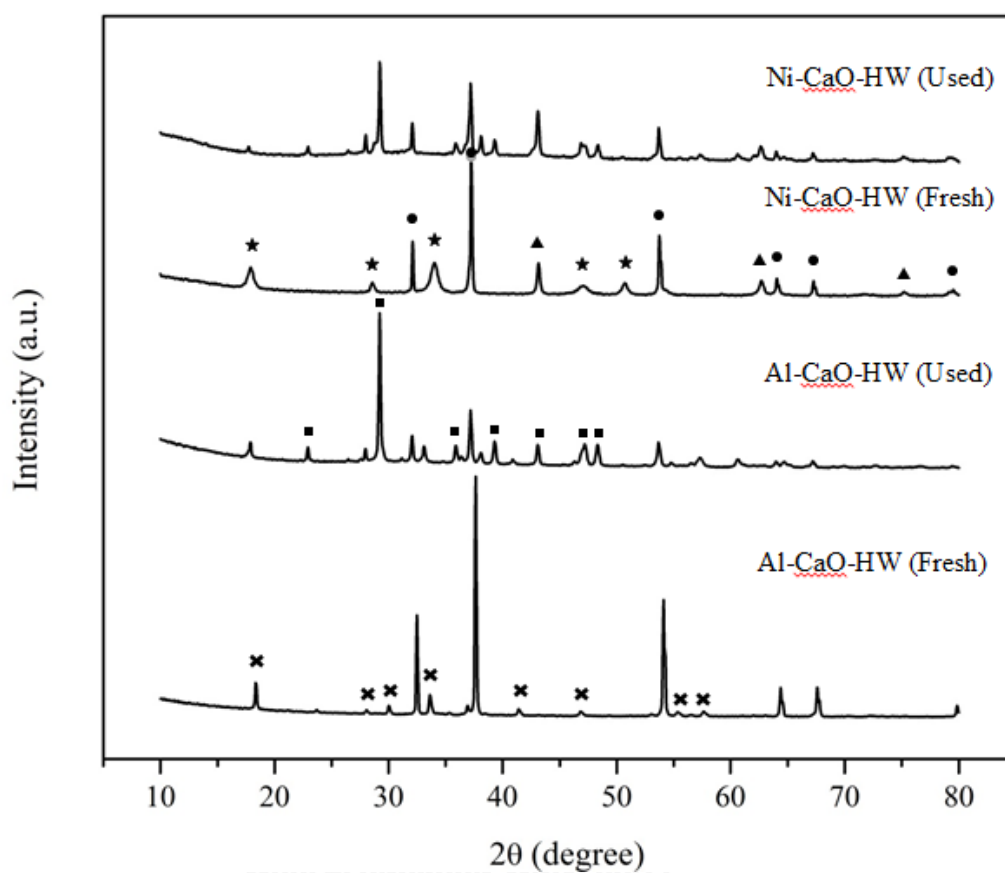


Figure 6.3 XRD pattern of modified sorbents Al-CaO-HW and Ni-CaO-HW: ● CaO,

★ Ca(OH)_2 , ▲ NiO, ✕ $\text{Ca}_{12}\text{Al}_{14}\text{O}_{33}$ and ■ CaCO_3 .

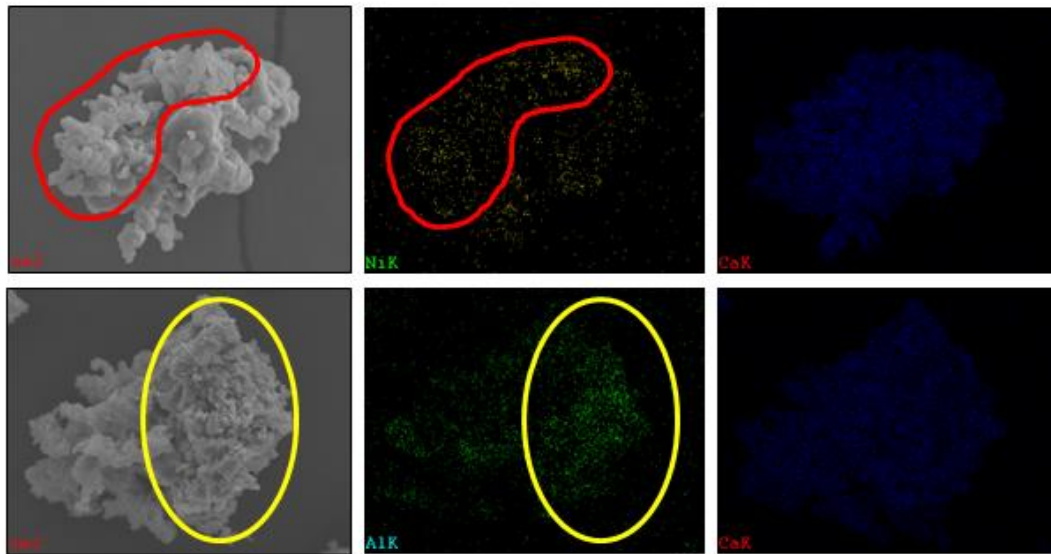


Figure 6.4 SEM-EDS images of (a) Ni-CaO-HW and (b) Al-CaO-HW after 10 CO₂ sorption/desorption cycles.

6.2 H₂ production by using multifunctional catalysts

As shown in section 6.1, both NiO and Ca₁₂Al₁₄O₃₃ can enhance the stability of CaO sorbent for high-temperature CO₂ sorption. As a consequence, the incorporation of metal ions into CaO was further tested for the sorption enhanced steam reforming process in this section.

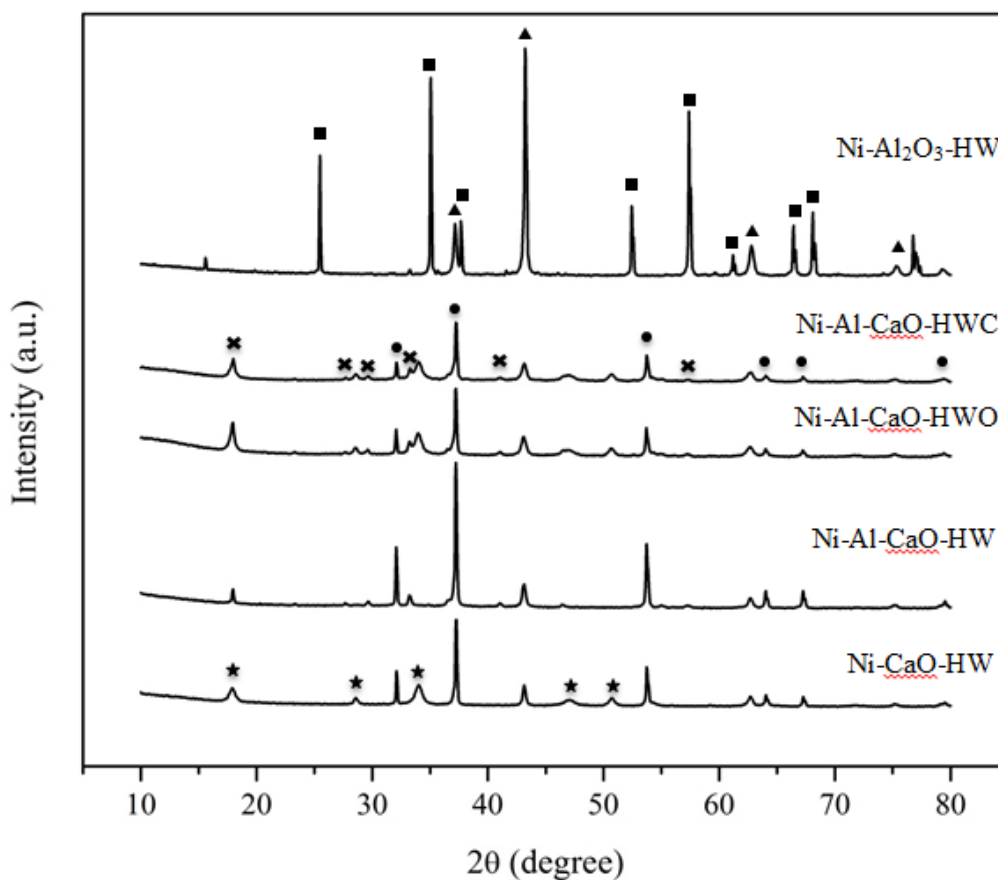


Figure 6.5 XRD pattern of different catalytic sorbents: ● CaO, ★ Ca(OH)₂,

▲ NiO, ✕ Ca₁₂Al₁₄O₃₃ and ■ Al₂O₃.

XRD patterns of different catalytic sorbents shown in Figure 6.5 reveal that the addition of Ni²⁺ results in Ni-CaO-HW and Ni-Al₂O₃-HW possessing separate phases of NiO, CaO and Ca(OH)₂ in the case of Ni-CaO-HW, and NiO and Al₂O₃ in the case of Ni-Al₂O₃-HW. On the other hand, a complex phase of Ca₁₂Al₁₄O₃₃ was formed in the presence of CaO and NiO when Al³⁺ ions were added into CaO as observed with Ni-Al-CaO-HW, Ni-Al-CaO-HWO and Ni-Al-CaO-HWC. Note that the observed Ca(OH)₂ phase was plausibly formed when CaO is exposed to atmospheric moisture. The crystallite

size of CaO for all samples did not differ significantly (46-51 nm) as shown in Table 6.1 Ni-Al-CaO-HW, Ni-Al-CaO-HWO and Ni-Al-CaO-HWC possess lower BET surface areas than Ni-CaO-HW, which could be explained by the presence of Al³⁺ in the CaO leading to the blockage of pores, resulting in reduced surface area and pore volume. Furthermore, Ni-Al-CaO-HWC exhibits a lower surface area than that of Ni-Al-CaO-HW and Ni-Al-CaO-HWO. This result is plausibly caused by the sequence of Ni²⁺ loading after formation of the modified sorbent (Ca₁₂Al₁₄O₃₃).

Table 6.1 BET surface areas and crystallite sizes of different catalytic sorbents.

Sample	BET surface area (m ² /g)	Pore size (nm)	Pore volume (cm ³ /g)	Crystallite size of CaO (nm)
Ni-CaO-HW	35.9	5.0	0.08	50.7
Ni-Al-CaO-HW	14.1	7.9	0.04	51.7
Ni-Al-CaO-HWO	18.3	7.9	0.06	46.3
Ni-Al-CaO-HWC	8.9	20.4	0.05	47.4

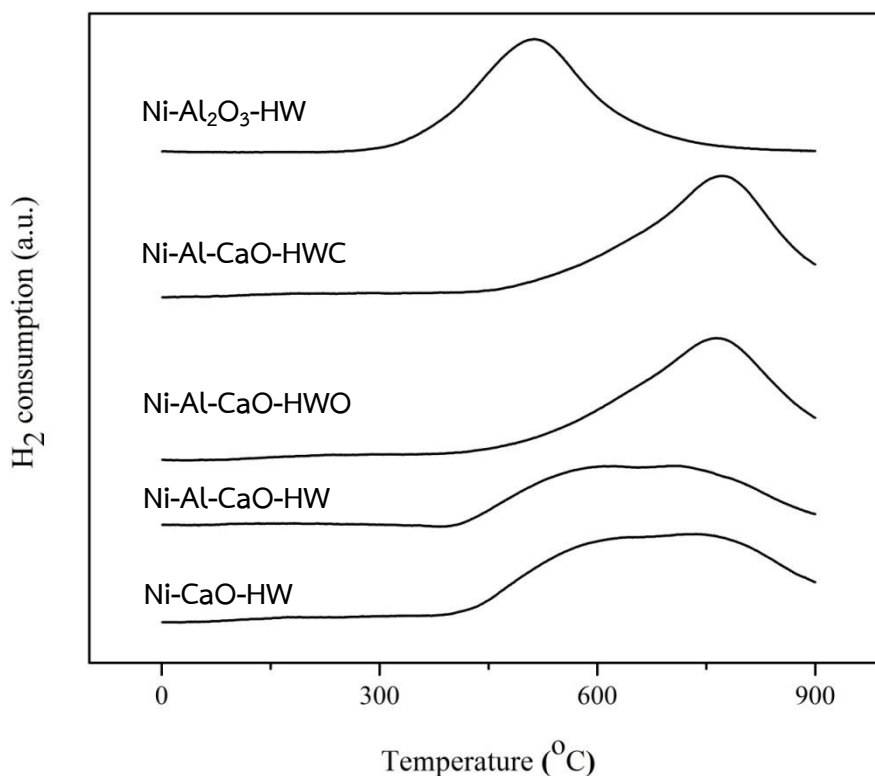


Figure 6.6 Temperature programmed reduction (TPR) profiles of Ni over multifunctional catalytic sorbents.

The reducibility of the multifunctional catalysts, which were synthesized by hydration followed by wet mixing, was tested by temperature program reduction (TPR) as shown in Figure 6.6. Ni-CaO-HW and Ni-Al-CaO-HW, which were fabricated in only a single synthesis step, show two peaks including (i) small peak at 560 °C, which could be a result of free NiO reduction [72], and (ii) larger peak at 720 °C, which could be attributed to Ni-Ca oxide interactions. Ni-Al-CaO-HWO and Ni-Al-CaO-HWC - fabricated in two synthesis steps - show only a single peak at 760 °C, which is probably due to the spinel phase of NiAl_2O_4 [72]. According to the results, Ni-Al-CaO-HWO and Ni-Al-CaO-HWC are more difficult to be reduced than Ni-CaO-HW and Ni-Al-CaO-HW, which

implies that NiO-Ca₁₂Al₁₄O₃₃ interactions formed by the two-step synthesis are stronger than that of NiO-Ca₁₂Al₁₄O₃₃ or NiO-CaO interactions synthesized in a single step. A reduction temperature of 850 °C, which is higher than the highest peak temperature, was therefore chosen to ensure the complete reduction of Ni with 10% v/v H₂ in N₂.

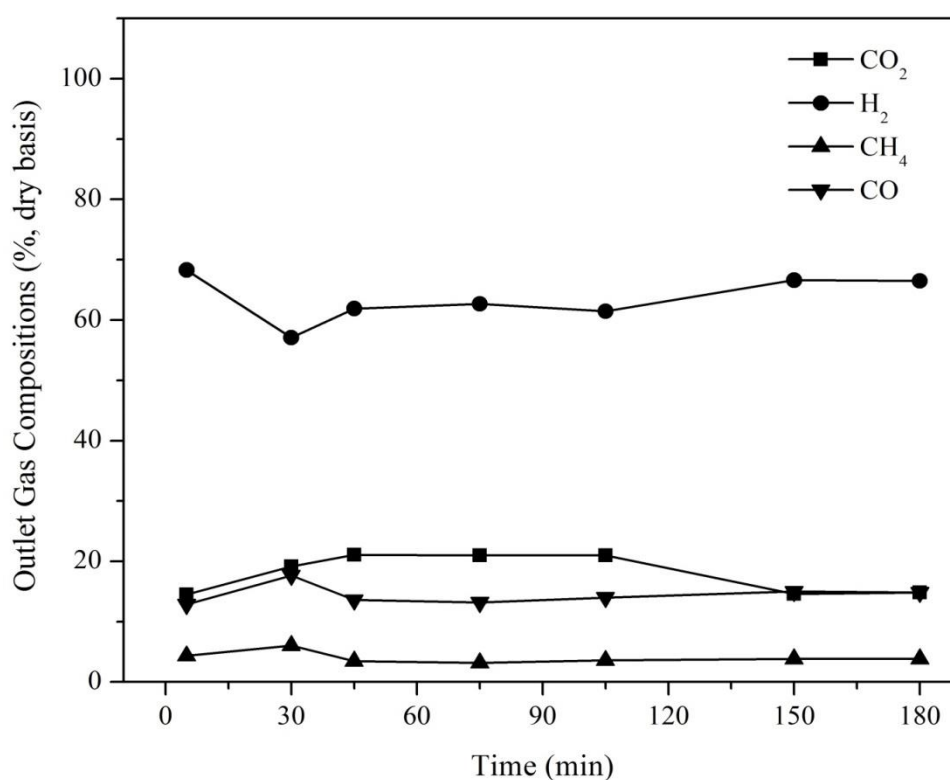


Figure 6.7 The performance of Ni-Al₂O₃-HW for hydrogen production from sorption enhanced steam reforming of biogas.

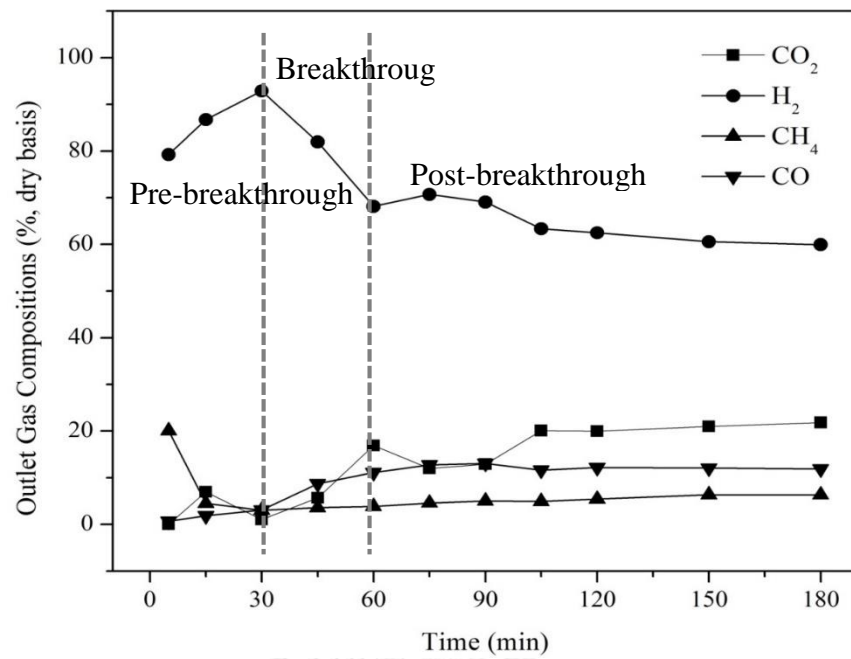


Figure 6.8 The performance of Ni-CaO-HW for hydrogen production from sorption enhanced steam reforming of biogas.

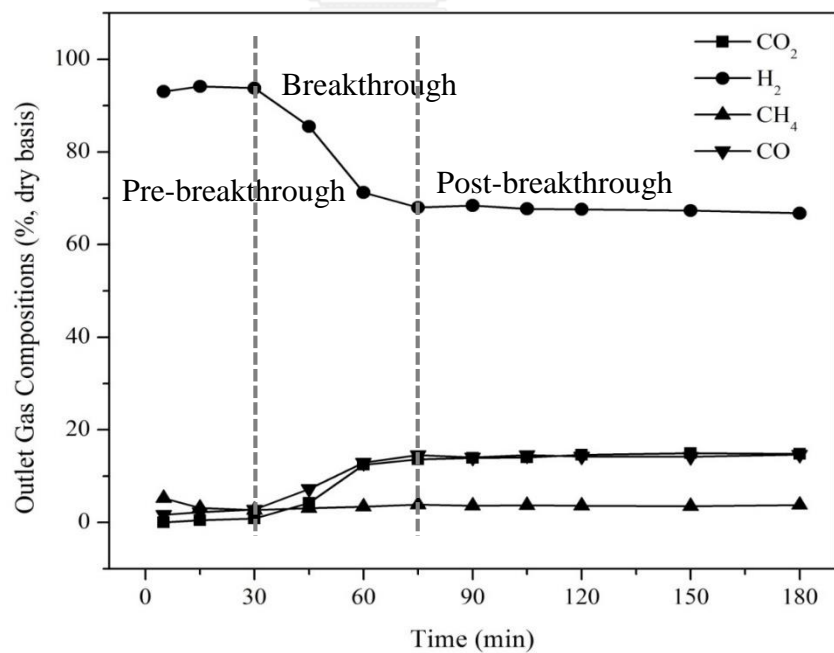


Figure 6.9 The performance of Ni-Al-CaO-HW for hydrogen production from sorption enhanced steam reforming of biogas.

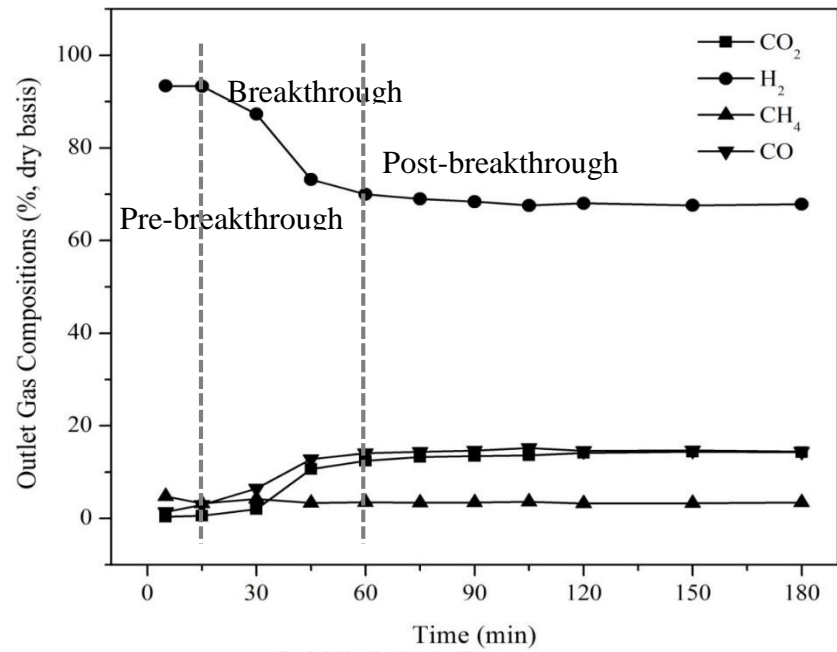


Figure 6.10 The performance of Ni-Al-CaO-HWO for hydrogen production from sorption enhanced steam reforming of biogas.

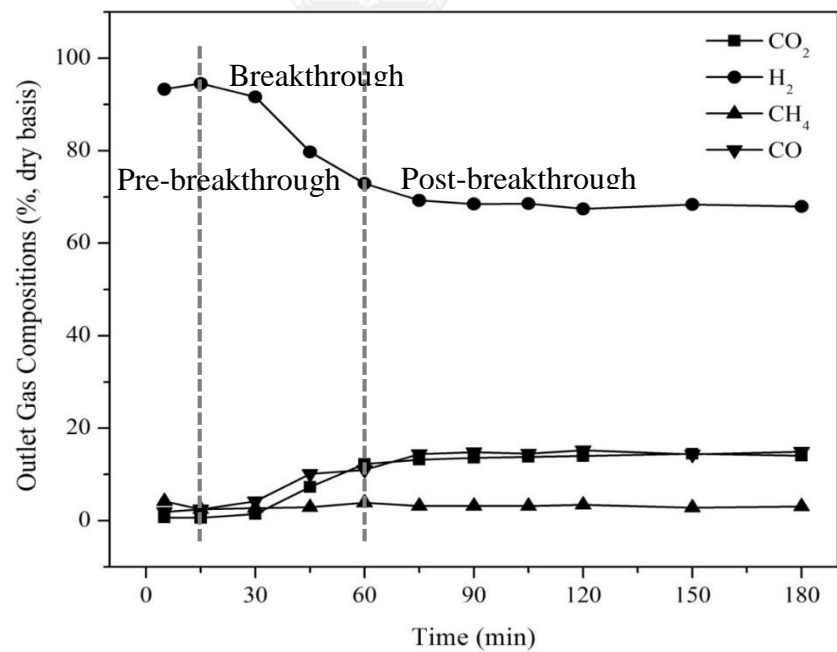


Figure 6.11 The performance of Ni-Al-CaO-HWC for hydrogen production from sorption enhanced steam reforming of biogas.

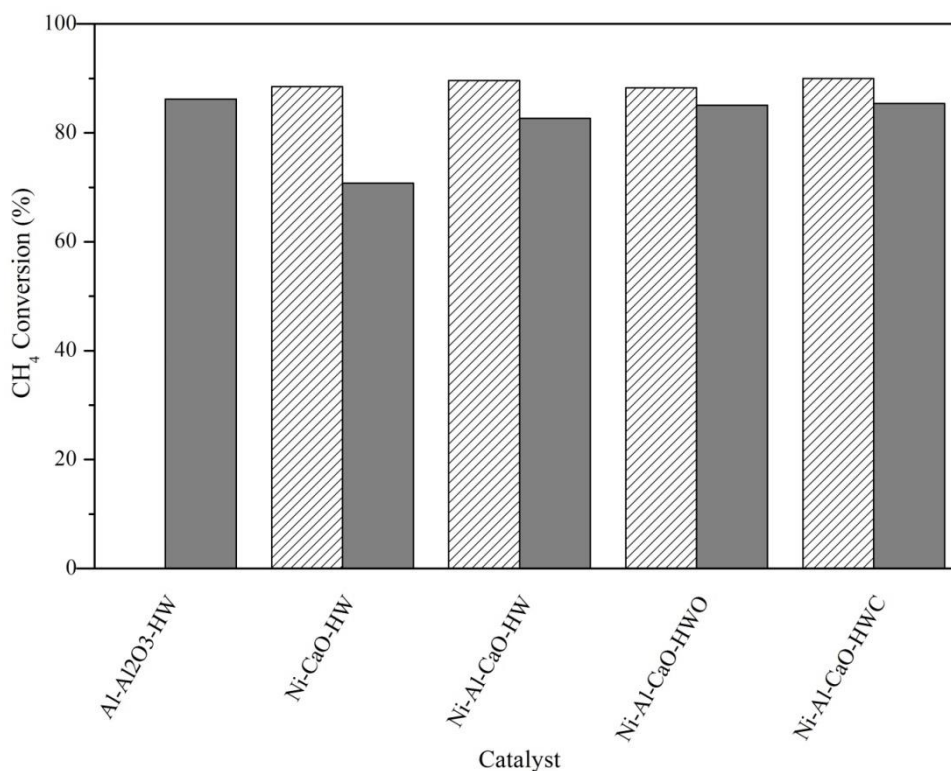




Figure 6.12 CH₄ conversions of Ni-Al₂O₃-HW, Ni-CaO-HW, Ni-Al-CaO-HW, Ni-Al-CaO-HWO and Ni-Al-CaO-HWC ( refers the pre-breakthrough period and  refers the post-breakthrough period).

Commercial catalyst Ni-Al₂O₃-HW was tested for use in hydrogen production via steam reforming of biogas as a base case as shown in Figure 6.7. The results show that approximately 67% hydrogen purity (Figure 6.7) and 88% CH₄ conversion (Figure 6.8) were achieved. Figure 6.12 shows the performance of Ni-CaO-HW for sorption enhanced biogas steam reforming. The results show that during the pre-breakthrough period the hydrogen purity increases from 79% to 93%, and after a further 30 min the CH₄ conversion was 91% as shown in Figure 6.12. As the reaction time progressed, CaO sorbent was gradually converted into CaCO₃ due to the reaction with CO₂, leading to

an increase of CO₂ concentration and hence a decrease of H₂ concentration in the product stream. After that, the H₂ purity dropped to equilibrium in the breakthrough period (approx. 68% H₂ purity and 87% CH₄ conversion at 60 min). The Ni-CaO-HW performance decreased with (i) H₂ purity dropping to 60% at 180 min and (ii) CH₄ conversion decreasing to 78% at 180 min. This is plausible because the catalyst lost its active sites as confirmed by XPS results shown in Table 6.2. The concentration of Ni at the surface decreased from 1.99% on the fresh catalyst (the binding energy of 854.8 eV indicated the formation of NiO) to 1.05% on the used catalyst (0.46% Ni and 0.56% NiO). The decrease in the number of active sites is plausible because a result of pore closure due to the formation of CaCO₃, confirmed by SEM images (Figure 6.13). Figure 6.13(a) suggests that CaCO₃ expansion is caused by densification resulting in the loss of active sites (Ni)

Al³⁺ ion is used to dope CaO in order to improve the thermal stability by the formation of an inert phase (Ca₁₂Al₁₄O₃₃). The sequence of Ni loading on to CaO to produce the modified sorbent (Ca₁₂Al₁₄O₃₃-CaO) was tested in order to investigate the effect on sorbent and hydrogen production performances. Figure 6.9 and Figure 6.12 show the performance of Ni-Al-CaO-HW on H₂ purity and CH₄ conversion. The results show that 94% H₂ purity and 90% CH₄ conversion could be obtained during the pre-breakthrough period. The pre-breakthrough time was 30 min, indicating that Ni-Al-CaO-HW can absorb CO₂ for 30 min. After that, CO₂ concentrations increases and remains constant in the post-breakthrough period. Meanwhile, H₂ purity decreased after 30 min

(breakthrough) and remained constant at 68% after the breakthrough period. The steady H₂ and CO₂ concentrations in the post-breakthrough period suggested that the sorbent can retain its original morphology as shown in Figure 6.13(b). Furthermore, the Ni-Al-CaO-HW result shows an increase in H₂ purity of 26% and an increase in CH₄ conversion of 5% between the pre-breakthrough and the post-breakthrough period.

Table 6.2 XPS analysis results of the multifunctional catalysts.

Sample	Binding Energy of Ni (eV)	Atomic concentration of elements on surface (%)			
		Ni 2p	O 1s	Ca 2p	Al 2p
Ni-CaO-HW	854.8	1.99	84.67	13.34	-
Ni-CaO-HW (Used)	853.1 854.7	0.49 0.56	89.56	9.39	-
Ni-Al-CaO-HW	854.6	2.56	82.54	11.55	3.35
Ni-Al-CaO-HWO	856.4	2.04	80.87	11.70	5.39
Ni-Al-CaO-HWC	857.2	2.89	80.83	10.10	6.18

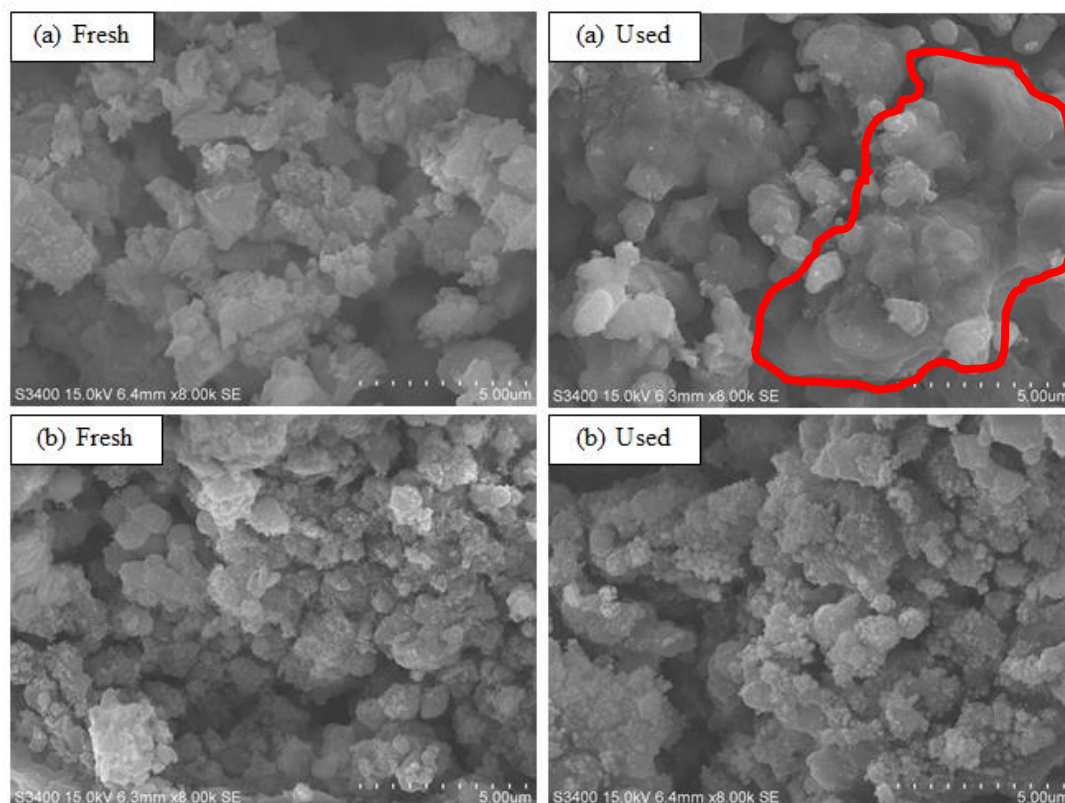


Figure 6.13 SEM images of multifunctional catalysts: (a) Ni-CaO-HW and
(b) Ni-Al-CaO-HW.

In the case of Ni-Al-CaO-HWO, 93% H₂ purity can be obtained (Figure 6.10) and the CH₄ conversion of 88% (Figure 6.12) was achieved in the pre-breakthrough period. The pre-breakthrough time of Ni-Al-CaO-HWO (15 min) was lower than that of Ni-Al-CaO-HW (30 min). Hence Ni-Al-CaO-HWO has a poorer CO₂ sorption performance than Ni-Al-CaO-HW. Previously, the XRD results indicated the formation of Ca₁₂Al₁₄O₃₃ phase in the presence of Al³⁺. The higher atomic concentration of Al at the surface of Ni-Al-CaO-HWO (Table 6.2) therefore suggests the presence of the inert phase (Ca₁₂Al₁₄O₃₃) is higher than that of Ni-Al-CaO-HW, resulting in reduced CO₂ sorption performance.

The performances of Ni-Al-CaO-HWC are shown in Figure 6.11 and Figure 6.12. The H₂ purity of 92% and CH₄ conversion of 90% were achieved in the pre-breakthrough period. The pre-breakthrough time of Ni-Al-CaO-HWC (15 min) is lower than that of Ni-Al-CaO-HW for the same reasons discussed in the case of Ni-Al-CaO-HWO.

It is suggested that the best sequence for loading Ni²⁺ on a modified sorbent (Ca₁₂Al₁₄O₃₃) is the single-step synthesis method, used to produce Ni-Al-CaO-HW. Low concentration of Al atomic at the surface, which indicates that Al can well disperse in the bulk of CaO, leads to the best CO₂ sorption performance. This performance is also confirmed by the longer pre-breakthrough period of Ni-Al-CaO-HW when compared with other samples. From these results, we therefore extended the investigation of the catalytic sorbent performance of Ni-Al-CaO-HW for the production of hydrogen under multiple cycles.

6.3 Stability of multifunctional catalyst

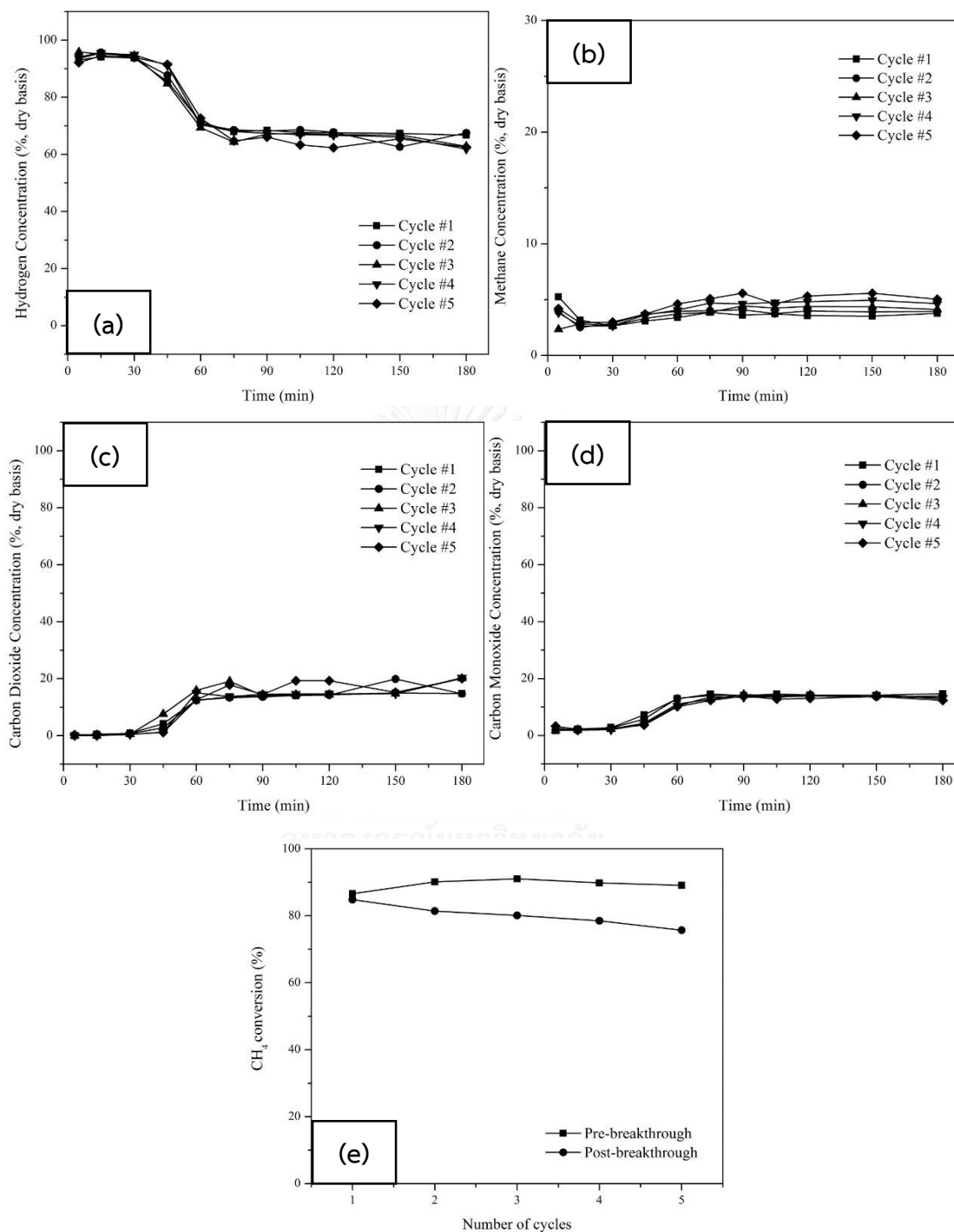


Figure 6.14 Gas product compositions and CH_4 conversion of Ni-Al-CaO-HW sample:

(a) hydrogen concentration, (b) methane concentration, (c) carbon dioxide concentration, (d) carbon monoxide concentration and (e) CH_4 conversion.

The stability of the multifunctional catalyst Ni-Al-CaO-HW over 5 cycles of biohydrogen production produced by sorption enhanced biogas steam reforming is shown in Figure 6.14. The results show that H₂ purity and CH₄ conversion can be maintained at about 94% and 90% in the pre-breakthrough period, respectively. However, during the post-breakthrough period, H₂ purity and CH₄ conversion decreases from 68% (1st cycle) to 64% (5th cycle) and from 85% (1st cycle) to 75% (5th cycle), respectively. A plausible explanation for the reduction of H₂ purity and CH₄ conversion in the post-breakthrough period is the formation of CaCO₃, which leads to pore blockage, reducing the number of active sites as indicated by the XPS results shown in Table 6.3. The binding energy of 854.6 eV for the fresh catalyst indicated that 2.56% of the atomic concentration of Ni at the surface is in the form of NiO. According to XPS results, after the 1st and the 5th cycles, the used catalysts contained two Ni species, one at (i) 852 – 853 eV attributed to metallic Ni and another at (ii) 855 – 856 eV attributed to NiAl₂O₄. These results suggested that the total concentration of Ni was reduced as the number of sorption/desorption cycles increases (2.56% Ni from the fresh catalyst decreased to 2.36 and 1.45% after the 1st cycle and the 5th cycle, respectively).

Table 6.3 XPS analysis results of Ni-Al-CaO-HW catalyst.

Sample	Binding energy of Ni (eV)	Atomic concentration on surface (%)			
		Ni 2p	O 1s	Ca 2p	Al 2p
Fresh	854.6	2.56	82.54	11.55	3.35
Used (1 st cycle)	852.8	0.44	83.64	9.16	4.84
	856.4	1.92			
Used (5 th cycle)	853.1	0.43	83.69	10.22	4.64
	855.7	1.02			

As shown above from our results that Ni-Al-CaO-HW provides a good performance for sorption enhanced hydrogen production from biogas both in terms of catalytic/sorption performance and stability. This might be due to well dispersed Al in the multifunctional catalyst as shown in Figure 6.15, which results in high CO₂ sorption capacity and stability. We proposed here the mechanism of H₂ production with the use of Ni-Al-CaO-HW with the comparison to the case of Ni-CaO-HW as shown in Figure 6.12. For Ni-Al-CaO-HW (Figure 6.16(a) pre-breakthrough), CH₄ and H₂O feed are adsorbed at the surface of Ni site and produced H₂ and CO₂ while CaO absorbs CO₂ both from the feed stream and from the steam reforming reaction enhancing hydrogen production yield and also high purity of H₂ in the product stream. Hydrogen production

was found to decrease in the post-breakthrough period due to part of the sorbent CaO has interacted with CO₂ and formed inactive phase of CaCO₃ as shown in Figure 6.16(a) post-breakthrough (1st cycle). At this stage, the concentration of H₂ in the product stream can be maintained for a long period of time because the densification and pore closure are inhibited by inert phase (Ca₁₂Al₁₄O₃₃). However, slight reduction of H₂ production over 5-cycle reused is attributed to partial densification of sorbents leading to the hindrance of Ni active site as shown in Figure 6.16(a) post-breakthrough (5th cycle). The good impact of adding metal into catalytic sorbent Ni-Al-CaO-HW is compared with that without metal Ni-CaO-HW as pictured in Figure 6.16(b), where lower H₂ production performance was obtained due to densification effect of CaCO₃.

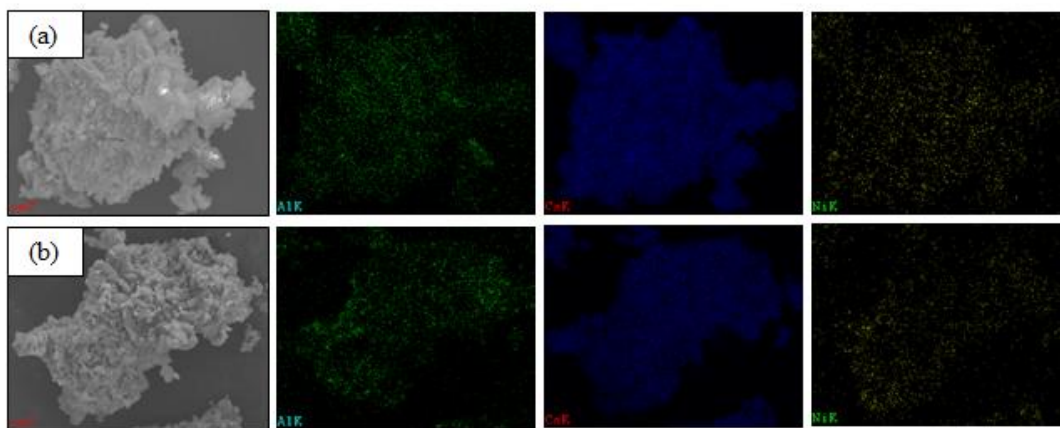


Figure 6.15 SEM-EDS images of Ni-Al-CaO-HW: (a) fresh and (b) used catalyst.

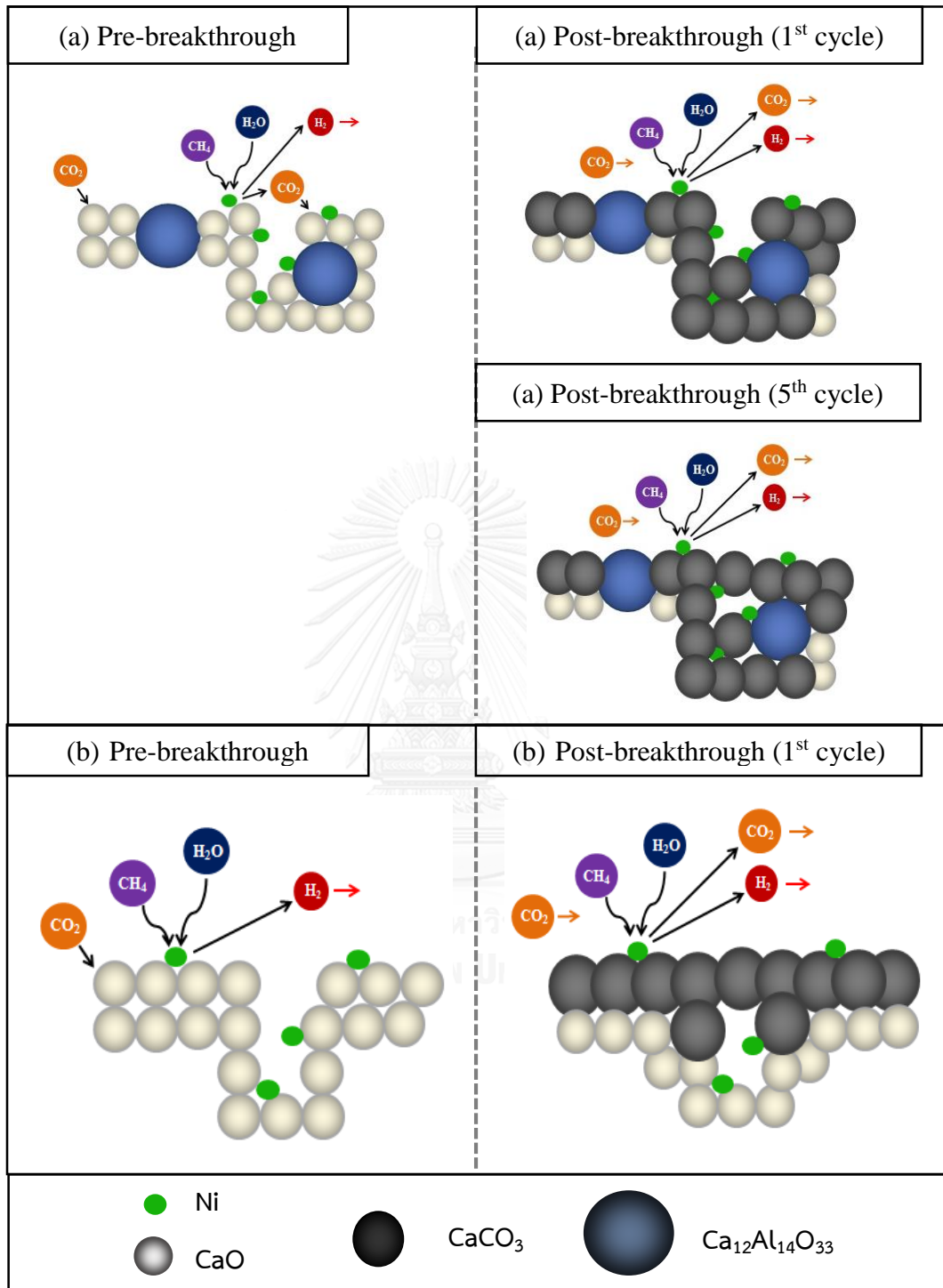


Figure 6.16 Schematic diagram of our proposed sorption enhanced H₂ production mechanism of (a) Ni-Al-CaO-HW and (b) Ni-CaO-HW at pre-breakthrough and post-breakthrough periods.

6.4 Effect of ultrasonic assistant in preparation method for CO₂ sorption/ desorption multiple cycles

The sorbent stabilities are shown in Figure 6.17. The modified sorbent (Al-CaO-UHW) showed stable CO₂ sorption capacity (approx. 0.28 g_{CO₂} / g_{sorbent}), while Al-CaO-HW showed a slight decrease of about 6% over 10 cycles. Furthermore, the CO₂ sorption capacity of Al-CaO-UHW is higher than Al-CaO-HW plausibly because Al-CaO-UHW has lower Al atomic concentration at the surface than Al-CaO-HW as shown in Table 6.4. This implies that at the surface of Al-CaO-UHW the sample has lower Ca₁₂Al₁₄O₃₃ inert phase. The high concentration of Ca₁₂Al₁₄O₃₃ phase at the surface might suppress carbonation reaction, which reduced the CO₂ sorption capacity.

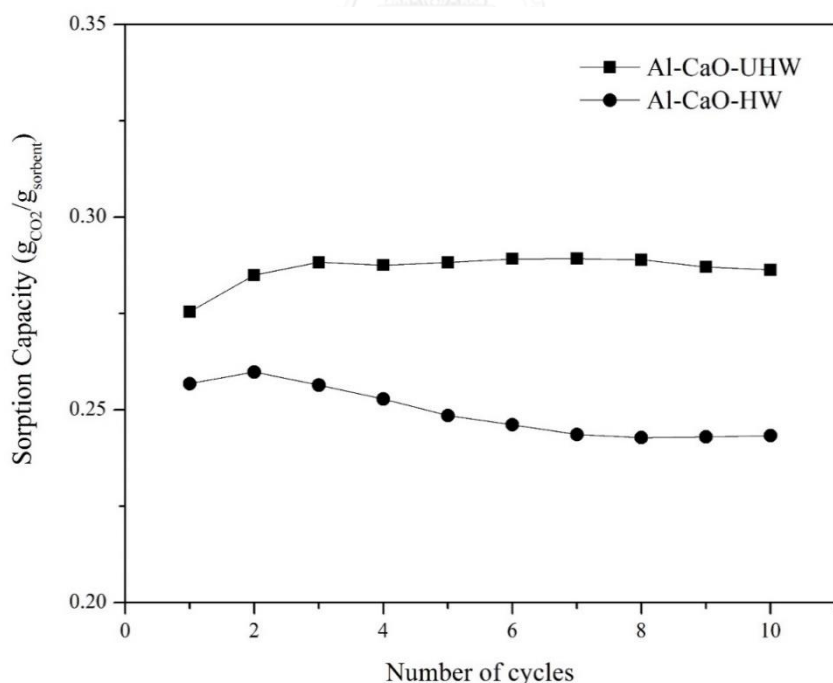


Figure 6.17 CO₂ sorption capacity using Al-CaO-HW and Al-CaO-UHW for 10 cycle operations.

Table 6.4 Atomic concentrations at the surface of modified sorbents.

Sample	Atomic concentration of elements on surface (%)		
	O 1s	Ca 2p	Al 2p
Al-CaO-HW	81.62	9.64	8.73
Al-CaO-UHW	82.83	11.76	5.41

6.5 Performance of multifunctional catalysts with/without ultrasonic assistant

The multifunctional catalysts with/without ultrasonic assistant in the preparation step (Ni-Al-CaO-HW and Ni-Al-CaO-UHW) were tested for H₂ production from sorption enhanced steam reforming of biogas as shown in Figure 6.18. The results indicated that H₂ purity is not different in pre-breakthrough period. In addition, the H₂ purity is maintained approximately 90% over 5 cycle operations. However, the CH₄ conversions by using Ni-Al-CaO-HW and Ni-Al-CaO-UHW showed the same trend which is decreased when increasing a number of cycles in pre-breakthrough and post-breakthrough period. This is possibly due to the amount of active site at the surface

of multifunctional catalysts are decreased when compared between at 1st cycle and 5th cycle as shown in Table 6.5 by pore closure from CaCO_3 formation.

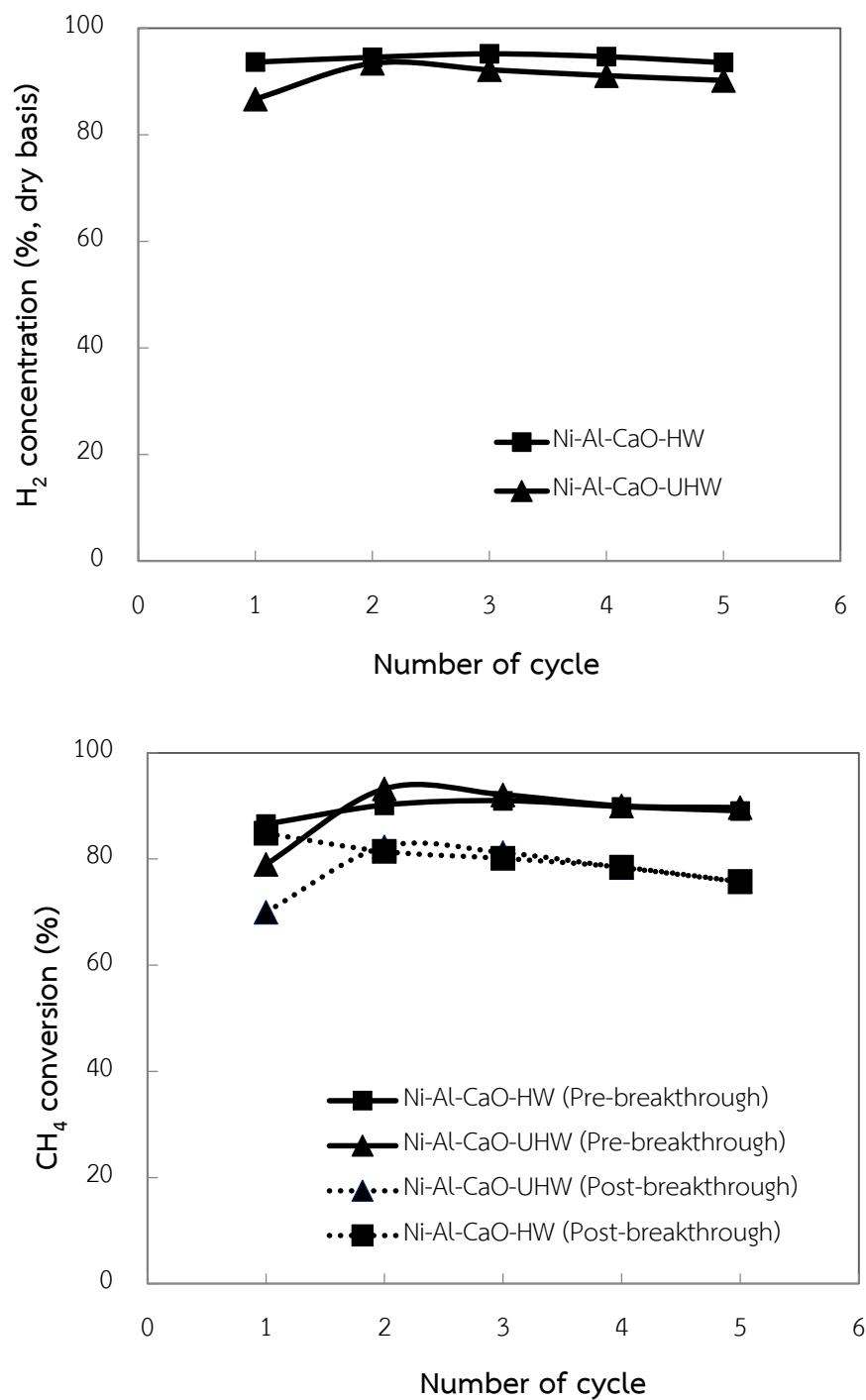


Figure 6.18 H₂ concentration and CH₄ conversion of Ni-Al-CaO-HW and Ni-Al-CaO-UHW.

Table 6.5 XPS analysis of Ni-Al-CaO-HW and Ni-Al-CaO-UHW before and after reaction.

Sample	Binding Energy of Ni (eV)	Atomic concentration of elements on surface (%)			
		Ni 2p	O 1s	Ca 2p	Al 2p
Ni-Al-CaO-HW (Fresh)	854.6	2.56	82.54	11.55	3.35
	853.1	0.43			
Ni-Al-CaO-HW (Used)	855.7	1.02	83.69	10.22	4.64
Ni-Al-CaO-UHW (Fresh)	855.8	3.12	79.18	10.40	7.30
Ni-Al-CaO-UHW (Used)	853.7	0.37	82.26	10.41	6.05
	855.8	0.91			

CHAPTER VII

H₂ production from sorption enhanced steam reforming of biogas using multifunctional catalysts of Ni over Zr-, Ce- and La-modified CaO sorbents

The work reported in this paper is composed of two investigations: (i) CO₂ sorption/desorption tests and (ii) H₂ production by sorption enhanced steam reforming of artificial biogas. In the first part, CaO was doped with various metal ions (Zr⁴⁺, Ce⁴⁺ and La³⁺), of which the corresponding metal oxides have Tammann temperatures greater than the calcination temperature (900 °C), by hydration followed by wet mixing and tested over multiple operation cycles. Hydrogen production was conducted with three modified sorbents (Ni-Zr-CaO, Ni-Ce-CaO and Ni-La-CaO).

7.1 CO₂ sorption stability of Zr-, Ce- and La-modified CaO sorbents

XRD patterns of the modified CaO sorbents are shown in Figure 7.1. These results indicate that (i) the Zr-CaO sorbent contained CaO, as well as a complex phase (CaZrO₃) formed by a reaction between CaO and ZrO₂ as shown in Eq. 7.1; (ii) the Ce-CaO sorbent contained separate CaO and CeO₂ phases and (iii) the La-CaO sorbent also contained CaO and La₂O₃ phases. After XRD analysis the sorbents were tested in multiple CO₂ sorption/desorption cycles in the fixed bed quartz reactor.

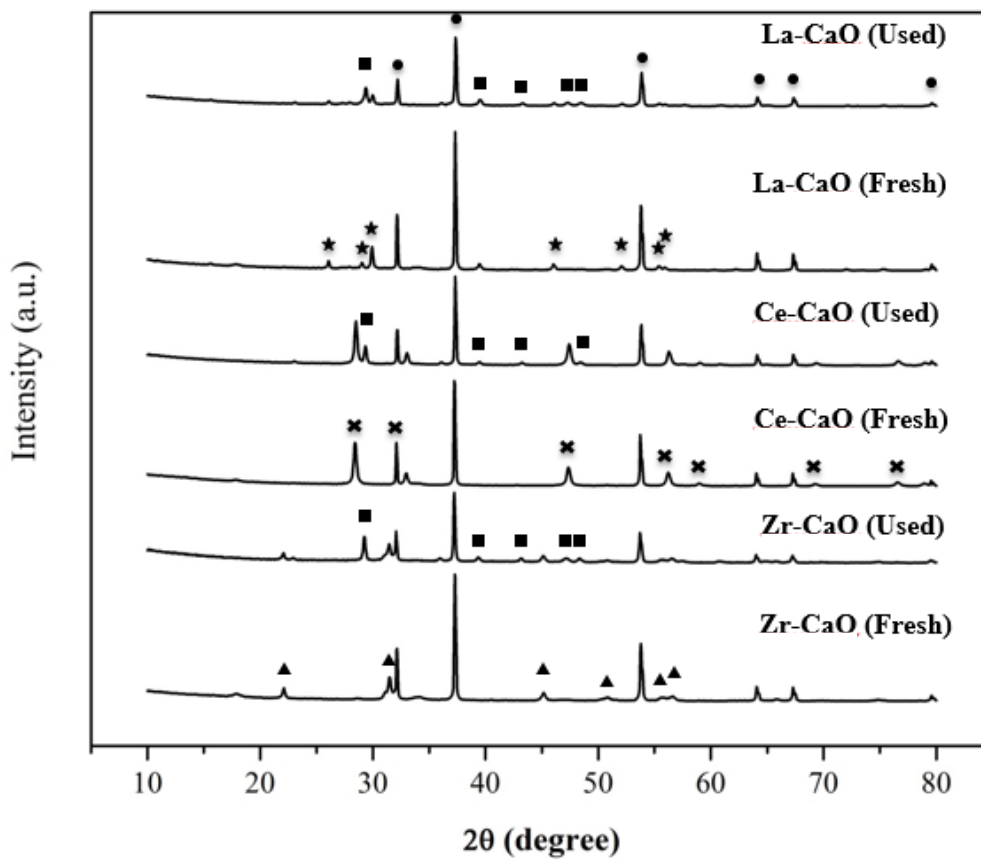
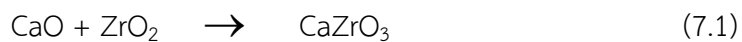


Figure 7.1 XRD patterns of modified sorbents: ● CaO, ■ CaCO₃, ▲ CaZrO₃,
✕ CeO₂ and ★ La₂O₃.

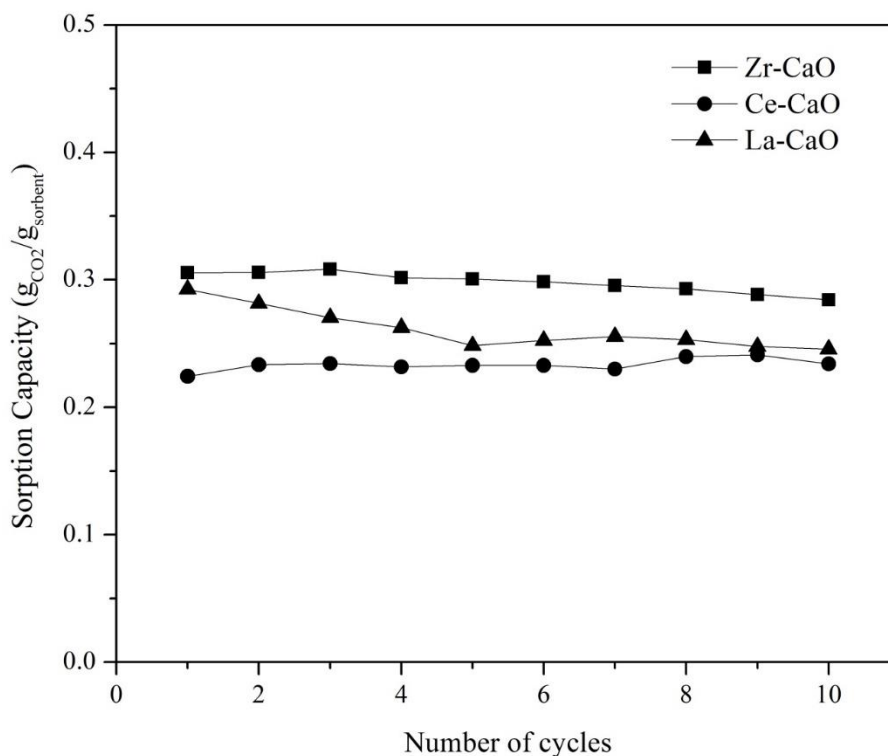


Figure 7.2 CO₂ sorption capacities of Zr⁴⁺, Ce⁴⁺ and La³⁺ modified CaO after the indicated number of sorption/desorption cycles.

The CO₂ sorption/desorption performances of Zr⁴⁺, Ce⁴⁺ and La³⁺ modified CaO are shown in Figure 7.2. The results indicate that the Zr-CaO and Ce-CaO sorbents possess the most stable sorption capacities, with CO₂ capacities of 0.306 and 0.224 g_{CO₂}/g_{Sorbent} after the 1st cycle and 0.284 and 0.234 g_{CO₂}/g_{Sorbent} after the 10th cycle, respectively. However, the La-CaO sorbent exhibited a significant decrease in its CO₂ sorption capacity from 0.293 g_{CO₂}/g_{Sorbent} after the 1st cycle to 0.246 g_{CO₂}/g_{Sorbent} after the 10th cycle, showing a 16% decrease. The decrease in the sorption capacity of La-CaO sorbent is possibly due to the partial densification by the volume expansion of CaCO₃, which results in pore closure as evidenced by the SEM images (Figure 7.3).

Figure 7.3(f) shows an SEM image of the used La-CaO sorbent, which indicates the partial densification (red outline) in comparison with the image of the fresh sample in Figure 7.3(e). In addition, the sintering of CaO was not observed as confirmed by the similar CaO crystallite sizes of both the fresh and used sorbents (Table 7.1).

Although, the Zr-CaO and Ce-CaO sorbents exhibited stable CO₂ sorption capacities over multiple cycles, the partial densification was observed nevertheless. The SEM images of the Zr-CaO (Figure 7.3(a) and (b)) and Ce-CaO (Figure 7.3(c) and (d)) show small partial densification areas. This phenomenon can be explained by the volume expansion due to the formation of CaCO₃, and the subsequent closure of void spaces between particles. However, the Zr-CaO and Ce-CaO sorbents possess a low temperature oxygen storage capability, as characterized by temperature program reduction oxidation (TPRO) (Figure 7.4 and Table 2). The low temperature oxygen storage results in the availability of relatively mobile oxygen atoms compared to the oxygen stored at higher temperatures. This characteristic leads to the promotion of CO₂ diffusion between the surface and bulk of modified CaO. Furthermore, the sorption capacities of Ce-CaO sorbent were shown to be more stable than those of the Zr-CaO sorbent between the 1st and 10th cycle because Ce-CaO has oxygen storage at low temperature of 1.76 mmol/g which is higher than that of Zr-CaO sorbent of 0.04 mmol/g. However, the Zr-CaO sorbent has a higher sorption capacity, which the authors argue is probably due to its higher BET surface area of 17.7 m²/g compared to

that of Ce-CaO of 8.2 m²/g. A higher surface area implies a greater number of active sites for CO₂ sorption. This has been reported in several investigations [111-113].

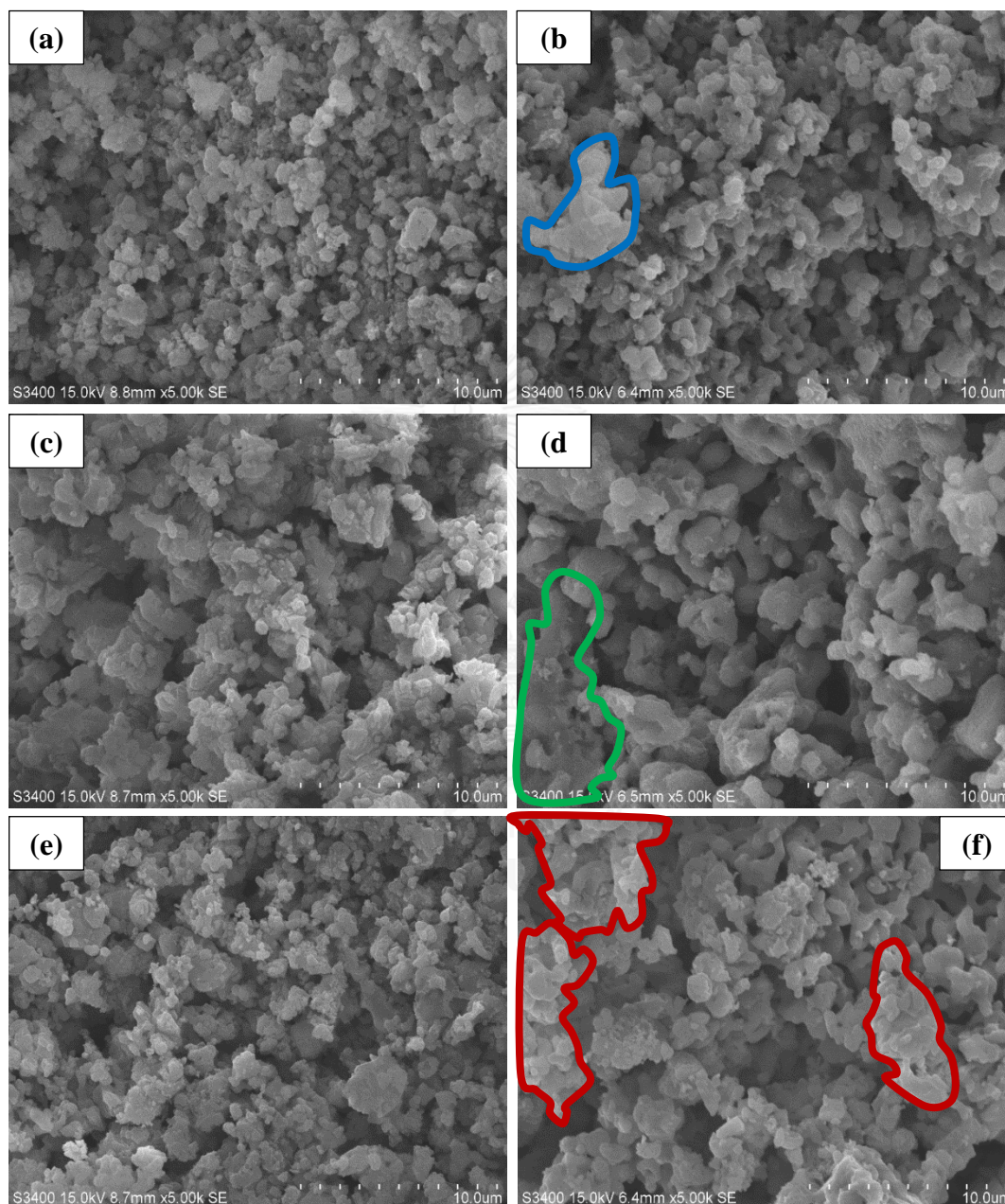


Figure 7.3 SEM images of modified sorbents: (a) Zr-CaO (Fresh), (b) Zr-CaO (Used), (c)

Ce-CaO (Fresh), (d) Ce-CaO (Used), (e) La-CaO (Fresh) and (f) La-CaO (Used).

Table 7.1 Properties of modified sorbents.

Sample	BET surface		Pore size (nm)	Pore volume (cm ³ /g)	Crystallize size (nm)			
	area (m ² /g)				CaO	CaZrO ₃	CeO ₂	La ₂ O ₃
Zr-CaO (Fresh)	17.7		5.62	0.04	55.1	40.2	-	-
Zr-CaO (Used)	-		-	-	53.9	41.6	-	-
Ce-CaO (Fresh)	8.2		9.75	0.03	56.6	-	33.5	-
Ce-CaO (Used)	-		-	-	55.3	-	34.0	-
La-CaO (Fresh)	13.1		6.32	0.03	56.0	-	-	45.4
La-CaO (Used)	-		-	-	53.5	-	-	45.5

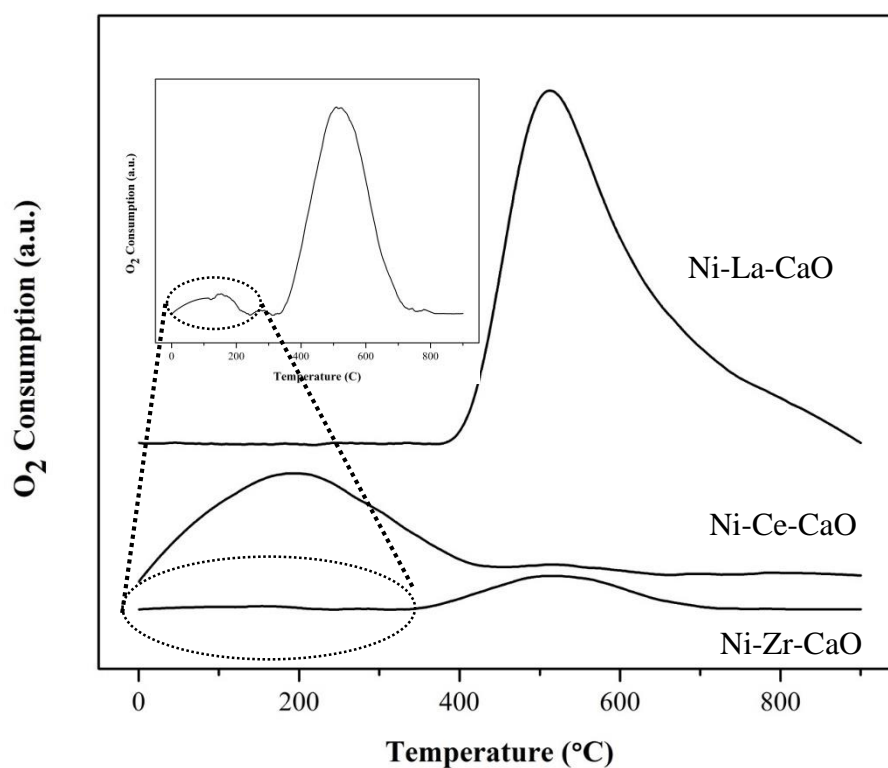


Figure 7.4 O₂ consumption from the temperature-programmed reduction oxidation of Zr⁴⁺, Ce⁴⁺ and La³⁺ modified CaO.

Table 7.2 Oxygen storage capacities of Zr⁴⁺, Ce⁴⁺ and La³⁺ modified CaO.

Sample	OSC* at low	OSC* at high	Total O ₂ OSC* (mmol/g)
	temperature (mmol/g)	temperature (mmol/g)	
Zr-CaO	0.04 (125 °C)	0.46 (520 °C)	0.50
Ce-CaO	1.76 (200 °C)	0.08 (530 °C)	1.84
La-CaO	-	2.08 (510 °C)	4.28
		2.19 (615 °C)	

*OSC refers to oxygen storage capacity (mmol/g)

7.2 H₂ production by using Ni over Zr-, Ce- and La-modified CaO multifunctional catalyst

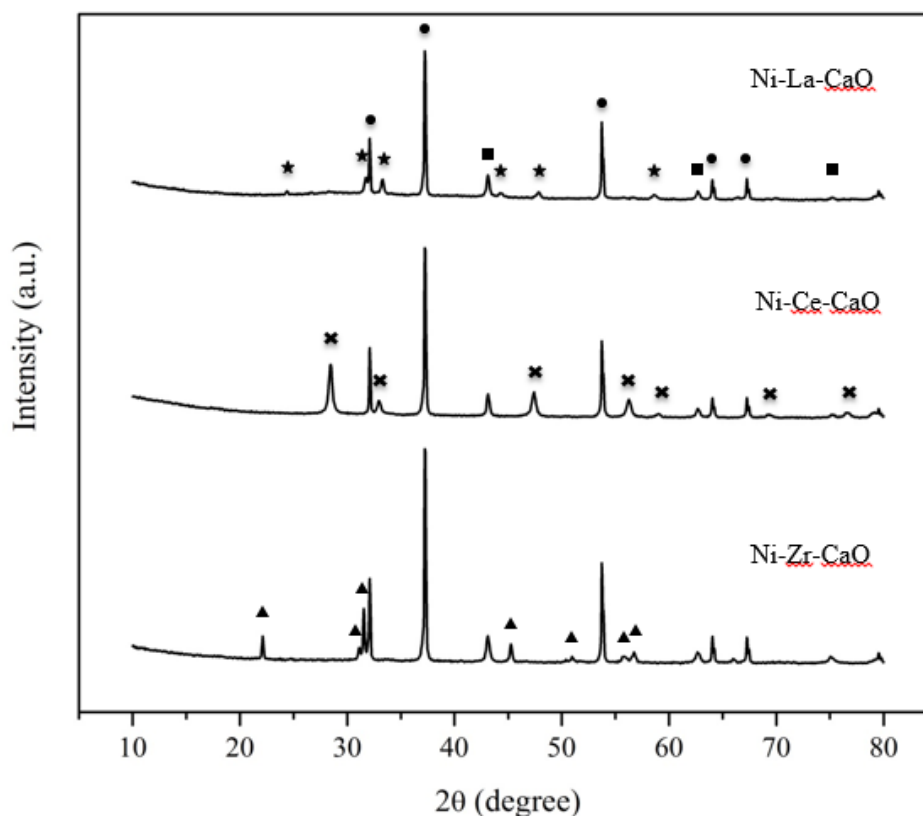


Figure 7.5 XRD patterns of multifunctional catalysts: ● CaO, ■ NiO, ▲ CaZrO₃,
 × CeO₂ and ★ (La_{1.7}Ca_{0.3})(NiO₄).

The multifunctional catalysts Ni-Zr-CaO, Ni-Ce-CaO and Ni-La-CaO were synthesized by CaO hydration followed by wet mixing. The phases of the multifunctional catalysts were characterized by XRD. The XRD patterns (Figure 7.5) indicates that (i) the Ni-Zr-CaO, Ni-Ce-CaO and Ni-La-CaO contained a NiO phase, which acts as the active sites for the catalyzed steam reforming; (ii) CaZrO₃ in the Ni-Zr-CaO samples and CeO₂ in the Ni-Ce-CaO samples are proposed to be inert materials

inhibiting the agglomeration of CaO, while the CaO phase acts as a catalyst support and CO₂ sorption material and (iii) the Ni-La-CaO samples contained a complex phase (La_{1.7}Ca_{0.3})(NiO₄) and a CaO phase acting as a support and CO₂ sorbent.

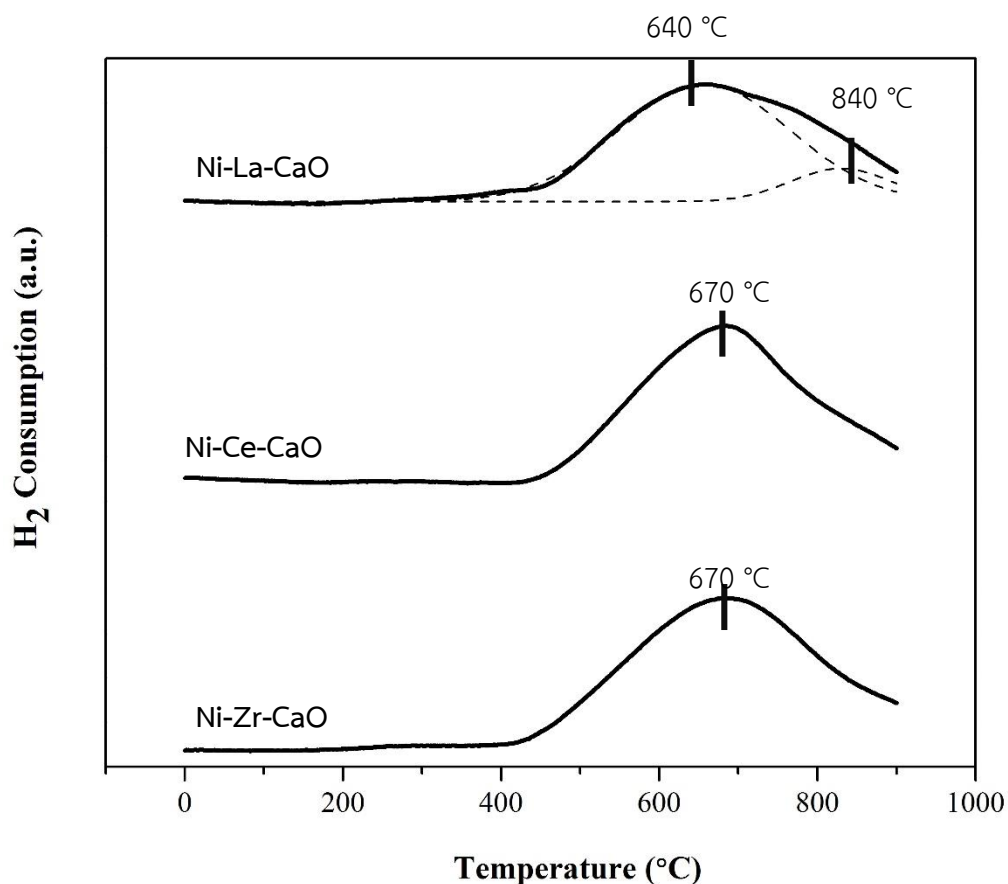


Figure 7.6 H₂ consumption from the temperature-programmed reduction of Ni over Zr⁴⁺, Ce⁴⁺ and La³⁺ modified CaO.

The reducibility of multifunctional catalysts Ni-Zr-CaO, Ni-Ce-CaO and Ni-La-CaO was tested by temperature-programmed reduction (TPR), the TPR profiles of which are presented in Figure 7.6. It is found that free NiO is not observed in all the samples (500-550 °C) [114, 115]. The profiles from the Ni-Zr-CaO and the Ni-Ce-CaO multifunctional catalysts have a single common peak at 670 °C, which refers to the

reduction of Ni^{2+} in low interaction with Zr-CaO or Ce-CaO. The profile for the Ni-La-CaO multifunctional catalyst possesses two peaks (i) at a lower temperature of 640 °C, which is attributed to weak Ni-La-CaO interactions and (ii) at a higher temperature of 830 °C referring to the reduction of more stable Ni(II) interacting with the support. This is probably an effect of progressive incorporation of Ni into the modified sorbent structure [116] supporting XRD evidence for the complex phase $((\text{La}_{1.7}\text{Ca}_{0.3})(\text{NiO}_4))$. For all multifunctional catalysts the TPR results imply that the temperature for the reduction of the Ni(II) active sites is higher than 830 °C.

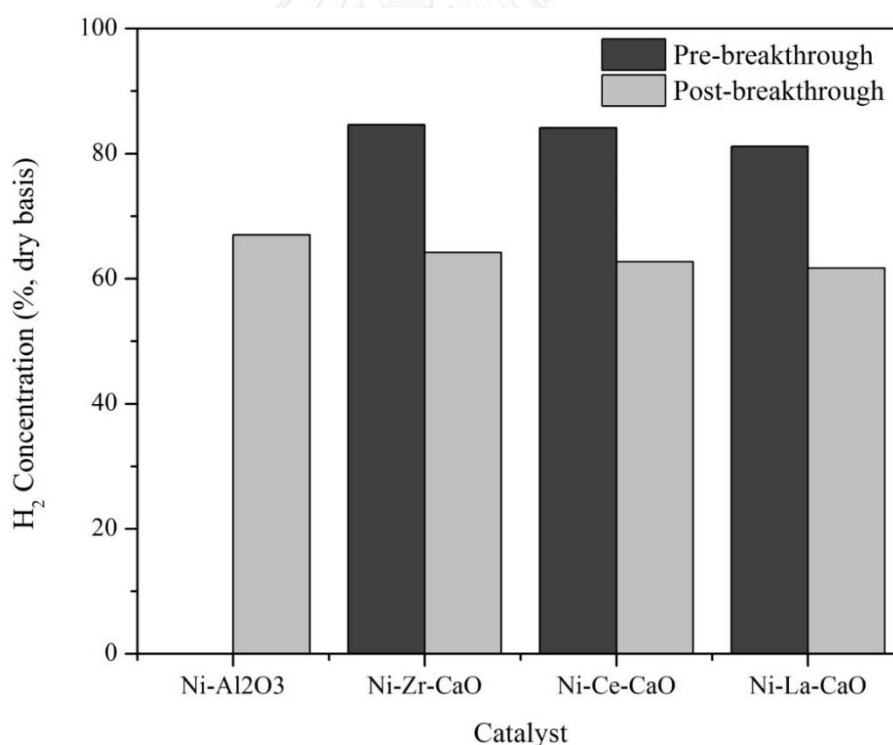


Figure 7.7 H₂ concentrations from sorption enhanced steam reforming of biogas with various multifunctional catalysts.

The multifunctional catalysts Ni-Zr-CaO, Ni-Ce-CaO and Ni-La-CaO were tested and compared with a commercial catalyst (Ni-Al₂O₃) used for SMR hydrogen production. Figure 7.7 shows the Ni-Al₂O₃ catalyst to produce H₂ at a purity of 67% while all the multifunctional catalysts produced H₂ at purities greater than 81% during the pre-breakthrough period of 30 min in the 1st cycle. However, the H₂ purities decreased towards the equilibrium concentration at approximately 64% in the post-breakthrough period of 180 min. During the pre-breakthrough period the purities of H₂ produced with the Ni-Zr-CaO and Ni-Ce-CaO multifunctional catalysts were similar (85% and 84%, respectively), but the purity of H₂ produced with Ni-La-CaO of 81% was significantly lower. This is possibly due to: (i) the lack of lower temperature oxygen storage leading to relatively poor oxygen mobility as shown in Figure 7.4 and Table 7.2 and (ii) the surface concentration of Ca of Ni-La-CaO samples being significantly lower (Table 7.3) and hence a lower concentration of active sites for CO₂ sorption resulting in lower CO₂ sorption rates. In the post-breakthrough period the H₂ purities from the multifunctional catalysts also exhibit the same trend as those during the pre-breakthrough period; The H₂ purities of Ni-Zr-CaO and Ni-Ce-CaO are 64% and 63%, respectively, compared to a significantly lower value of 61% from Ni-La-CaO.

To test the performance of the multifunctional catalysts over multiple cycles, the samples were regenerated at 850 °C under N₂ flow and reduced at the same temperature under 10% v/v H₂ balanced with N₂. Five cycles of operations were performed and the results are presented in the next section.

7.3 Stability of Ni over Zr-, Ce- and La-modified CaO multifunctional catalysts

for 5 cycles H₂ production

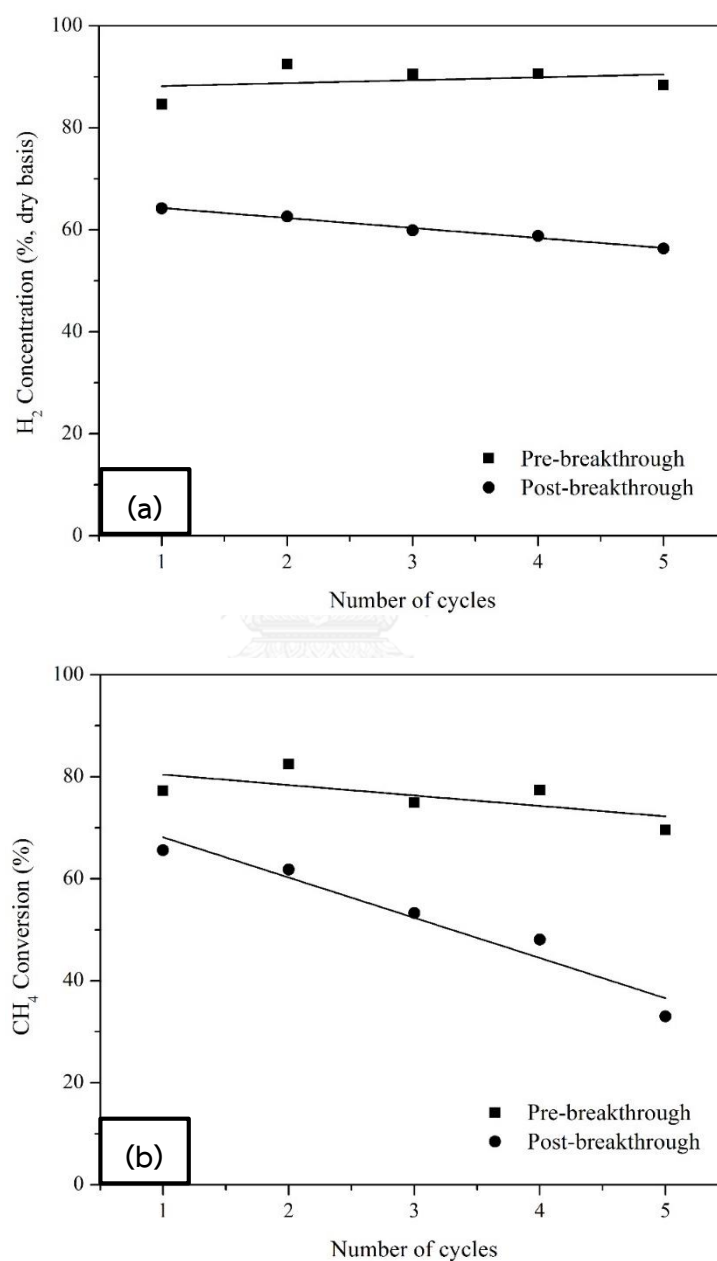


Figure 7.8 The hydrogen production performance of Ni-Zr-CaO: (a) H₂ concentration and (b) CH₄ conversion.

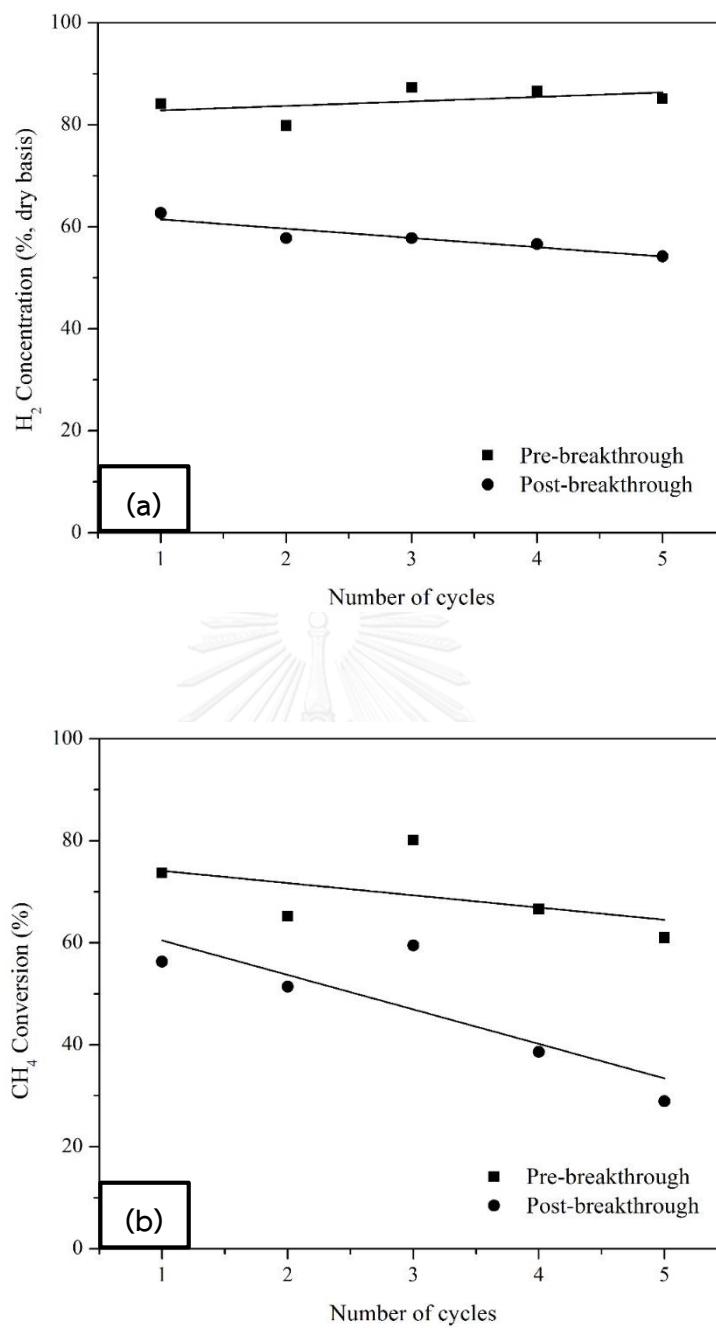


Figure 7.9 The hydrogen production performance of Ni-Ce-CaO: (a) H₂ concentration and (b) CH₄ conversion.

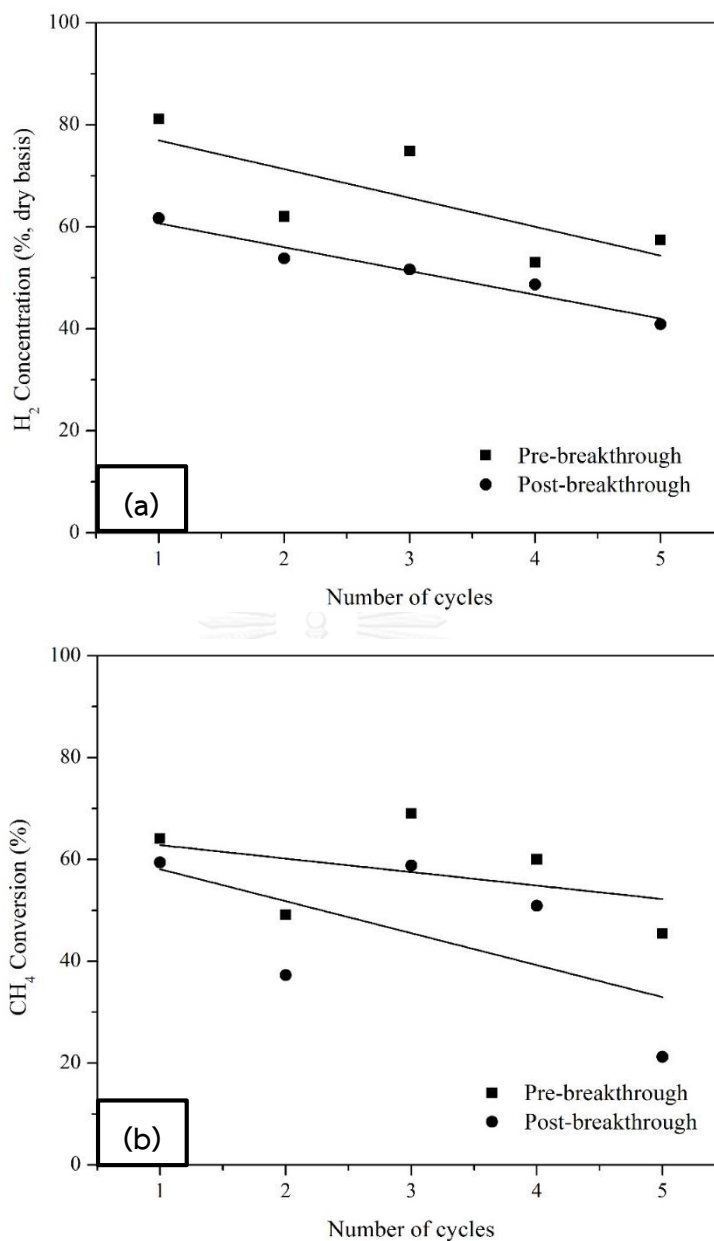


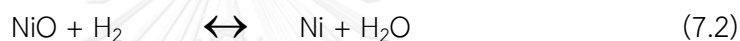
Figure 7.10 The hydrogen production performance of Ni-La-CaO: (a) H₂ concentration and (b) CH₄ conversion.

Figures 7.8 – 7.10 indicates the performance of the multifunctional catalysts Ni-Zr-CaO, Ni-Ce-CaO and Ni-La-CaO tested by sorption enhanced steam reforming of biogas over five operation cycles. The Ni-Zr-CaO and Ni-Ce-CaO (Figures 7.8(a) and 7.9

(a)) offered the most stable H₂ purities over the five cycles, producing 85% and 84% at the 1st cycle and 88% and 85% at the 5th cycle, respectively, during the pre-breakthrough period. This can be attributed to the most stable sorption capacities of Zr-CaO and Ce-CaO present in Ni-Zr-CaO and Ni-Ce-CaO. However, Ni-La-CaO (Figure 7.10 (a)) exhibited low stability. The H₂ purity of the product gas from Ni-La-CaO decreased significantly from 81% during the 1st cycle to 57% during the 5th cycle. The associated deactivation of the Ni-La-CaO is explained by the same reasons discussed in the previous section.

The pre-breakthrough CH₄ conversions of Ni-Zr-CaO and Ni-Ce-CaO are shown to decrease slightly from 77% and 74% at 1st cycle to 70% and 61% at the 5th cycle, respectively, while in the post-breakthrough period the CH₄ conversions decreased rapidly with increasing number of cycles. This is attributed to the loss of Ni active sites confirmed by XPS results shown in Table 7.3 due to pore closure as shown in Figure 7.11 possibly caused by CaCO₃ formation [117]. In addition, it should be noted that the Ni species at the surface of the multifunctional catalysts have different chemical states as indicated by the XPS data, which shows that nickel at the surface has binding energies (B.E.) of 852-853 eV for metallic Ni [118, 119] and 854-855 eV for NiO [118-120]. The concentration of these nickel active sites at the surface of the fresh multifunctional catalysts are 3.4% (B.E. of 855.4 eV indicates the chemical state of NiO), 2.5% (B.E. of 855.8 eV indicates the chemical state of NiO) and 2.8% (B.E. of 855.4 eV indicates the chemical state of NiO), for Ni-Zr-CaO, Ni-Ce-CaO and Ni-La-CaO,

respectively. After the reaction the total nickel concentrations at the surface become significantly lower: (i) 1.2% of total nickel species consisting of 0.1% for metallic Ni (B.E. of 851.8 eV) and 1.1% for NiO (B.E. of 855.3 eV) on the Ni-Zr-CaO sample, (ii) 1.5% of metallic Ni (B.E. of 854.1 eV) on the Ni-Ce-CaO sample and (iii) 0.9% of total nickel species consisting of 0.6% for metallic Ni (B.E. of 852.4 eV) and 0.3% for NiO (B.E. of 855.4 eV) on the Ni-La-CaO sample. The presence of metallic nickel is due to the reduction of NiO in the fresh multifunctional catalysts by H₂, while the presence of NiO is caused by the oxidation of metallic nickel by steam according to Eq. 7.2.



Note that observations from the SEM images (Figure 7.11) and XPS results (Table 7.3) indicate the deactivation of the catalyst observed in this work could be due to the expansion of CaCO₃, resulting in pore closure and the loss of Ni active sites, rather than coke formation. It would be interesting to determine the amount of carbon deposition on the catalysts. However, the typical techniques such as thermogravimetric analysis (TGA) and temperature-programmed oxidation (TPO) are inapplicable for the measurement of the amount of carbon deposition on our used multifunctional catalysts (Ni on Zr-, Ce- and La-modified CaO) because CaCO₃ can release CO₂ during the measurements, therefore the weight loss from the TGA and the amount of CO₂ from the TPO cannot distinguish between those from CaCO₃ and those from carbon deposition. However, it is likely that the carbon deposition in this study is not pronounced owing to the following reasons; (i) Zr, Ce and La are the oxygen promoters

that inhibit coke formation [121-124] – the oxygen storage in ZrO_2 , CeO_2 and La_2O_3 can promote oxygen to react with carbon on the catalyst to form CO or CO_2 ; (ii) an excess amount of steam is fed into the reactor – steam can readily react with carbon to form CO and H_2 as shown in Eq. 9 [125]; and (iii) CaO is a basic support which resists carbon formation [126]. Nevertheless, it is plausible that the deactivation was due to the densification of the multifunctional catalysts which is evidenced by the SEM images (Figure 7.11). This indicates that all the multifunctional catalysts underwent densification due to the volume expansion accompanying the formation of $CaCO_3$, which resulted in pore closure and the loss of Ni active sites. The schematic illustration of the proposed mechanism of the densification of $CaCO_3$ is presented in Figure 7.12.

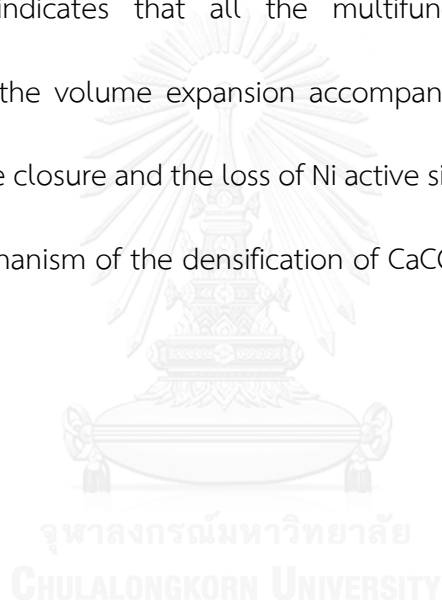


Table 7.3 Atomic concentration at the surface of the multifunctional catalysts before and after reaction.

Sample	Binding energy of Ni (eV)	Atomic concentration at surface (%)						
		Ni	Zr	Ce	La	Ca	O	
Ni-Zr-CaO (Fresh)	856.8	3.4	1.2	-	-	12.7	82.7	
Ni-Zr-CaO (Used)	854.3	1.1	1.0	-	-	12.3	85.4	
Ni-Ce-CaO (Fresh)	854.4	2.5	-	1.2	-	12.4	83.9	
Ni-Ce-CaO (Used)	852.5	1.5	-	1.5	-	12.0	85.0	
Ni-La-CaO (Fresh)	855.4	2.8	-	-	4.6	11.8	80.8	
Ni-La-CaO (Used)	854.2	0.3	-	-	2.4	11.0	85.6	
Ni-La-CaO (Used)	852.4	0.6	-	-	-	-	-	

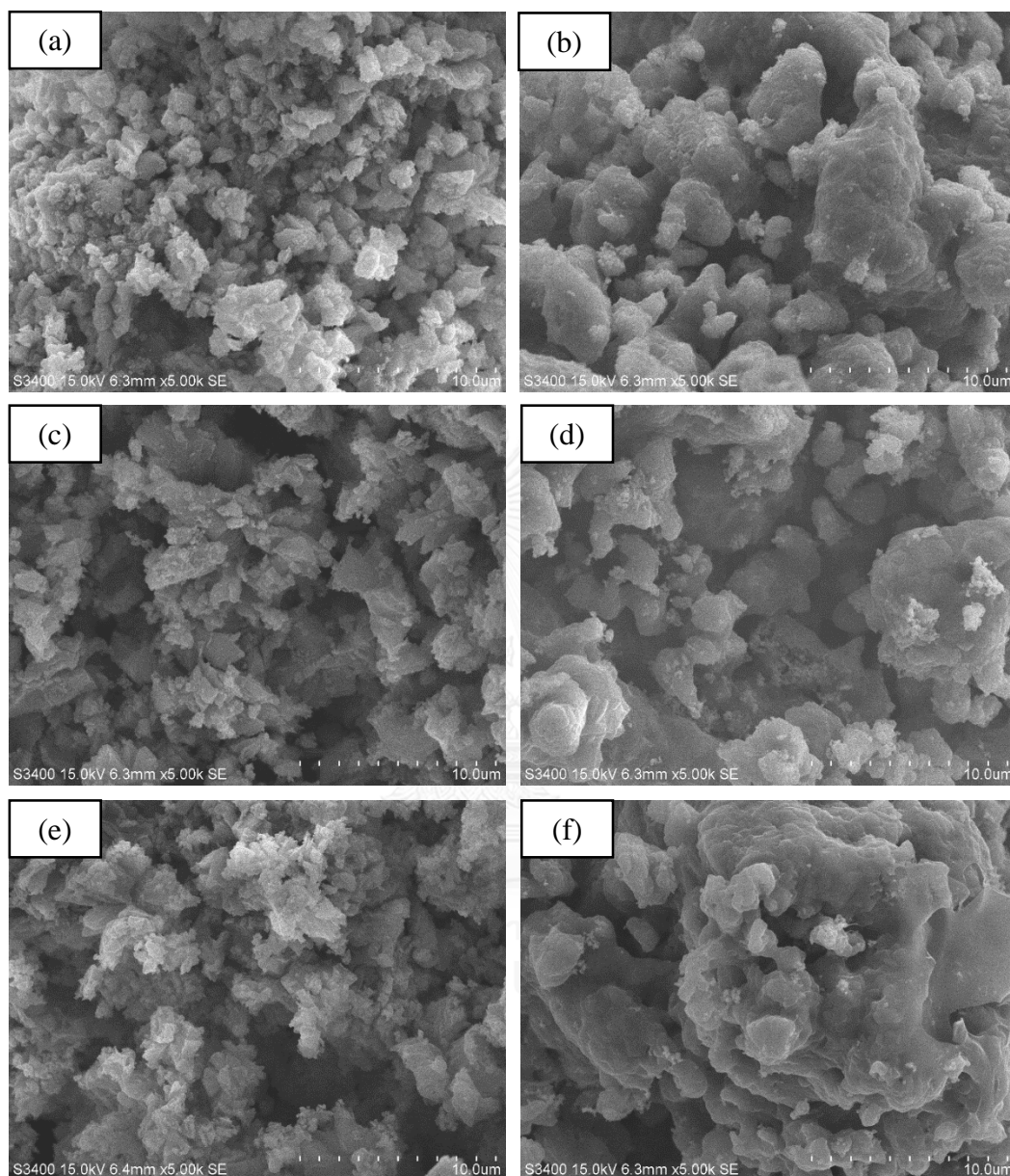


Figure 7.11 SEM images of multifunctional catalysts: (a) Ni-Zr-CaO (Fresh), (b) Ni-Zr-CaO (Used), (c) Ni-Ce-CaO (Fresh), (d) Ni-Ce-CaO (Used), (e) Ni-La-CaO (Fresh) and (f) Ni-La-CaO (Used).

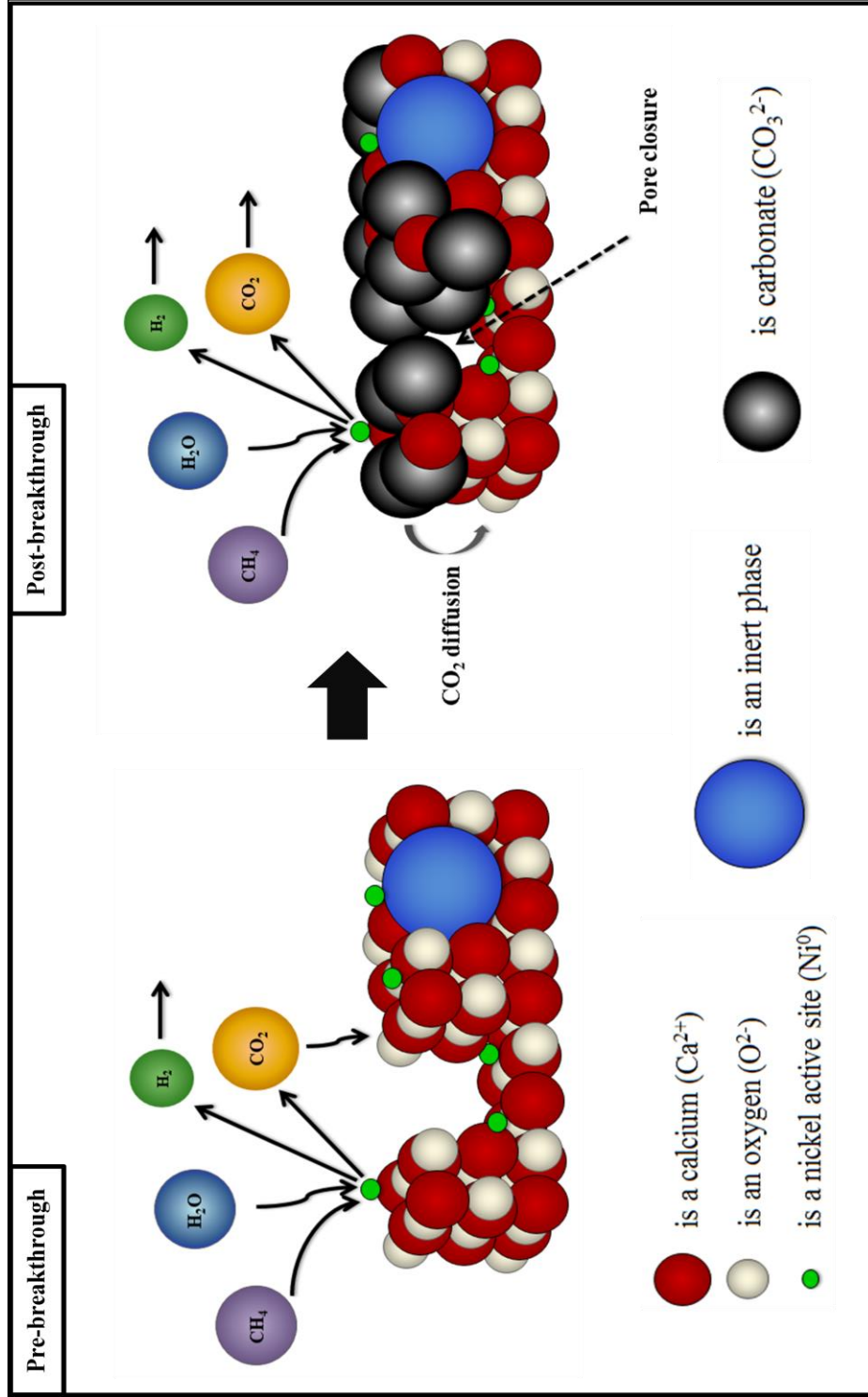


Figure 7.12 Proposed mechanism of the densification of CaCO_3 .

CHAPTER VIII

Conclusions and recommendations

8.1 Conclusions

8.1.1 CO₂ sorption

The material with the highest CO₂ sorption capacity was found to be CaO (0.571 g_{CO₂} / g_{sorbent}), in comparison with MgO (0.038 g_{CO₂} / g_{sorbent}), SrO (0.065 g_{CO₂} / g_{sorbent}) and Al₂O₃ (0.037 g_{CO₂} / g_{sorbent}) at temperature of 600 °C. Modified sorbents produced by using the dry powder mixing method (Mg-CaO-D, Sr-CaO-D and Al-CaO-D) were shown to have similar CO₂ sorption capacities (0.256, 0.219, 0.248 g_{CO₂} / g_{sorbent} for Mg-CaO-D, Sr-CaO-D and Al-CaO-D, respectively), as a result of them all containing the same amount of CaO.

Modified sorbents by wet mixing (Mg-CaO-W, Sr-CaO-W and Al-CaO-W) exhibited decreasing CO₂ sorption capacity with an increasing number of cycles due to decreasing surface area and pore volume; both of which result in a decrease in the capacity for surface adsorption but also decrease the rate at which absorption into the bulk can take place.

The CaO hydration step was implemented to increase the pore volume and surface area of CaO and thus improved diffusion of CO₂ into the bulk material. The first group of metals loading is Mg²⁺, Sr²⁺ and Al³⁺. The experimental results indicate

that over 10 cycles the Mg-CaO-HW performed the best in terms of CO₂ sorption/desorption (CO₂ sorption capacity of 0.259 for 1st cycle to 0.252 g_{CO₂} / g_{sorbent} for the 10th cycle). Whereas Al-CaO-HW and Sr-CaO-HW exhibited a decrease in CO₂ sorption capacity corresponding to a 6 and 12 % decrease over 10 cycles (0.257 and 0.286 g_{CO₂} / g_{sorbent} for 1st cycle dropping to 0.243 and 0.251 g_{CO₂} / g_{sorbent} for 10th cycle, respectively).

The second group of metals loading on CaO is Zr⁴⁺, Ce⁴⁺ and La³⁺ and its performances indicated that Zr-CaO-HW and Ce-CaO-HW possessed stable CO₂ capacities over the 10 cycles. On the other hand, La-CaO-HW was shown to have a decrease in the CO₂ sorption capacity of 16% over the 10 cycles. This was due to the low-temperature oxygen storage properties of Zr-CaO and Ce-CaO, which enhanced the mobility of oxygen. This behavior promoted the CO₂ diffusion from the surface to the bulk and vice versa (sorption/desorption) of the modified CaO.

8.1.2 H₂ production

In the H₂ production section, three sequences of Ni²⁺ loading on modified CaO were investigated: (i) simultaneous adding Ni²⁺ and Al³⁺ into CaO solution (Ni-Al-CaO-HW), (ii) adding Ni²⁺ after drying the modified sorbent (Ni-Al-CaO-HWO) and (iii) adding Ni²⁺ after calcination the modified sorbent (Ni-Al-CaO-HWC). The results show that the sorbent synthesized by loading Ni²⁺ and Al³⁺ simultaneously (Ni-Al-CaO-HW) is the best catalytic sorbent for H₂ production as the longest pre-breakthrough time (30 min) could

be obtained. Nevertheless, H₂ purity and CH₄ conversion are not significantly different when compared to other samples (94% H₂ purity and 90% CH₄ conversion in the pre-breakthrough period). The stability of Ni-Al-CaO-HW in the production of H₂ was tested over 5 cycles. The results show that CH₄ conversion is still higher than 90% during the pre-breakthrough period for 5 cycle operations. However, during the post-breakthrough period the CH₄ conversion decreases slightly from 85% to 75% at 1st to 5th cycle, respectively. The plausible explanation is due to the reduction of Ni concentration at the surface of the catalyst (Ni concentration at surface of 1.93% after 1st cycle and of 1.02% after 5th cycle) caused from pore blockage by CaCO₃.

Ni(II) was loaded on the modified sorbents Zr-CaO-HW, Ce-CaO-HW and La-CaO-HW for H₂ production via sorption enhanced steam reforming of biogas. The results showed that Ni-Zr-CaO-HW and Ni-Ce-CaO-HW produced H₂ at stable purities but with decreasing CH₄ conversions. This was attributed to the loss of nickel active sites at the surface of the multifunctional catalysts due to the formation of CaCO₃. The Ni-La-CaO-HW was shown to produce H₂ at decreasing purity and decreasing CH₄ conversion in both the pre-breakthrough and the post-breakthrough periods. This was explained in terms of the unstable CO₂ sorption capacities of the support (La-CaO-HW) and the subsequent loss of Ni active sites confirmed by the XPS results.

8.2 Recommendations

1. CaO sorbent can be developed by changing the Ca precursors such as calcium acetate, calcium nitrate and calcium carbonate. Dissolved and non-dissolved calcium precursors can promote the open pore of modified CaO sorbent.

2. The mixture Ce-Zr oxide is an interesting material for adding into CaO sorbent. The literature indicated that it has high oxygen storage which can promote the CO₂ diffusion into the deep layer of CaO particle.

3. The investigation of CaO dispersion on high surface area supports such as SiO₂ nanoparticle, TiO₂ nanotube and zeolite is the alternative method to improve the CO₂ sorption/desorption performance of CaO.

4. The sorption enhanced steam reforming can be used for several feed stocks such ethanol, glycerol, toluene, phenol and other hydrocarbons.

5. A number of CO₂ sorption/desorption cycle tests of modified sorbents at more cycles should be carried out to compare with the performance of CaO.

6. The investigation of CO₂ sorption on modified on CaO and H₂ production by multifunctional catalysts (Ni over modified CaO) mechanisms need further studies such as how CO₂ diffuses to deep layers of modified CaO.

REFERENCES



- [1] Westermann, P., Jørgensen, B., Lange, L., Ahring, B., and Christensen, C. Maximizing renewable hydrogen production from biomass in a bio/catalytic refinery. International Journal of Hydrogen Energy 32(17) (2007): 4135-4141.
- [2] Kalinci, Y., Hepbasli, A., and Dincer, I. Biomass-based hydrogen production: A review and analysis. International Journal of Hydrogen Energy 34(21) (2009): 8799-8817.
- [3] Soaring demand 2004. Available from: http://news.bbc.co.uk/2/shared/spl/hi/pop_ups/04/sci_nat_global_energy_crisis/html/1.stm
- [4] Brisse, A., Schefold, J., and Zahid, M. High temperature water electrolysis in solid oxide cells. International Journal of Hydrogen Energy 33(20) (2008): 5375-5382.
- [5] Carmo, M., Fritz, D.L., Mergel, J., and Stolten, D. A comprehensive review on PEM water electrolysis. International Journal of Hydrogen Energy 38(12) (2013): 4901-4934.
- [6] Rasten, E., Hagen, G., and Tunold, R. Electrocatalysis in water electrolysis with solid polymer electrolyte. Electrochimica Acta 48(25-26) (2003): 3945-3952.
- [7] Stojić, D.L., Marčeta, M.P., Sovilj, S.P., and Miljanić, Š.S. Hydrogen generation from water electrolysis—possibilities of energy saving. Journal of Power Sources 118(1-2) (2003): 315-319.

- [8] Zeng, K. and Zhang, D. Recent progress in alkaline water electrolysis for hydrogen production and applications. Progress in Energy and Combustion Science 36(3) (2010): 307-326.
- [9] Laoun, B. Thermodynamics aspect of high pressure hydrogen production by water electrolysis. Revue des Energies Renouvelables 10 (2007): 435 – 444.
- [10] Carrieri, D., Ananyev, G., Garcia Costas, A.M., Bryant, D.A., and Dismukes, G.C. Renewable hydrogen production by cyanobacteria: Nickel requirements for optimal hydrogenase activity. International Journal of Hydrogen Energy 33(8) (2008): 2014-2022.
- [11] Dholam, R., Patel, N., Adami, M., and Miotello, A. Hydrogen production by photocatalytic water-splitting using Cr- or Fe-doped TiO₂ composite thin films photocatalyst. International Journal of Hydrogen Energy 34(13) (2009): 5337-5346.
- [12] Li, Z., Wang, Y., Liu, J., Chen, G., Li, Y., and Zhou, C. Photocatalytic hydrogen production from aqueous methanol solutions under visible light over Na(Bi_xTa_{1-x})O₃ solid-solution. International Journal of Hydrogen Energy 34(1) (2009): 147-152.
- [13] Wang, X., Maeda, K., Thomas, A., Takahashi, K., Xin, G., Carlsson, J.M., Domen, K., and Antonietti, M. A metal-free polymeric photocatalyst for hydrogen production from water under visible light. Nat Mater 8(1) (2009): 76-80.

- [14] Xing, C., Zhang, Y., Yan, W., and Guo, L. Band structure-controlled solid solution of $\text{Cd}_{1-x}\text{Zn}_x\text{S}$ photocatalyst for hydrogen production by water splitting. International Journal of Hydrogen Energy 31(14) (2006): 2018-2024.
- [15] Yan, H., Yang, J., Ma, G., Wu, G., Zong, X., Lei, Z., Shi, J., and Li, C. Visible-light-driven hydrogen production with extremely high quantum efficiency on Pt-PdS/CdS photocatalyst. Journal of Catalysis 266(2) (2009): 165-168.
- [16] Yang, H., Guo, L., Yan, W., and Liu, H. A novel composite photocatalyst for water splitting hydrogen production. Journal of Power Sources 159(2) (2006): 1305-1309.
- [17] Moon, S.-C., Mametsuka, H., Tabata, S., and Suzuki, E. Photocatalytic production of hydrogen from water using TiO_2 and B/ TiO_2 . Catalysis Today 58(2-3) (2000): 125-132.
- [18] Sreethawong, T., Junbua, C., and Chavadej, S. Photocatalytic H_2 production from water splitting under visible light irradiation using Eosin Y-sensitized mesoporous-assembled Pt/ TiO_2 nanocrystal photocatalyst. Journal of Power Sources 190(2) (2009): 513-524.
- [19] Dholam, R., Patel, N., and Miotello, A. Efficient H_2 production by water-splitting using indium-tin-oxide/V-doped TiO_2 multilayer thin film photocatalyst. International Journal of Hydrogen Energy 36(11) (2011): 6519-6528.

- [20] Peppley, B.A., Amphlett, J.C., Kearns, L.M., and Mann, R.F. Methanol steam reforming on Cu/ZnO/Al₂O₃. Part 1: the reaction network. Applied Catalysis A: General 179 (1999): 21–29.
- [21] Hong, X. Selective hydrogen production from methanol oxidative steam reforming over Zn–Cr catalysts with or without Cu loading. International Journal of Hydrogen Energy 33(2) (2008): 700-708.
- [22] Basile, A., Parmaliana, A., Tosti, S., Iulianelli, A., Gallucci, F., Espro, C., and Spooen, J. Hydrogen production by methanol steam reforming carried out in membrane reactor on Cu/Zn/Mg-based catalyst. Catalysis Today 137(1) (2008): 17-22.
- [23] Huang, T.-J. and Chen, H.-M. Hydrogen production via steam reforming of methanol over Cu/(Ce,Gd)O_{2-x} catalysts. International Journal of Hydrogen Energy 35(12) (2010): 6218-6226.
- [24] Casanovas, A., de Leitenburg, C., Trovarelli, A., and Llorca, J. Ethanol steam reforming and water gas shift reaction over Co–Mn/ZnO catalysts. Chemical Engineering Journal 154(1-3) (2009): 267-273.
- [25] Carrero, A., Calles, J.A., and Vizcaino, A.J. Effect of Mg and Ca addition on coke deposition over Cu–Ni/SiO₂ catalysts for ethanol steam reforming. Chemical Engineering Journal 163(3) (2010): 395-402.

- [26] Youn, M.H., Seo, J.G., Lee, H., Bang, Y., Chung, J.S., and Song, I.K. Hydrogen production by auto-thermal reforming of ethanol over nickel catalysts supported on metal oxides: Effect of support acidity. Applied Catalysis B: Environmental 98(1-2) (2010): 57-64.
- [27] Pistonesi, C., Juan, A., Irigoyen, B., and Amadeo, N. Theoretical and experimental study of methane steam reforming reactions over nickel catalyst. Applied Surface Science 253(9) (2007): 4427-4437.
- [28] Lertwittayanon, K., Atong, D., Aungkavattana, P., Wasanapiarnpong, T., Wada, S., and Sricharoenchaikul, V. Effect of CaO–ZrO₂ addition to Ni supported on γ -Al₂O₃ by sequential impregnation in steam methane reforming. International Journal of Hydrogen Energy 35(22) (2010): 12277-12285.
- [29] Maluf, S.S. and Assaf, E.M. Ni catalysts with Mo promoter for methane steam reforming. Fuel 88(9) (2009): 1547-1553.
- [30] Frusteri, F., Arena, F., Calogero, G., Torre, T., and Parmaliana, A. Potassium-enhanced stability of Ni/MgO catalysts in the dry-reforming of methane. Catalysis Communications 2(2) (2001): 49-56.
- [31] Juan-Juan, J., Román-Martínez, M.C., and Illán-Gómez, M.J. Effect of potassium content in the activity of K-promoted Ni/Al₂O₃ catalysts for the dry reforming of methane. Applied Catalysis A: General 301(1) (2006): 9-15.

- [32] Barelli, L., Bidini, G., Gallorini, F., and Servili, S. Hydrogen production through sorption-enhanced steam methane reforming and membrane technology: A review. Energy 33(4) (2008): 554-570.
- [33] Jang, H.M., Lee, K.B., Caram, H.S., and Sircar, S. High-purity hydrogen production through sorption enhanced water gas shift reaction using K_2CO_3 -promoted hydrotalcite. Chemical Engineering Science 73 (2012): 431-438.
- [34] Johnsen, K., Ryu, H.J., Grace, J.R., and Lim, C.J. Sorption-enhanced steam reforming of methane in a fluidized bed reactor with dolomite as CO_2 -acceptor. Chemical Engineering Science 61(4) (2006): 1195-1202.
- [35] Martavaltzi, C.S., Pampaka, E.P., Korkakaki, E.S., and Lemonidou, A.A. Hydrogen Production via Steam Reforming of Methane with Simultaneous CO_2 Capture over $CaO-Ca_{12}Al_{14}O_{33}$. Energy & Fuels 24(4) (2010): 2589-2595.
- [36] Ochoa-Fernández, E., Haugen, G., Zhao, T., Rønning, M., Aartun, I., Rytter, E., Rønnekleiv, M., and Chen, D. Process design simulation of H_2 production by sorption enhanced steam methane reforming: evaluation of potential CO_2 acceptors. Green Chemistry 9(6) (2007): 654.
- [37] Hong, L., Reddy, E.P., and Smirniotis, P.G. Calcium Oxide Based Sorbents for Capture of Carbon Dioxide at High Temperatures. Industrial and Engineering Chemistry Research 45 (2006): 3944-3949.

- [38] Zou Y. and Rodrigues, A.E. Hydrotalcite-like compounds as adsorbents for carbon dioxide. Energy Conversion and Management 43 (2002): 1865–1876.
- [39] Oliveira, E.L.G., Grande, C.A., and Rodrigues, A.E. CO₂ sorption on hydrotalcite and alkali-modified (K and Cs) hydrotalcites at high temperatures. Separation and Purification Technology 62(1) (2008): 137-147.
- [40] Bhatta, L.K.G., Subramanyam, S., Chengala, M.D., Olivera, S., and Venkatesh, K. Progress in hydrotalcite like compounds and metal-based oxides for CO₂ capture: a review. Journal of Cleaner Production 103 (2015): 171-196.
- [41] Hanif, A., Dasgupta, S., Divekar, S., Arya, A., Garg, M.O., and Nanoti, A. A study on high temperature CO₂ capture by improved hydrotalcite sorbents. Chemical Engineering Journal 236 (2014): 91-99.
- [42] Pramod, C.V., Upendar, K., Mohan, V., Sarma, D.S., Dhar, G.M., Prasad, P.S.S., Raju, B.D., and Rao, K.S.R. Hydrotalcite-SBA-15 composite material for efficient carbondioxide capture. Journal of CO₂ Utilization 12 (2015): 109-115.
- [43] Bretado, M.E., Guzmán Velderrain, V., Lardizábal Gutiérrez, D., Collins-Martínez, V., and Ortiz, A.L. A new synthesis route to Li₄SiO₄ as CO₂ catalytic/sorbent. Catalysis Today 107-108 (2005): 863-867.
- [44] Guo, L., Wang, X., Zhong, C., and Li, L. Synthesis and CO₂ capture property of high aspect-ratio Li₂ZrO₃ nanotubes arrays. Applied Surface Science 257(18) (2011): 8106-8109.

- [45] López Ortiz, A., Escobedo Bretado, M.A., Guzmán Velderrain, V., Meléndez Zaragoza, M., Salinas Gutiérrez, J., Lardizábal Gutiérrez, D., and Collins-Martínez, V. Experimental and modeling kinetic study of the CO₂ absorption by Li₄SiO₄. International Journal of Hydrogen Energy 39(29) (2014): 16656-16666.
- [46] Ochoa-Fernández, E., Rusten, H.K., Jakobsen, H.A., Rønning, M., Holmen, A., and Chen, D. Sorption enhanced hydrogen production by steam methane reforming using Li₂ZrO₃ as sorbent: Sorption kinetics and reactor simulation. Catalysis Today 106(1-4) (2005): 41-46.
- [47] Olivares-Marín, M., Drage, T.C., and Maroto-Valer, M.M. Novel lithium-based sorbents from fly ashes for CO₂ capture at high temperatures. International Journal of Greenhouse Gas Control 4(4) (2010): 623-629.
- [48] Shan, S., Jia, Q., Jiang, L., Li, Q., Wang, Y., and Peng, J. Novel Li₄SiO₄-based sorbents from diatomite for high temperature CO₂ capture. Ceramics International 39(5) (2013): 5437-5441.
- [49] Wang, K., Zhao, P., Guo, X., Li, Y., Han, D., and Chao, Y. Enhancement of reactivity in Li₄SiO₄-based sorbents from the nano-sized rice husk ash for high-temperature CO₂ capture. Energy Conversion and Management 81 (2014): 447-454.

- [50] Xiao, Q., Tang, X., Liu, Y., Zhong, Y., and Zhu, W. Citrate route to prepare K-doped Li_2ZrO_3 sorbents with excellent CO_2 capture properties. Chemical Engineering Journal 174(1) (2011): 231-235.
- [51] H. Lu, A. Khan, S.E. Pratsinis, and Smirniotis, P.G. Flame-Made Durable Doped-CaO Nanosorbents for CO_2 Capture. Energy & Fuels 23 (2009): 1093–1100.
- [52] Zhou, Z., Qi, Y., Xie, M., Cheng, Z., and Yuan, W. Synthesis of CaO-based sorbents through incorporation of alumina/aluminate and their CO_2 capture performance. Chemical Engineering Science 74 (2012): 172-180.
- [53] Wang, X., Wang, N., and Wang, L. Hydrogen production by sorption enhanced steam reforming of propane: A thermodynamic investigation. International Journal of Hydrogen Energy 36(1) (2011): 466-472.
- [54] Chang, C.-C., Wang, J.-W., Chang, C.-T., Liaw, B.-J., and Chen, Y.-Z. Effect of ZrO_2 on steam reforming of methanol over $\text{CuO}/\text{ZnO}/\text{ZrO}_2/\text{Al}_2\text{O}_3$ catalysts. Chemical Engineering Journal 192 (2012): 350-356.
- [55] Das, D., Llorca, J., Dominguez, M., Colussi, S., Trovarelli, A., and Gayen, A. Methanol steam reforming behavior of copper impregnated over $\text{CeO}_2\text{-ZrO}_2$ derived from a surfactant assisted coprecipitation route. International Journal of Hydrogen Energy 40(33) (2015): 10463-10479.

- [56] Deshmane, V.G., Abrokwhah, R.Y., and Kuila, D. Synthesis of stable Cu-MCM-41 nanocatalysts for H₂ production with high selectivity via steam reforming of methanol. International Journal of Hydrogen Energy 40(33) (2015): 10439-10452.
- [57] Lytkina, A.A., Zhilyaeva, N.A., Ermilova, M.M., Orekhova, N.V., and Yaroslavtsev, A.B. Influence of the support structure and composition of Ni–Cu-based catalysts on hydrogen production by methanol steam reforming. International Journal of Hydrogen Energy 40(31) (2015): 9677-9684.
- [58] Tesser, R., Di Serio, M., and Santacesaria, E. Methanol steam reforming: A comparison of different kinetics in the simulation of a packed bed reactor. Chemical Engineering Journal 154(1-3) (2009): 69-75.
- [59] Yang, R.-X., Chuang, K.-H., and Wey, M.-Y. Hydrogen production through methanol steam reforming: Effect of synthesis parameters on Ni–Cu/CaO–SiO₂ catalysts activity. International Journal of Hydrogen Energy 39(34) (2014): 19494-19501.
- [60] Essaki, K., Muramatsu, T., and Kato, M. Effect of equilibrium-shift in the case of using lithium silicate pellets in ethanol steam reforming. International Journal of Hydrogen Energy 33(22) (2008): 6612-6618.
- [61] Bednarczuk, L., Ramírez de la Piscina, P., and Homs, N. H₂-production from CO₂-assisted ethanol steam reforming: The regeneration of Ni-based catalysts. International Journal of Hydrogen Energy 40(15) (2015): 5256-5263.

- [62] Chiou, J.Y.Z., Lai, C.L., Yu, S.-W., Huang, H.-H., Chuang, C.-L., and Wang, C.-B. Effect of Co, Fe and Rh addition on coke deposition over Ni/Ce_{0.5}Zr_{0.5}O₂ catalysts for steam reforming of ethanol. International Journal of Hydrogen Energy 39(35) (2014): 20689-20699.
- [63] Ma, H., Zeng, L., Tian, H., Li, D., Wang, X., Li, X., and Gong, J. Efficient hydrogen production from ethanol steam reforming over La-modified ordered mesoporous Ni-based catalysts. Applied Catalysis B: Environmental 181 (2016): 321-331.
- [64] Ma, R., Castro-Dominguez, B., Mardilovich, I.P., Dixon, A.G., and Ma, Y.H. Experimental and simulation studies of the production of renewable hydrogen through ethanol steam reforming in a large-scale catalytic membrane reactor. Chemical Engineering Journal 303 (2016): 302-313.
- [65] Rossetti, I., Compagnoni, M., and Torli, M. Process simulation and optimization of H₂ production from ethanol steam reforming and its use in fuel cells. 2. Process analysis and optimization. Chemical Engineering Journal 281 (2015): 1036-1044.
- [66] Vaidya, P.D. and Rodrigues, A.E. Insight into steam reforming of ethanol to produce hydrogen for fuel cells. Chemical Engineering Journal 117(1) (2006): 39-49.

- [67] Wu, Y.J., Li, P., Yu, J.G., Cunha, A.F., and Rodrigues, A.E. Sorption-enhanced steam reforming of ethanol on NiMgAl multifunctional materials: Experimental and numerical investigation. Chemical Engineering Journal 231 (2013): 36-48.
- [68] Wu, Y.-J., Li, P., Yu, J.-G., Cunha, A.F., and Rodrigues, A.E. Sorption-enhanced steam reforming of ethanol for continuous high-purity hydrogen production: 2D adsorptive reactor dynamics and process design. Chemical Engineering Science 118 (2014): 83-93.
- [69] Dou, B., Dupont, V., Rickett, G., Blakeman, N., Williams, P.T., Chen, H., Ding, Y., and Ghadiri, M. Hydrogen production by sorption-enhanced steam reforming of glycerol. Bioresource Technology 100(14) (2009): 3540-3547.
- [70] Lima da Silva, A. and Müller, I.L. Hydrogen production by sorption enhanced steam reforming of oxygenated hydrocarbons (ethanol, glycerol, n-butanol and methanol): Thermodynamic modelling. International Journal of Hydrogen Energy 36(3) (2011): 2057-2075.
- [71] Ashok, J., Kathiraser, Y., Ang, M.L., and Kawi, S. Bi-functional hydrotalcite-derived NiO–CaO–Al₂O₃ catalysts for steam reforming of biomass and/or tar model compound at low steam-to-carbon conditions. Applied Catalysis B: Environmental 172-173 (2015): 116-128.

- [72] Ashok, J. and Kawi, S. Steam reforming of toluene as a biomass tar model compound over CeO₂ promoted Ni/CaO–Al₂O₃ catalytic systems. International Journal of Hydrogen Energy 38(32) (2013): 13938-13949.
- [73] Gao, N., Liu, S., Han, Y., Xing, C., and Li, A. Steam reforming of biomass tar for hydrogen production over NiO/ceramic foam catalyst. International Journal of Hydrogen Energy 40(25) (2015): 7983-7990.
- [74] Oh, G., Park, S.Y., Seo, M.W., Kim, Y.K., Ra, H.W., Lee, J.-G., and Yoon, S.J. Ni/Ru–Mn/Al₂O₃ catalysts for steam reforming of toluene as model biomass tar. Renewable Energy 86 (2016): 841-847.
- [75] Zamboni, I., Zimmermann, Y., Kiennemann, A., and Courson, C. Improvement of steam reforming of toluene by CO₂ capture using Fe/CaO–Ca₁₂Al₁₄O₃₃ bi-functional materials. International Journal of Hydrogen Energy 40(15) (2015): 5297-5304.
- [76] Ahmed, S., Lee, S.H.D., and Ferrandon, M.S. Catalytic steam reforming of biogas – Effects of feed composition and operating conditions. International Journal of Hydrogen Energy 40(2) (2015): 1005-1015.
- [77] Appari, S., Janardhanan, V.M., Bauri, R., and Jayanti, S. Deactivation and regeneration of Ni catalyst during steam reforming of model biogas: An experimental investigation. International Journal of Hydrogen Energy 39(1) (2014): 297-304.

- [78] Italiano, C., Vita, A., Fabiano, C., Laganà, M., and Pino, L. Bio-hydrogen production by oxidative steam reforming of biogas over nanocrystalline Ni/CeO₂ catalysts. International Journal of Hydrogen Energy 40(35) (2015): 11823-11830.
- [79] Alves, H.J., Bley Junior, C., Niklevicz, R.R., Frigo, E.P., Frigo, M.S., and Coimbra-Araújo, C.H. Overview of hydrogen production technologies from biogas and the applications in fuel cells. International Journal of Hydrogen Energy 38(13) (2013): 5215-5225.
- [80] Kolbitsch, P., Pfeifer, C., and Hofbauer, H. Catalytic steam reforming of model biogas. Fuel 87(6) (2008): 701-706.
- [81] Kohn, M.P., Castaldi, M.J., and Farrauto, R.J. Biogas reforming for syngas production: The effect of methyl chloride. Applied Catalysis B: Environmental 144 (2014): 353-361.
- [82] Ganzoury, M.A. and Allam, N.K. Impact of nanotechnology on biogas production: A mini-review. Renewable and Sustainable Energy Reviews 50 (2015): 1392-1404.
- [83] Chasnyk, O., Sołowski, G., and Shkarupa, O. Historical, technical and economic aspects of biogas development: Case of Poland and Ukraine. Renewable and Sustainable Energy Reviews 52 (2015): 227-239.
- [84] Biogas Plant Design 2011. Available from: <http://bio-gas-plant.blogspot.com/2011/04/biogas-plant-design.html>

- [85] Maier, L., Schädel, B., Herrera Delgado, K., Tischer, S., and Deutschmann, O. Steam Reforming of Methane Over Nickel: Development of a Multi-Step Surface Reaction Mechanism. Topics in Catalysis 54(13-15) (2011): 845-858.
- [86] Haan, A.B.d. Process Technology: An Introduction. 2015.
- [87] McCabe, W., Smith, J., and Harriott, P. Unit Operations of Chemical Engineering. Seven ed.: McGraw-Hill.
- [88] Mass Transfer Zone and Breakthrough Available from: http://www.separationprocesses.com/Adsorption/AD_Chp02c.htm
- [89] Roh, H.-S., Koo, K.Y., Jeong, J.H., Seo, Y.T., Seo, D.J., Seo, Y.-S., Yoon, W.L., and Park, S.B. Combined reforming of methane over supported Ni catalysts. Catalysis Letters 117(1-2) (2007): 85-90.
- [90] Chaubey, R., Sahu, S., James, O.O., and Maity, S. A review on development of industrial processes and emerging techniques for production of hydrogen from renewable and sustainable sources. Renewable and Sustainable Energy Reviews 23 (2013): 443-462.
- [91] LeValley, T.L., Richard, A.R., and Fan, M. The progress in water gas shift and steam reforming hydrogen production technologies – A review. International Journal of Hydrogen Energy 39(30) (2014): 16983-17000.

- [92] Dong, W.-S., Roh, H.-S., Jun, K.-W., Park, S.-E., and Oh, Y.-S. Methane reforming over NiCe-ZrO₂ catalysts effect of nickel content. Applied Catalysis A: General 226(1-2) (2002): 63-72.
- [93] Lu, H., Reddy, E.P., and Smirniotis, P.G. Calcium Oxide Based Sorbents for Capture of Carbon Dioxide at High Temperatures. Industrial and Engineering Chemistry Research 45 (2006): 3944-3949.
- [94] Reddy, E.P. and Smirniotis, P.G. High-Temperature Sorbents for CO₂ Made of Alkali Metals Doped on CaO Supports. Journal of Physical Chemistry B 108 (2004): 7794 7800.
- [95] Hong Lu and Smirniotis, P.G. Calcium Oxide Doped Sorbents for CO₂ Uptake in the Presence of SO₂ at High Temperatures. Industrial and Engineering Chemistry Research 48 (2009): 5454–5459.
- [96] Vieille, L., Govin, A., and Grosseau, P. Improvements of calcium oxide based sorbents for multiple CO₂ capture cycles. Powder Technology 228 (2012): 319-323.
- [97] Mastin, J., Aranda, A., and Meyer, J. New synthesis method for CaO-based synthetic sorbents with enhanced properties for high-temperature CO₂ - capture. Energy Procedia 4(0) (2011): 1184-1191.
- [98] Wang, Q., Wu, Z., Tay, H.H., Chen, L., Liu, Y., Chang, J., Zhong, Z., Luo, J., and Borgna, A. High temperature adsorption of CO₂ on Mg–Al hydrotalcite: Effect of

- the charge compensating anions and the synthesis pH. Catalysis Today 164(1) (2011): 198-203.
- [99] Chanburanasiri, N., Ribeiro, A.M., Rodrigues, A.E., Arpornwichanop, A., Laosiripojana, N., Praserttham, P., and Assabumrungrat, S. Hydrogen Production via Sorption Enhanced Steam Methane Reforming Process Using Ni/CaO Multifunctional Catalyst. Industrial & Engineering Chemistry Research 50(24) (2011): 13662-13671.
- [100] Chen, Y., Zhao, Y., Zhang, J., and Zheng, C. Hydrogen production through CO₂ sorption-enhanced methane steam reforming: Comparison between different adsorbents. Science China Technological Sciences 54(11) (2011): 2999-3008.
- [101] C. S. Martavaltzi, T. D. Pefkos, and Lemonidou, A.A. Operational Window of Sorption Enhanced Steam Reforming of Methane over CaO Ca₁₂Al₁₄O₃₃. Industrial and Engineering Chemistry Research 50 (2011): 539–545.
- [102] Feng, H.Z., Lan, P.Q., and Wu, S.F. A study on the stability of a NiO–CaO/Al₂O₃ complex catalyst by La₂O₃ modification for hydrogen production. International Journal of Hydrogen Energy 37(19) (2012): 14161-14166.
- [103] Wu, S.F. and Wang, L.L. Improvement of the stability of a ZrO₂-modified Ni–nano-CaO sorption complex catalyst for ReSER hydrogen production. International Journal of Hydrogen Energy 35(13) (2010): 6518-6524.

- [104] Ochoa-Fernández, E., Lacalle-Vilà, C., Christensen, K.O., Walmsley, J.C., Rønning, M., Holmen, A., and Chen, D. Ni catalysts for sorption enhanced steam methane reforming. Topics in Catalysis 45(1-4) (2007): 3-8.
- [105] Hans Kristian Rusten, Esther Ochoa-Fernández, Håvard Lindborg, De Chen, and Jakobsen, H.A. Hydrogen Production by Sorption-Enhanced Steam Methane Reforming Using Lithium Oxides as CO₂-Acceptor. Industrial and Engineering Chemistry Research 46 (2007): 8729-8737.
- [106] Esther Ochoa-Fernández, Claudia Lacalle-Vilà, Tiejun Zhao, Magnus Rønning, and Chen, D. Experimental demonstration of H₂ production by CO₂ sorption enhanced steam methane reforming using ceramic acceptors. Natural Gas Conversion VIII (2007): 159-164.
- [107] Martavaltzi, C.S. and Lemonidou, A.A. Hydrogen production via sorption enhanced reforming of methane: Development of a novel hybrid material—reforming catalyst and CO₂ sorbent. Chemical Engineering Science 65(14) (2010): 4134-4140.
- [108] Halabi, M.H., de Croon, M.H.J.M., van der Schaaf, J., Cobden, P.D., and Schouten, J.C. A novel catalyst–sorbent system for an efficient H₂ production with in-situ CO₂ capture. International Journal of Hydrogen Energy 37(6) (2012): 4987-4996.

- [109] Izquierdo, U., Barrio, V.L., Requies, J., Cambra, J.F., Güemez, M.B., and Arias, P.L. Tri-reforming: A new biogas process for synthesis gas and hydrogen production. International Journal of Hydrogen Energy 38(18) (2013): 7623-7631.
- [110] Carbon Dioxide Capture and Storage, ed. Bert Metz, L.K., Susan Solomon, Stephen O. Andersen, Ogunlade Davidson, José Pons, David de Jager, Tahl Kestin, Martin Manning, and Leo Meyer. Cambridge University Press, 2005.
- [111] Antzara, A., Heracleous, E., and Lemonidou, A.A. Improving the stability of synthetic CaO-based CO₂ sorbents by structural promoters. Applied Energy 156 (2015): 331-343.
- [112] Lu, H., Khan, A., Pratsinis, S.E., and Smirniotis, P.G. Flame-Made Durable Doped-CaO Nanosorbents for CO₂ Capture. Energy & Fuels 23 (2009): 1093-1100.
- [113] Cesário, M.R., Barros, B.S., Courson, C., Melo, D.M.A., and Kiennemann, A. Catalytic performances of Ni–CaO–mayerite in CO₂ sorption enhanced steam methane reforming. Fuel Processing Technology 131 (2015): 247-253.
- [114] Sanchezsanchez, M., Navarro, R., and Fierro, J. Ethanol steam reforming over Ni/M_xO_y–Al₂O₃ (M=Ce, La, Zr and Mg) catalysts: Influence of support on the hydrogen production. International Journal of Hydrogen Energy 32(10-11) (2007): 1462-1471.
- [115] Phromprasit, J., Powell, J., Wongsakulphasatch, S., Kiatkittipong, W., Bumroongsakulsawat, P., and Assabumrungrat, S. Activity and stability

- performance of multifunctional catalyst (Ni/CaO and Ni/Ca₁₂Al₁₄O₃₃-CaO) for bio-hydrogen production from sorption enhanced biogas steam reforming. International Journal of Hydrogen Energy 41(18) (2016): 7318-7331.
- [116] Djaidja, A., Libs, S., Kiennemann, A., and Barama, A. Characterization and activity in dry reforming of methane on NiMg/Al and Ni/MgO catalysts. Catalysis Today 113(3-4) (2006): 194-200.
- [117] Donat, F., Florin, N.H., Anthony, E.J., and Fennell, P.S. Influence of high-temperature steam on the reactivity of CaO sorbent for CO₂ capture. Environ Sci Technol 46(2) (2012): 1262-9.
- [118] Kin, K.S. and Winograd, N. X-ray photoelectron spectroscopic studies of nickel-oxygen surfaces using oxygen and argon ion-bombardment. Surface Science 43 (1974): 625-643.
- [119] Klein, J.C. and Hercules, D.M. Surface Characterization of Model Urushibara Catalysts. Journal of catalysis 82 (1983): 424-441.
- [120] Molina, R. and Poncelet, G. r-Alumina-Supported Nickel Catalysts Prepared with Nickel Acetylacetonate. 2. A Study of the Thermolysis of the Metal Precursor. Journal of Physical Chemistry B 103 (1999): 11290-11296.
- [121] Takeguchi, T., Kani, Y., Yano, T., Kikuchi, R., Eguchi, K., Tsujimoto, K., Uchida, Y., Ueno, A., Omoshiki, K., and Aizawa, M. Study on steam reforming of CH₄ and C₂

- hydrocarbons and carbon deposition on Ni-YSZ cermets. Journal of Power Sources 112 (2002): 588–595.
- [122] Nichele, V., Signoretto, M., Pinna, F., Menegazzo, F., Rossetti, I., Cruciani, G., Cerrato, G., and Di Michele, A. Ni/ZrO₂ catalysts in ethanol steam reforming: Inhibition of coke formation by CaO-doping. Applied Catalysis B: Environmental 150-151 (2014): 12-20.
- [123] Al-Fatesh, A.S., Naeem, M.A., Fakeeha, A.H., and Abasaeed, A.E. Role of La₂O₃ as Promoter and Support in Ni/γ-Al₂O₃ Catalysts for Dry Reforming of Methane. Chinese Journal of Chemical Engineering 22(1) (2014): 28-37.
- [124] Yang, X., Da, J., Yu, H., and Wang, H. Characterization and performance evaluation of Ni-based catalysts with Ce promoter for methane and hydrocarbons steam reforming process. Fuel 179 (2016): 353-361.
- [125] Jang, W.-J., Jeong, D.-W., Shim, J.-O., Kim, H.-M., Roh, H.-S., Son, I.H., and Lee, S.J. Combined steam and carbon dioxide reforming of methane and side reactions: Thermodynamic equilibrium analysis and experimental application. Applied Energy 173 (2016): 80-91.
- [126] Quincoces, C.E., Dicundo, S., Alvarez, A.M., and Gonzalez, M.G. Effect of addition of CaO on Ni/Al₂O₃ catalysts over CO₂ reforming of methane. Materials Letters 50 (2001): 21-27.



APPENDIX A

CALCULATIONS OF ADSORPTION CAPACITY

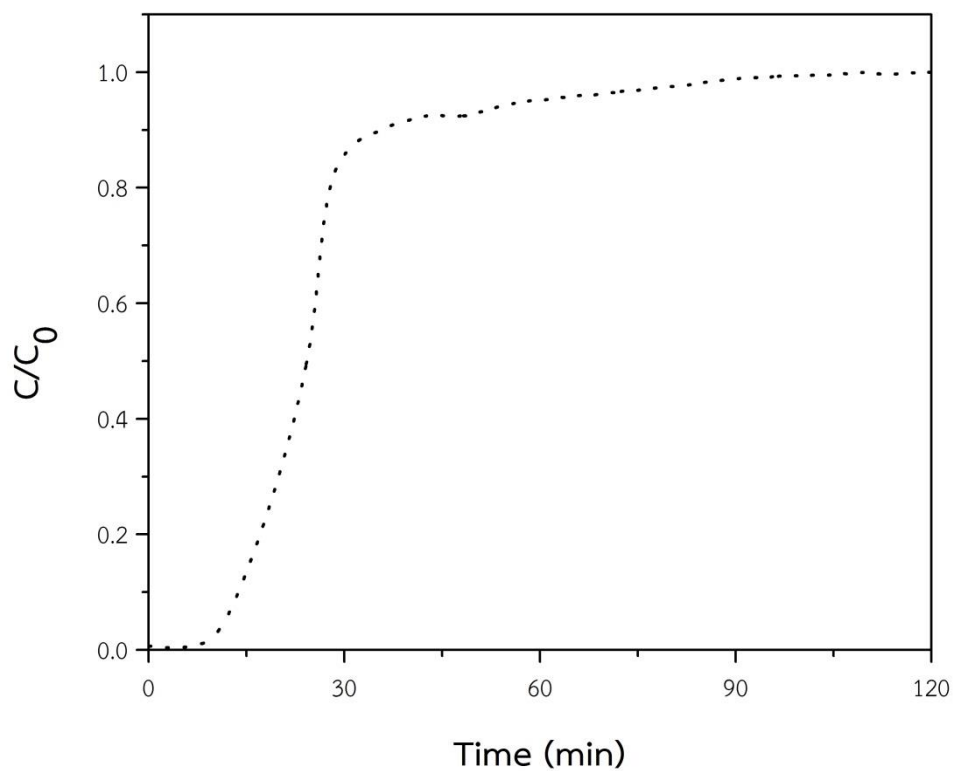


Figure A.1 CO₂ sorption by CaO at adsorption temperature of 500 °C, atmospheric pressure and 8% CO₂ in N₂ feed.

Sorption capacities of sorbents are calculated by Eq. A.1

$$\text{Sorption capacity } \left(\frac{g_{\text{CO}_2}}{g_{\text{sorbent}}} \right) = \frac{F_{\text{CO}_2} \times \int_0^t \left(1 - \frac{C}{C_0} \right) dt}{W} \quad (\text{A.1})$$

Where F_{CO_2} is the feed rate $\left(\frac{g}{min}\right)$, C is the CO_2 concentration at the outlet of reactor (%), C_0 is the CO_2 concentration at inlet of reactor (%), W is the sorbent weight (g) and t is sorption time (min). Eq. A.1 is derived as shown below:

In

$$m_{CO_2, in} (g) = \int_0^t u_{total, in} \left(\frac{mL}{min}\right) \cdot C_{CO_2, in} \left(\frac{mol}{mL}\right) \cdot MW \left(\frac{g}{mol}\right) dt$$

Out

$$m_{CO_2, out} (g) = \int_0^t u_{total, out} \left(\frac{mL}{min}\right) \cdot C_{CO_2, out} \left(\frac{mol}{mL}\right) \cdot MW \left(\frac{g}{mol}\right) dt$$

In - Out = Accumulation

$$m_{CO_2, in} - m_{CO_2, out} (g) = \left(\int_0^t u_{Total, in} \cdot C_{CO_2, in} \cdot MW dt \right) - \left(\int_0^t u_{Total, out} \cdot C_{CO_2, out} \cdot MW dt \right)$$

$$m_{CO_2, in} - m_{CO_2, out} (g) = MW \int_0^t (u_{Total, in} \cdot C_{CO_2, in} - u_{Total, out} \cdot C_{CO_2, out}) dt$$

$$m_{CO_2, in} - m_{CO_2, out} (g) = u_{Total, in} \cdot C_{CO_2, in} \cdot MW \int_0^t \left(1 - \frac{u_{Total, out} \cdot C_{CO_2, out}}{u_{Total, in} \cdot C_{CO_2, in}} \right) dt \dots (A.2)$$

From

$$y_{\text{CO}_2} = \frac{U_{\text{CO}_2}}{(U_{\text{CO}_2} + U_{\text{N}_2})}$$

$$U_{\text{CO}_2} = y_{\text{CO}_2} \cdot U_{\text{CO}_2} + y_{\text{CO}_2} \cdot U_{\text{N}_2}$$

$$U_{\text{CO}_2} - y_{\text{CO}_2} \cdot U_{\text{CO}_2} = y_{\text{CO}_2} \cdot U_{\text{N}_2}$$

$$U_{\text{CO}_2} = \frac{y_{\text{CO}_2} \cdot U_{\text{N}_2}}{(1 - y_{\text{CO}_2})} \quad \dots \text{(A.3)}$$

From

$$U_{\text{Total, out}} = (U_{\text{N}_2} + U_{\text{CO}_2}) \quad \dots \text{(A.4)}$$

Substitute (A.3) to (A.4)

$$U_{\text{Total, out}} = \left(U_{\text{N}_2} + \frac{y_{\text{CO}_2} \cdot U_{\text{N}_2}}{(1 - y_{\text{CO}_2})} \right)$$

$$U_{\text{Total, out}} = U_{\text{N}_2} \left(1 + \frac{y_{\text{CO}_2}}{(1 - y_{\text{CO}_2})} \right) \quad \dots \text{(A.5)}$$

Substitute (A.5) to (A.2)

$$m_{\text{CO}_2, \text{in}} - m_{\text{CO}_2, \text{out}} \text{ (g)} =$$

$$= U_{\text{Total, in}} \cdot C_{\text{CO}_2, \text{in}} \cdot \text{MW} \int_0^t \left(1 - \left(\frac{U_{\text{N}_2}}{U_{\text{Total, in}}} \cdot \left(1 + \frac{y_{\text{CO}_2}}{(1 - y_{\text{CO}_2})} \right) \cdot \frac{C_{\text{CO}_2, \text{out}}}{C_{\text{CO}_2, \text{in}}} \right) \right)$$

$$= F_{\text{CO}_2, \text{in}} \times \int_0^t \left(1 - \left(\frac{u_{\text{N}_2}}{u_{\text{Total, in}}} \cdot \left(1 + \frac{y_{\text{CO}_2}}{(1 - y_{\text{CO}_2})} \right) \cdot \frac{C_{\text{CO}_2, \text{out}}}{C_{\text{CO}_2, \text{in}}} \right) \right) dt$$

Therefore

$$\text{Sorption capacity} = \frac{F_{\text{CO}_2, \text{in}} \times \int_0^t \left(1 - \left(\frac{u_{\text{N}_2}}{u_{\text{Total, in}}} \cdot \left(1 + \frac{y_{\text{CO}_2}}{(1 - y_{\text{CO}_2})} \right) \cdot \frac{C_{\text{CO}_2, \text{out}}}{C_{\text{CO}_2, \text{in}}} \right) \right) dt}{W}$$

$$\text{Sorption capacity} = \frac{F_{\text{CO}_2, \text{in}} \times \int_0^t \left(1 - A \cdot \frac{C_{\text{CO}_2, \text{out}}}{C_{\text{CO}_2, \text{in}}} \right) dt}{W} \quad \dots \text{(A.6)}$$

$$\text{Where } A \text{ is } \frac{u_{\text{N}_2}}{u_{\text{Total, in}}} \cdot \left(1 + \frac{y_{\text{CO}_2}}{(1 - y_{\text{CO}_2})} \right)$$

APPENDIX B

CALCULATIONS FOR SORPTION ENHANCED BIOGAS STEAM REFORMING

PROCESS

Biogas steam reforming process is a process whose main reactions are methane steam reforming (Equation B.1) and dry methane reforming (Equation B.3). Moreover, the side reaction is water gas shift reaction (Equation B.2). For this study, the experiments were performed using excess steam at S/C of 3. Calculations for methane/carbon dioxide ratio, steam/carbon ratio and methane conversion equations are shown in Equations B.4-B.6, respectively.



Methane/carbon dioxide ratio

$$\begin{aligned} \text{CH}_4 / \text{CO}_2 &= \frac{\% \text{ composition of methane}}{\% \text{ composition of carbon dioxide}} \quad \dots \text{ (B.4)} \\ &= \frac{60 (\%)}{40 (\%)} \\ &= 1.5 \end{aligned}$$

Steam/carbon molar ratio:

$$\begin{aligned}
 S/C &= \frac{Y_{\text{H}_2\text{O},\text{in}}}{Y_{\text{CH}_4,\text{in}}} && (\text{mol/mol}) && \dots \text{ (B.5)} \\
 &= \frac{3 \text{ mole}}{1 \text{ mole}} \\
 &= 3
 \end{aligned}$$

The conversions of substance CH_4 :

$$\text{Conversion } (\text{CH}_4) = \frac{F_{\text{CH}_4,\text{in}} - F_{\text{CH}_4,\text{out}}}{F_{\text{CH}_4,\text{in}}} \times (100\%) \quad \dots \text{ (B.6)}$$

Where $F_{\text{CH}_4,\text{in}}$ is the molar flow rate of methane at the inlet stream (mol/min)

and $F_{\text{CH}_4,\text{out}}$ is the molar flow rate of methane at the outlet stream (mol/min).

The energy efficiency

Net energy = [Energy from H_2 – Energy from CH_4] – Energy used in SMR +

Energy from CO_2 sorption

$$\begin{aligned}
 &= \left[\left(4 \text{ mol H}_2 \times 142 \frac{\text{MJ}}{\text{kg}} \right) - \left(1 \text{ mol CH}_4 \times 45 \frac{\text{MJ}}{\text{kg}} \right) \right] - 165 \frac{\text{kJ}}{\text{mol}} + 176.8 \frac{\text{kJ}}{\text{mol}} \\
 &= \left[\left(1136 \frac{\text{kJ}}{\text{mol}} \right) - \left(720 \frac{\text{kJ}}{\text{mol}} \right) \right] - 165 \frac{\text{kJ}}{\text{mol}} + 176.8 \frac{\text{kJ}}{\text{mol}} \\
 &= \left[\left(1136 \frac{\text{kJ}}{\text{mol}} \right) - \left(720 \frac{\text{kJ}}{\text{mol}} \right) \right] + 11.8 \frac{\text{kJ}}{\text{mol}} \\
 &= 427.8 \frac{\text{kJ}}{\text{mol}}
 \end{aligned}$$

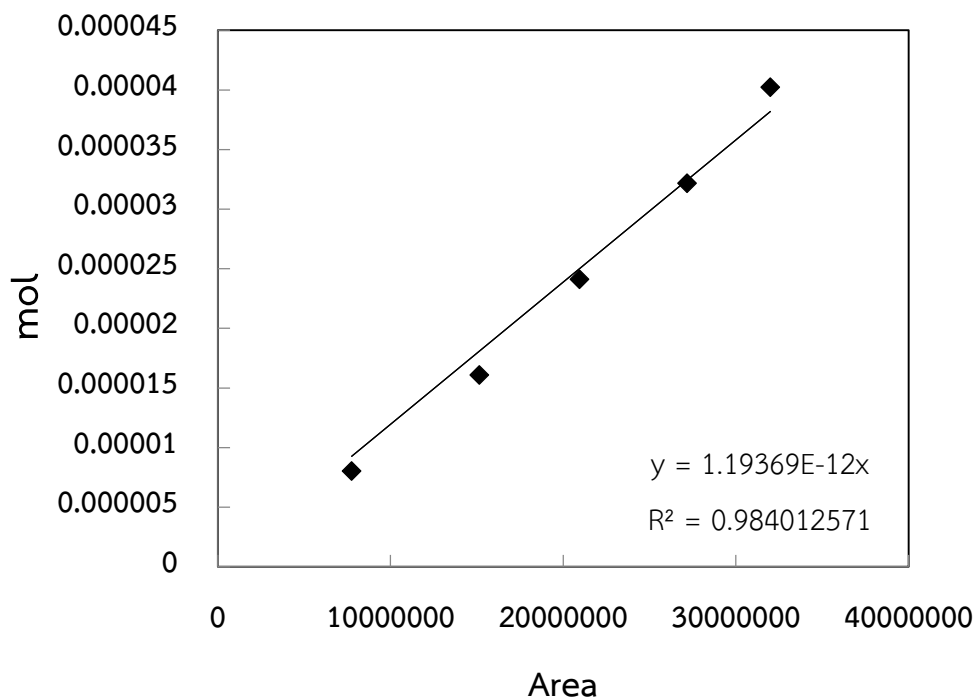
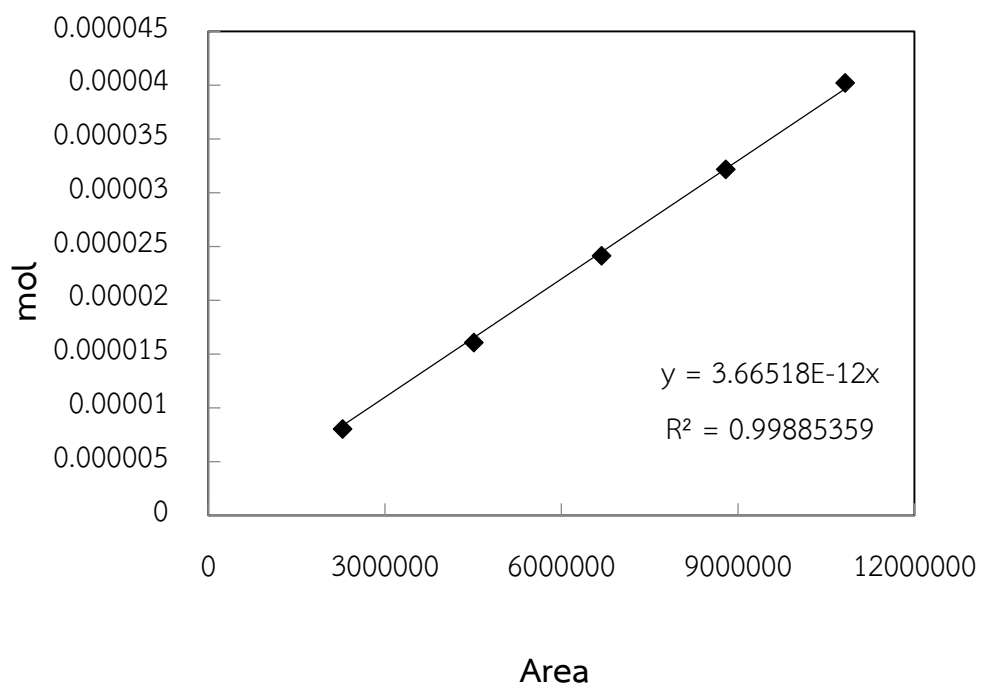
APPENDIX C

CALIBRATION CURVES

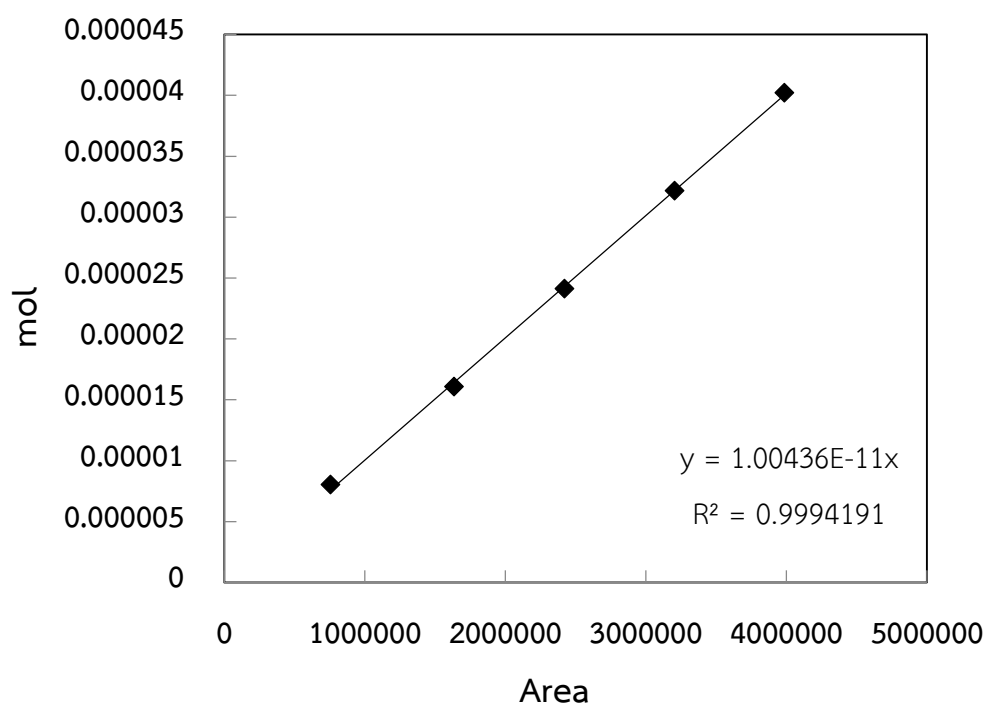
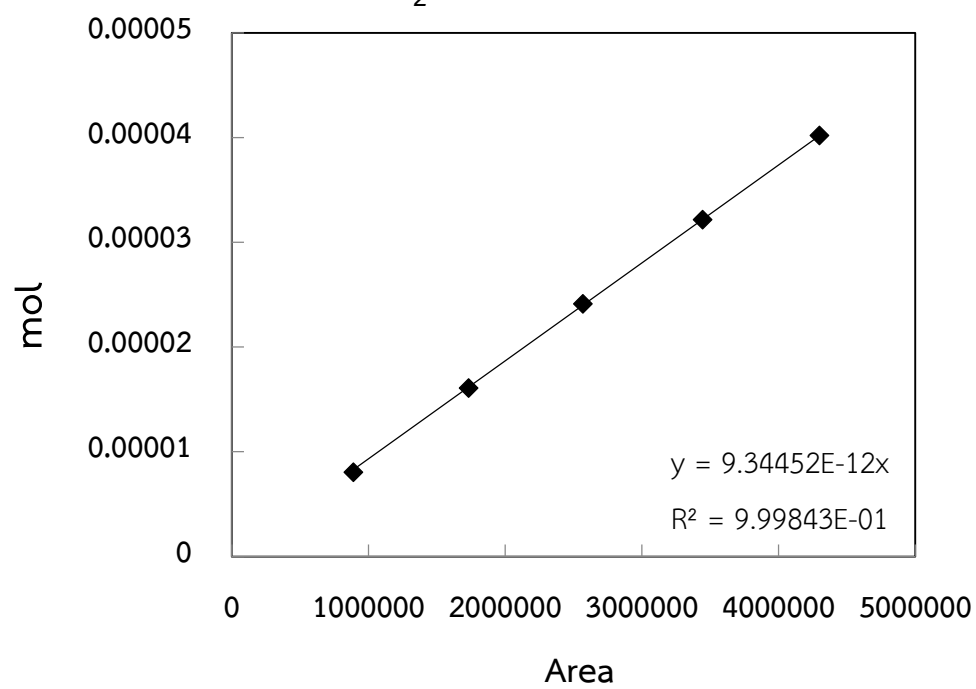
Calibration curve is done from gas chromatography (GC-8A) equipped with two columns that are Molecular Sieve and Poraplot column. Table C.1 shows the operating conditions for gas chromatography. The gas standard is injected to gas chromatography at different concentrations and we get peak area from GC for each concentration. Then, plot graph between peak area of gas chromatography and mole of gas that we inject into gas chromatography. Calibration curves are shown in Figures C.1-C.5 for CO₂, H₂, N₂, CH₄ and CO, respectively.

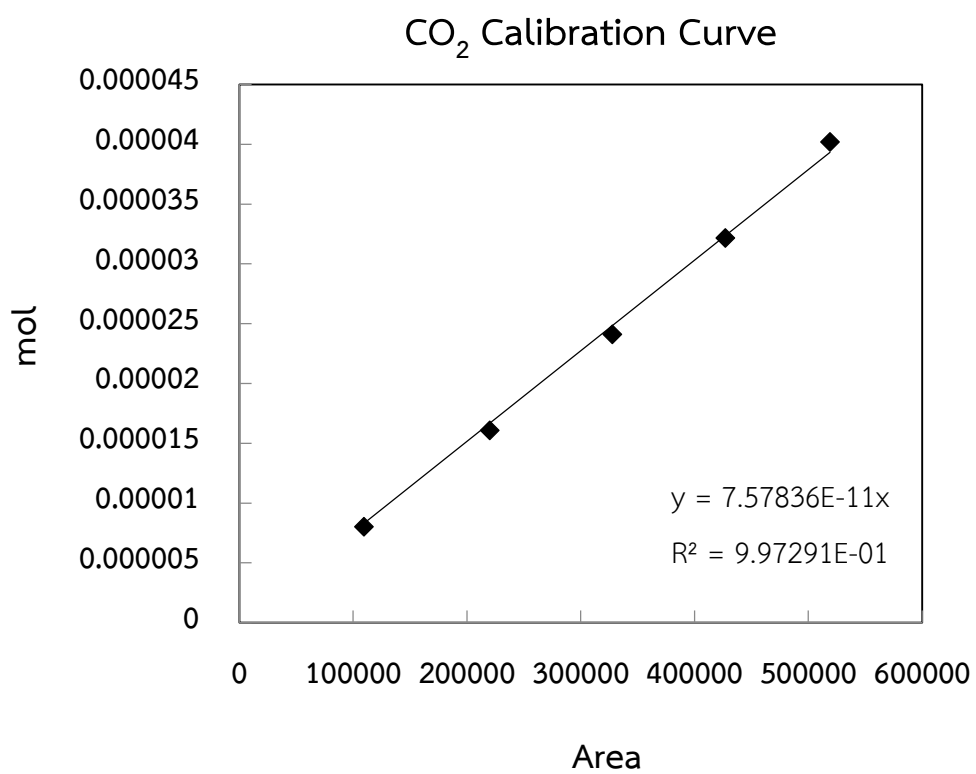
Table C.1 Operating conditions for gas chromatography

Gas Chromatography	Shimadzu GC-8A	
Detector	TCD	
Column	Molecular sieve 5A	Porapak-Q
- Column material	SUS	SUS
- Length (m)	2	2
- Outer diameter (mm)	4	4
- Inner diameter (mm)	3	3
- Mesh range	60/80	60/80
- Maximum temperature (°C)	350	350
Carrier gas	Ar (99.999%)	Ar (99.999%)
Column temperature		
- initial (°C)	50	50
- final (°C)	50	50
Injector temperature (°C)	70	70
Detector temperature (°C)	100	100
Current (mA)	70	70
Analyzed gas	N ₂ , H ₂ , CO, CH ₄	CO ₂

H₂ Calibration CurveCH₄ Calibration Curve

CO Calibration Curve

N₂ Calibration Curve



APPENDIX D

LIST OF PUBLICATIONS

International Publications

1. Janewit Phromprasit, Jonathan Powell and Suttichai Assabumrungrat, “Metals (Mg, Sr and Al) modified CaO based sorbent for CO₂ sorption/desorption stability in fixed bed reactor for high temperature application”, Chemical Engineering Journal, (2016) 284, 1212-1223.
2. Janewit Phromprasit, Jonathan Powell, Suwimol Wongsakulphasatch, Worapon Kiatkittipong, Palang Bumroongsakulsawat, Suttichai Assabumrungrat, “Activity and stability performance of multifunctional catalyst (Ni/CaO and Ni/Ca₁₂Al₁₄O₃₃-CaO) for bio-hydrogen production from sorption enhanced biogas steam reforming”, International Journal of Hydrogen Energy, (2016) 41, 7318-7331.
3. Janewit Phromprasit, Jon Powell, Suwimol Wongsakulphasatch, Worapon Kiatkittipong, Palang Bumroongsakulsawat, Suttichai Assabumrungrat, “H₂ production from sorption enhanced steam reforming of biogas using multifunctional catalysts of Ni over Zr-, Ce- and La-modified CaO sorbents”, Chemical Engineering Journal (Accepted)

International Conferences

1. Janewit Phromprasit, Jonathan Powell, Suwimol Wongsakulphasatch, Worapon Kiatkittipong, Palang Bumroongsakulsawat, Suttichai Assabumrungrat, “Hydrogen Production from Sorption Enhanced Biogas Steam Reforming using CaO based Catalyst”, RGJ-Ph.D. Congress XVII, Pataya, Thailand; June 8-11, 2016.
2. Janewit Phromprasit, Jon Powell, Suwimol Wongsakulphasatch, Worapon Kiatkittipong, Palang Bumroongsakulsawat, Suttichai Assabumrungrat, “Ni-Ca₁₂Al₁₄O₃₃ multifunctional catalyst prepared by ultrasonic assisted method for bio-hydrogen from sorption enhanced biogas steam reforming”, XXII International Conference on Chemical Reactors, London, United Kingdom; September 19-23, 2016.

Awards

1. Outstanding poster presentation in RGJ-Ph.D. congress XVII from RGJ-Ph.D. programme, Pataya, Thailand; June 8-11, 2016.
2. Presentation award of Royal Society of Chemistry from XXII International Conference on Chemical Reactors, London, United Kingdom; September 19-23, 2016.

VITA

Mr. Janewit Phromprasit was born in Surin province, Thailand, on September 7, 1987. He finished high school from Pibulwittayalai School, Lob Buri, Thailand, in 2006. He received his Bachelor's Degree of Chemical Engineering, Thammasat University, Thailand, in 2010. He received his Master's Degree of Chemical Engineering, Chulalongkorn University, Thailand, 2012. He has been studied Doctoral's Degree of Chemical Engineering, Chulalongkorn University, Thailand, since 2012



